EFFECT OF WELD SCHEDULE VARIATION ON THE WELDABILITY AND DURABILITY OF AHSS SPOT WELD JOINTS

by

ERIC RAYMOND WEISHAUPT

MARK E. BARKEY, COMMITTEE CHAIR
RICHARD C. BRADT
JAMES P. HUBNER
JOHN E. JACKSON
MARK L. WEAVER

A DISSERTATION

Submitted in partial fulfillment of the requirements
for the degree of Doctor of Philosophy
in the Department of Aerospace Engineering and Mechanics
in the Graduate School of
The University of Alabama

TUSCALOOSA, ALABAMA

2012

ABSTRACT

Tensile strength testing and high cycle fatigue testing of advanced high strength steel spot welded shear lap joints were performed for the various weld conditions. The materials used in this study were DP 980, DP 780 and TRIP 780. The microstructure and microhardness of the shear lap joints were examined in an effort to identify the effect of microstructural changes on the strength and fatigue durability of the spot weld specimens. The occurrence of interfacial failure was recorded for the differing weld processes.

Several weld schedules were examined and used to produce shear lap spot weld joints, specifically varying the squeeze force and the average current. The weld force used to produce a spot weld does not have a significant effect on the fracture mode of the specimen given the average current is constant. The average current used to produce a spot weld has a significant effect on the fracture mode of the spot weld for several squeeze forces. Interfacial failure of spot welded TRIP 780 can be mitigated using a certain range of currents when welding. This appears to come as a tradeoff for sacrificing the strength of the joint. Higher values of weld strength were obtainable; however, welds that failed with higher strengths also experienced interfacial failure.

A fracture mechanics approach to estimating the high cycle fatigue life of the shear lap specimen is also proposed and represents a conservative estimate of the shear lap specimen durability.

DEDICATION

For Dad.

LIST OF ABBREVIATIONS AND SYMBOLS

a	Flaw size
AHSS	Advance high strength steel
b	Nugget diameter
C	Paris law material constant coefficient
DP	Dual phase (in reference to dual phase steel)
d	Nugget diameter
$\frac{da}{dN}$	Crack growth rate
dc	Critical weld diameter size
F	Force
$f(g)$	Geometry factor
$H_{\max}$	Maximum HAZ hardness
$H_{\min}$	Minimum HAZ hardness
HAZ	Heat affected zone
HRC	Rockwell “C” scale Hardness
HV	Vickers Hardness
kA	kiloAmpere
K_{eq}	Equivalent stress intensity factor
$K_{\max}$	Stress Intensity associated with maximum load

K_{min}	Stress Intensity associated with minimum load
K_I	Mode I stress intensity factor
K_{II}	Mode II stress intensity factor
K_{III}	Mode III stress intensity factor Computed value of *t* test
K_{Ic}	Mode I critical fracture toughness
m	Paris law material constant exponent
mm	Millimeter
MPa	Megapascal
N	Newton
Nf	Cycles to failure
TRIP	Transformation induced plasticity (in reference to Transformation induced plasticity steel)
TSFc	Critical tensile shear force
UTS	Ultimate tensile strength
ΔK_{eq}	Equivalent stress intensity range
ΔK	stress intensity range
$\Delta\sigma$	Applied stress range
σ_b^{++}	Symmetrical radial bending stress
σ_b^{+-}	Antisymmetrical radial bending stress

σ^{+-} Antisymmetrical radial membrane stress

$\tau_{\perp}^{++}$ Symmetrical transverse shear stress

$\tau_{\perp}^{+-}$ Antisymmetrical transverse shear stress

$\tau_{\parallel}^{+-}$ Antisymmetrical longitudinal shear stress

μm micrometer

ACKNOWLEDGMENTS

I would like to sincerely thank my advisor Dr. Mark Barkey, he has proven to be an excellent mentor, this endeavor certainly would not be possible without his honest advice, expertise, and encouragement.

I am pleased to have this opportunity to thank my committee, Dr. Richard Bradt, Dr. Paul Hubner, Dr. John Jackson, and Dr. Mark Weaver for graciously supplying their time not only in this matter, but myriad other subjects.

I also would like to thank Dr. Benda Yan of ArcelorMittal for providing the steel used in this study, in addition to his valuable insight. A thank you is overdue to Dr. Michael Stevenson and Jeffrey McDougall for their insight and mentorship.

This endeavor could not have been successful without the support of my entire family, Starnes, Weishaupt, and Sissen. I specifically would like to recognize Mom, Dad and Edie for their support. Finally, thank you to my wife, Kristen, for all of your sacrifice and encouragement.

CONTENTS

LIST OF TABLES

LIST OF FIGURES

Chapter 1

Introduction

The automotive industry has long used steel products for various components throughout vehicles. It is no surprise that the automotive industry has also been one of the greatest sources of material innovation for steel products, specifically in the forming, joining, and advanced materials communities. Automotive manufacturers consistently strive to reduce weight and improve performance of vehicles by introducing new materials and joining methods. Currently, an overwhelming sense of urgency to increase the efficiency of the average automobile is all too apparent. This heightened sense of urgency is due to increasing fuel costs, environmental concerns and economic uncertainty. Reasons such as these are driving automakers to establish new material and performance standards which will prepare them for the next step in automobile manufacturing, including upcoming United States government fuel consumption regulations (EPA and NHTSA, 2011).

Advanced high strength steels (AHSS) are currently being explored as resources to lead to a safer and more efficient automobile (Long et al. 2007). Two specific types of AHSS are dual phase (DP) steels and transformation induced plasticity (TRIP) steels. These steels not only have superior strength when compared to standard carbon steels but the formability, ductility and fatigue endurance limit are also favorable for use in the automotive industry (Fredrikson et al.

1988, El-Sayed 1996). The information available regarding AHSS is limited when compared to that of carbon steel. Metallurgical and mechanical investigations regarding potential applications for these materials are equally limited. Further knowledge regarding the performance of these materials in automotive applications is imperative to ensure the automotive industry thrives in the foreseeable future.

DP steels are currently being used as a replacement for high-strength low-alloy (HSLA) steels in structural components. DP steels exhibit higher strength and higher fatigue resistance resulting in a lower part weight (Yan et al. 2003, ASM Handbook Vol. 1). TRIP steels exhibit increased ductility over the DP steels, allowing for more intricate part shapes to be formed while maintaining a strength and fatigue resistance comparable to that of the DP steels (Yan et al. 2003, ASM Handbook Vol. 1). DP and TRIP steels both exhibit unique work hardening properties due to their respective microstructures. The durability of spot welded joints fabricated from TRIP and DP steels is a topic garnering increased interest. Techniques common in the materials science, metallurgy, and mechanics communities must be utilized to develop an enhanced understanding of the material behavior and mechanical performance of these steels in spot welded applications. Research regarding the spot weld joint behavior is crucial to developing durability, manufacturing, and design standards which will allow these materials to be implemented in automotive manufacturing. Relationships between the material, mechanical properties, fracture mode, and resulting overall durability of the spot welded joint will be formulated and refined during the course of this study to provide a useful solution to an important problem.

The metallurgical composition of AHSS materials that provide the characteristically high strength also present new challenges and opportunities, particularly with regard to spot weldability. Changes in cooling rate following welding can result in differences in the metallurgical composition of the heat affected zone (HAZ) adjacent to the spot welds. These HAZ properties are fundamental to the durability characteristics of spot welded joints, as most fatigue cracks initiate in the HAZ near spot welds (Wang et al. 2006). By controlling the cooling rate, the HAZ properties of these steels can be optimized for durability performance of these joints. In a production environment, the only practical way to control the microstructure is to alter the welding process, or weld schedule, so that the optimal microstructure is obtained - i.e. via an *in-situ* tempering process.

This research will investigate how altering welding parameters can be used to create a microstructure to optimize both fatigue and strength properties of TRIP 780, while maintaining a consistent fracture mode. Interfacial failure is a fracture mechanism that results in spot weld fracture through the nugget. Interfacial failure is often associated with a lack of deformation in the base material prior to failure of the joint, specifically when compared to the conventional nugget pullout failure mode which consists of the nugget remaining intact and the fracture propagating through the base material. Figures 1.1 and 1.2 compare the conventional nugget pullout fracture mechanism to the interfacial failure fracture mechanism. Currently, interfacial failure of advanced high strength steels is limiting the use of spot welded structures to components that are not overtly susceptible to this type of failure, mainly components that would

experience primarily compressive loading at the welded joint. Local microstructures developed during welding may lead to unfavorable fracture mechanisms, including interfacial fracture. Since mass scale heat treatment of automotive parts is both costly and inefficient, by adjusting the weld schedule and possibly the cooling parameters, one can alter the resulting microstructure of the weld. Changing welding parameters may suppress the formation of undesirable local microstructures. Optimizing the spot weld procedure to establish the most favorable strength and fatigue results will potentially allow advanced high strength steels to replace traditional carbon and deep draw steels in a majority of applications.

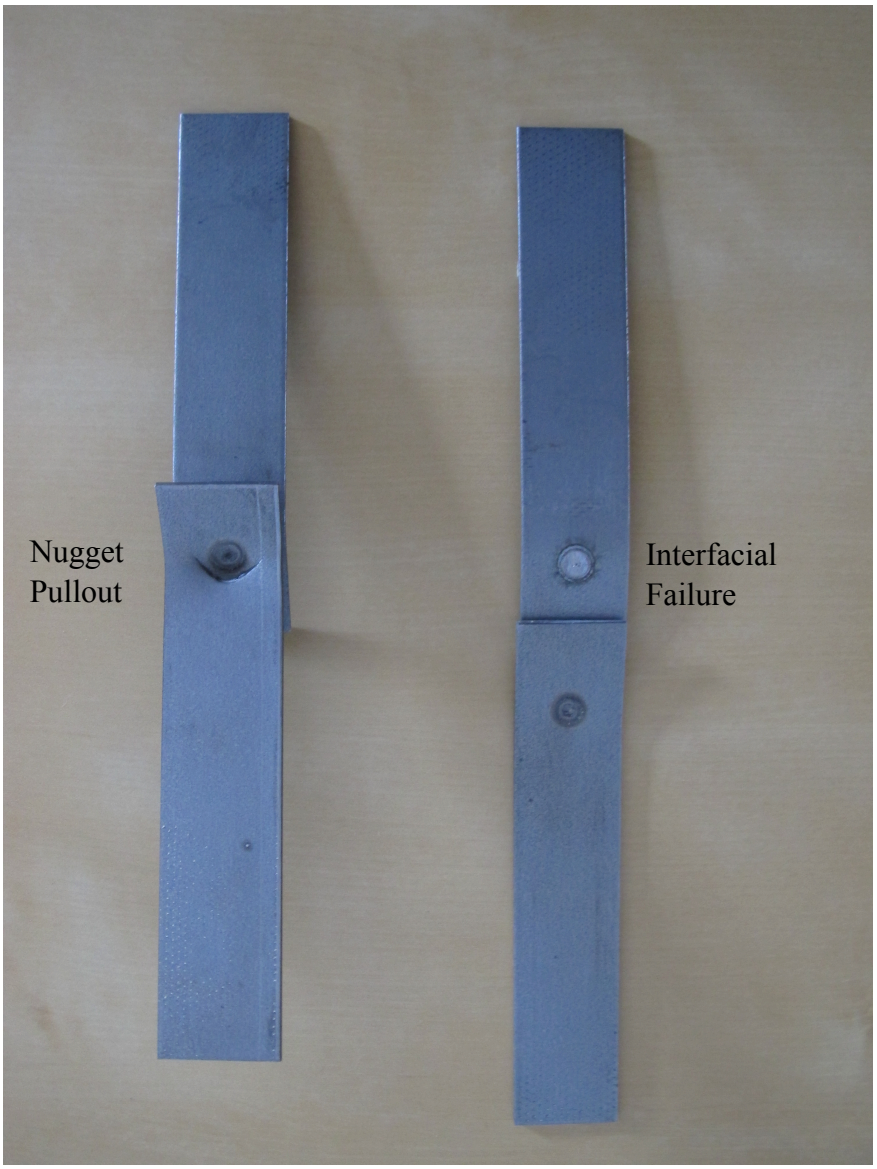

Figure 1.1 Comparison of nugget pullout failure to interfacial failure

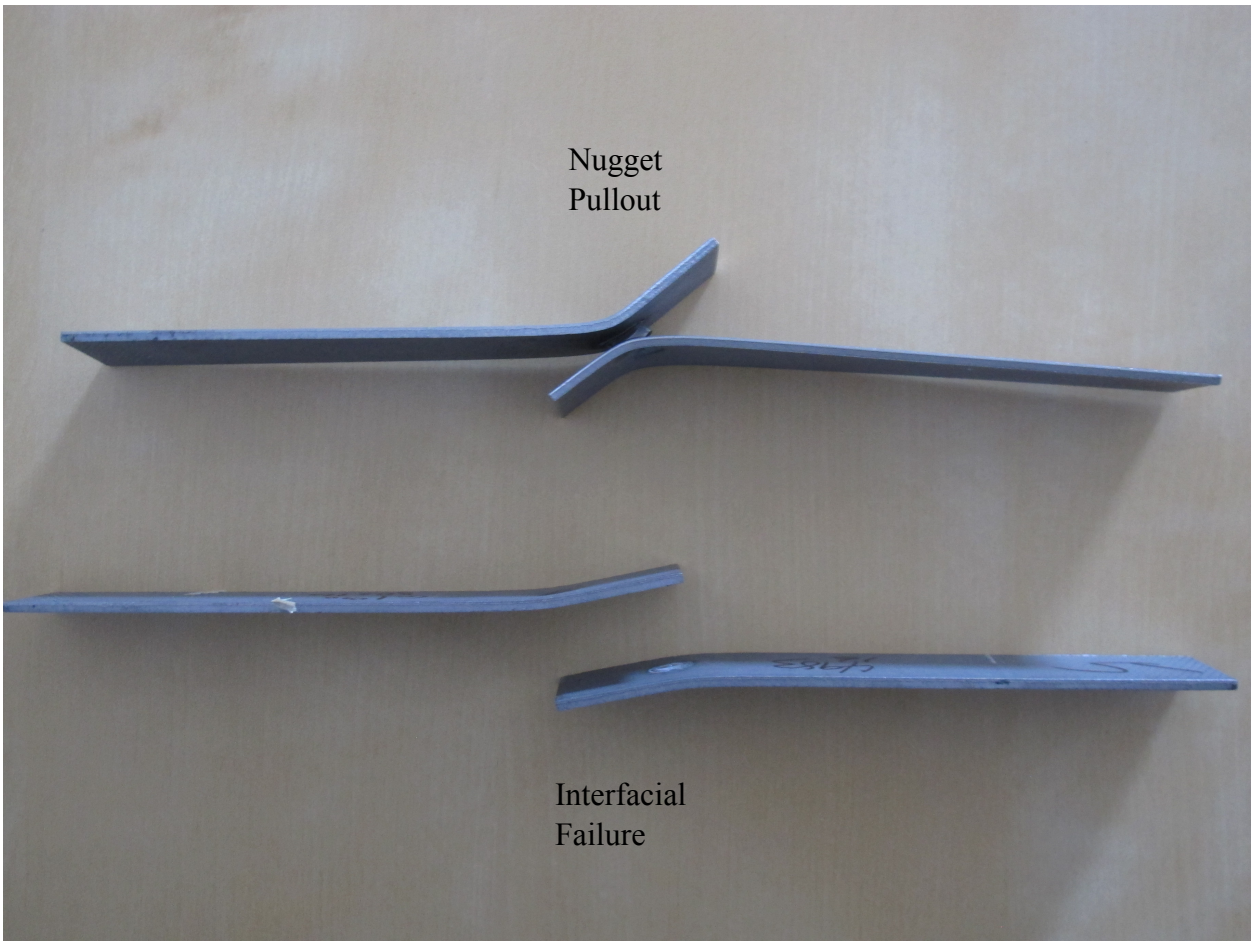

Figure 1.2 Comparison of nugget pullout failure to interfacial failure (cont.)

In the current study, TRIP and DP steels will be evaluated and compared. Shear lap fatigue fracture mechanisms will be examined with changing welding procedures; the shear lap joints will be welded using a multiple pulses and compared to a traditional one pulse weld schedule. To develop a weld schedule that potentially mitigates interfacial failure in TRIP 780 the squeeze force and the average welding current for the shear lap joints were altered. Altering these parameters allowed an adequate welding schedule to be defined for the TRIP 780 steel. Additionally, this research project focuses on damage mechanisms associated with fatigue durability and strength of AHSS spot welded joints. The high cycle fatigue life of the AHSS spot welded joints is compared using a stress intensity approach. A model is developed to conservatively estimate the high cycle fatigue life of the AHSS shear lap joints, using material properties for steels and the Paris power law.

Chapter 2

Literature Review

Several research projects have recently examined the effectiveness and feasibility of AHSS in spot welded applications. Initial studies into the base properties of TRIP and DP steels have indicated that the steels show desirable strength and fatigue properties when compared to steels currently used in spot-welded sheet applications (Yan et al. 2003). The use of DP steels has become increasingly popular for components where high strengths are required and decreased part weight is paramount. The following section will examine previous research on both of the steels used for this study, the structure of a spot weld joint and the associated nomenclature, failure modes of spot weld joints, and numerical models used to calculate the durability of spot weld joints.

2.1 Dual Phase Steels

Dual phase steels are a type of steel achieved through an intercritical heat treatment process. Figure 2.1 shows a portion of the an Fe - C phase diagram that depicts some representative annealing temperatures to produce DP steel (Krauss 1980). The steel is cooled from its annealing temperature to form a microstructure that is composed of ferrite and martensite phases, hence the term “dual phase” steel.

This intercritical heat treatment creates a continuously yielding steel that displays excellent tensile strength and strain hardening (ASM Handbook Vol. 1). A high density of dislocations are introduced to the ferrite upon cooling from the intercritical temperature and begin to migrate immediately upon the application of stress, which attributes to the continuous yielding observed (Krauss 1980). The martensite will provide dispersion strengthening to the DP steels. This results in a relationship between the strength of the DP steel and the amount of martensite present. It is also indicated that the configuration of the martensite will contribute to the ability of the steel to effectively work harden and maintain ductility (Krauss 2005).

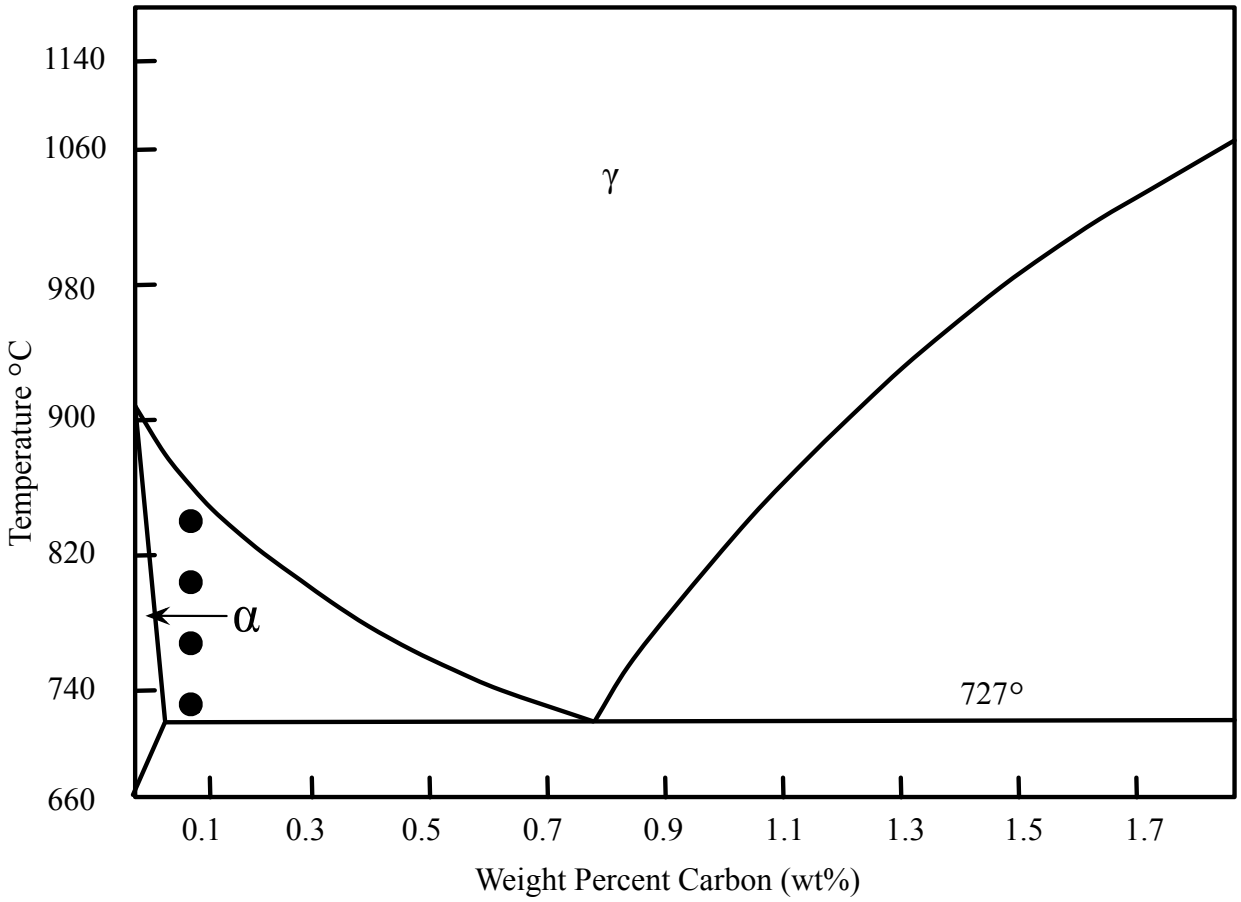

Figure 2.1 Portion of Fe - C phase diagram indicating example intercritical annealing temperatures (Adopted from Krauss 1980)

2.2 TRIP Steels

Transformation Induced Plasticity (TRIP) steels are a class of steel that is typically achieved through an intercritical annealing step followed by an isothermal transformation (Krauss, 2005). TRIP microstructures are created using a thermomechanical process that was initially examined extensively by Matsumura, Sakuma, and Tkechi (Matsumura et al. 1987, Matsumura et al. 1987, Sakuma et al. 1991, Sakuma et al. 1991). The primary phases present in TRIP steels are polygonal ferrite, bainite, and retained austenite (Timokhina et al. 2004).

The TRIP steels, like the DP steels, are a continuously yielding steel and also exhibit excellent tensile strength while maintaining ductility. A unique characteristic of TRIP steels is the phase transformation that occurs during deformation. The retained austenite phase of the TRIP steels will, upon sufficient deformation, transform to martensite. Austenite is a phase of steel that is stable at high temperatures (Krauss 1980). Following the aforementioned isothermal transformation TRIP steels undergo, austenite remains at ambient temperatures. The phase transformation from austenite to martensite is a diffusionless, athermal, shear transformation. Martensite is a hard phase formed in steels and often is attributed with giving steels a high tensile strength.

This transformation is believed by many to be responsible for the high strength of TRIP steels, while maintaining excellent ductility, specifically, uniform elongation during plastic deformation. Consequently, the effect of the presence of retained austenite in TRIP steels has been the subject of many recent studies (Matsumura et al. 1987, Matsumura et al. 1992). The literature also indicates that this consequence may be overstated and the ductility observed along with the high tensile strength may be attributable to the composite microstructure of the TRIP steels, not unlike the DP steels (Bhadeshia, 2002, Chaterjee 2006, Chatterjee 2007).

2.3 The Spot Weld Joint

The spot weld joint contains three microstructural zones of primary interest that will be described based on the proximity to the weld. Figure 2.2 displays the three zones of interest.

The first zone is the weld zone or weld nugget, this zone contains the portion of the spot weld that creates the joint or interface between workpieces. The weld nugget contains the sections of the material that becomes molten and resolidifies during the welding and subsequent cooling.

The heat affected zone (HAZ) is located directly adjacent to the weld nugget. This section of the weld has not been melted; however, significant thermal affects are evident. Several microstructural changes can occur in the HAZ. The HAZ of a spot weld is a metallurgical transition zone.

The final zone is the base material. This zone is adjacent to the HAZ and represents the portion of the spot weld joint that has not been affected by the welding process and is comprised of the parent material used to produce the weld.

Several early studies on the mechanical properties of spot weld joints have investigated the effect of various aspects of the microstructural zones. Several of these early studies, often conducted on carbon steel, are outlined in the next section of this chapter. At the time of this study researchers continue to study the effect of various aspects of the microstructural zones on AHSS.

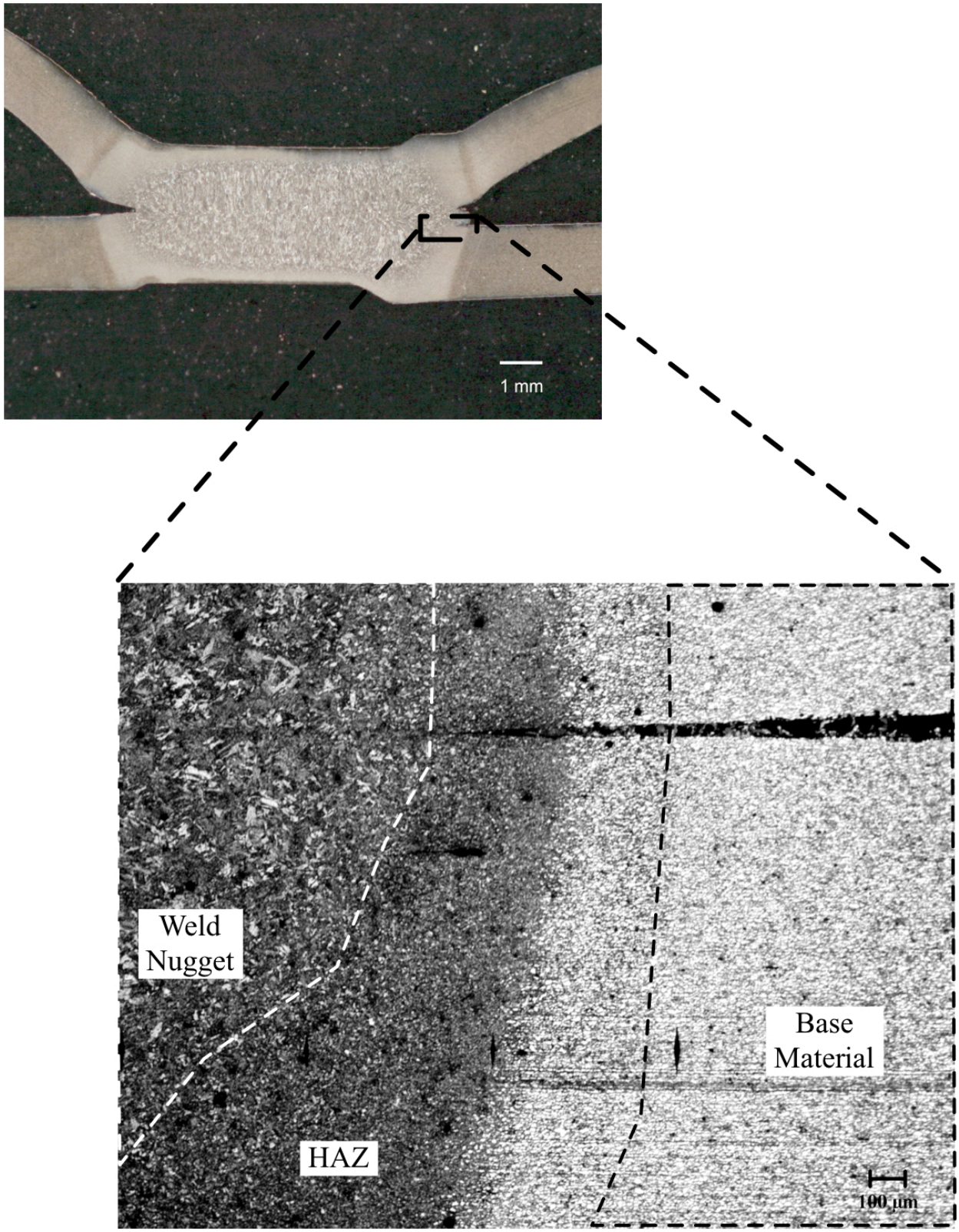

Figure 2.2 Metallurgical zones of the spot weld joint

Several authors have studied various aspects of the spot weld geometry (including specimen thickness, nugget size, and weld spacing) and its relation to the fatigue life and mechanical properties. In general, it has been found that increasing the thickness of the sheet used to make a spot weld joint will increase the fatigue life (Pollard 1982, Jung et al. 1996, Kitagwa et al. 1985, Davidson et al. 1984). However, increasing sheet thickness to increase the fatigue life of a spot weld joint is a cumbersome task when design considerations are factored, such as reduced part weight.

Nugget size may also have a beneficial effect on the fatigue life of some spot weld materials. For increasing nugget diameter it has been found that the fatigue life can increase (Pollard 1982, Wilson et al. 1981). The benefits of increasing nugget size are negligible in the high cycle fatigue regime (Davidson 1983). Weld spacing and edge distance were examined for low carbon steel joints by Zhang et al. (Zhang et al. 2008). It was found that decreasing spacing between welds in multiple welded joints reduced the strength of the joint.

In addition to spot weld geometry, these studies have investigated the effect of base material strength on the fatigue life of spot weld joints. The results of several studies have concluded that a higher base material strength result in enhanced fatigue life in the low cycle fatigue regime of approximately 10^4 cycles and lower (Davidson et al. 1984, Kitagwa et al. 1985). The beneficial effect of increased base material strength is negligible in the high cycle fatigue regime for spot welded joints (Pollard 1982). Increasing base material strength will influence the crack initiation

life of the spot weld joint; however, it appears to have a negligible effect on the crack propagation life (Abe et al. 1986).

2.4 AHSS Spot Weld Failure Modes

Recently, DP steels have been used in spot welded applications as well. Since the onset of this usage spot welded DP parts have been plagued by issues regarding interfacial fracture, especially in the mid to low cycle fatigue regimes (Barkey et al. 2007). The inherent shape of spot welded joints introduces undesirable local geometry, resulting in a notch. Toughness is an equally critical property to consider in the design of a spot welded part. The highly martensitic microstructure commonly formed in spot welded joints can result in high hardness but a drastically reduced toughness when compared to the base material.

Interfacial failure of DP spot welds has been found to be associated with welding parameters; interfacial failure is associated with low welding force or low weld current for the dual phase steel joints. (Ma et al.). Ma et al. found that voids and/or cracks formed during solidification may lead to interfacial failure in both static load testing and fatigue loading. The interfacial failure is associated with low welding force or low weld current for the dual phase steel joints. The interfacial failure of the dual phase steel was also found to be more prolific in high load fatigue failures.

Interfacial failure of DP steels has also been found to be more prevalent in spot weld joints produced using higher strength base material (Marya et al. 2006). In Marya's study, a value for the critical weld diameter was developed to predict the failure mode of the spot weld.

An empirical equation was developed by Marya that relates HAZ hardness values and sheet thickness to a critical weld diameter size. The dimension dependent equation is presented below:

$$d_c = 0.53t^{3.22} + 8.48\left(\frac{H_{\max}}{H_{\min}}\right)^{-1.24}, \qquad (2.1)$$

where

d_c = Critical Weld diameter size (mm),

t = sheet thickness (mm),

$H_{\max}$ = Maximum HAZ hardness (HV),

$H_{\min}$ = Minimum HAZ hardness (HV).

This equation was used to accurately model the failure mode of DP 780, DP 600, and DP 980 steels. The critical diameter value describes a threshold that below which interfacial failure can be expected. This model was derived using a shear lap spot weld configuration. The above equation was also used in combination with observations regarding the tensile shear failure force to develop a relationship between the tensile shear failure force and the HAZ hardness ratio and sheet thickness. The dimension dependent equation is described below:

$$TSF_c = 831\left[0.53t^{3.22} + 8.48\left(\frac{H_{\max}}{H_{\min}}\right)^{-1.24}\right]^{1.68}, \quad (2.2)$$

where

TSF_c = Critical Tensile Shear Force (N).

Several failure modes have been recorded for DP steels other than the aforementioned interfacial failure. For low fatigue loads, cracks typically initiate at the interface of the nugget and HAZ on the inner surface of the joint and propagate in the direction of the outer surface through the thickness of the weld (Long et al. 2007). At high fatigue load levels the cracks may initiate in the HAZ near the nugget, while at intermediate load levels it has been observed that cracks initiate at the nugget boundary and propagate around the circumference of the nugget before growing into the base material (Ma et al. 2007).

For spot welds produced from TRIP steels interfacial failure has also been found to be associated with welding parameters (Gould et al. 2006, Gould et al.1998). The work by Gould et al. shows that the interfacial failure is associated with small nugget diameters with thicker sections that may cause high stress triaxiality. This type of stress state is known to promote interfacial failure (Chuko et al. 2002, Rathbun et al. 2003). Interfacial failure for TRIP steels was again noted to occur with more frequency in the low cycle fatigue regime.

Several failure modes have been recorded for TRIP steels other than the aforementioned interfacial failure. For low fatigue loads or in the high cycle regime, cracks typically initiate at the tongue of the weld (Rathbun et al. 2003). The tongue of the weld refers to a structure that can result from molten metal being ejected from the weld nugget. An example of the tongue structure is displayed in Figure 2.3.

In the high cycle fatigue regime cracks were found to initiate at the tongue structure, using the inherit geometry of the structure as a "precrack". The majority of the life of the fatigue joint is spent in crack propagation. The cracks initiated at the tongue would propagate through the HAZ on the inner surface of the joint and propagate in the direction of the outer surface through the thickness of the weld. A similar observation regarding the crack path from the tongue structure in fatigue cracks in both the high and low cycle fatigue regime was observed in an additional study (Long et al. 2007).

Interfacial failure of TRIP spot weld joints has been found to occur as a mixture of both intergranular and transgranular fracture (Hilditch et al. 2007). It was also shown in the Hilditch et al. study that interfacial failure of TRIP steel spot weld joints do not necessarily translate into a lower value of weld strength when compared to conventional spot weld failure modes, like button pullout. This study also indicated that there was no acceptable correlation between weld hardness and the strength of the spot weld joint or the failure mechanism.

Interfacial failure has also been associated with an odd phenomenon observed in TRIP spot welds joined in a cross tension orientation, with a decrease in fatigue life observed for decreasing loads (Rathbun et al. 2007). This behavior was observed in the intermediate fatigue load range with no interfacial failure being reported in the high cycle fatigue regime.

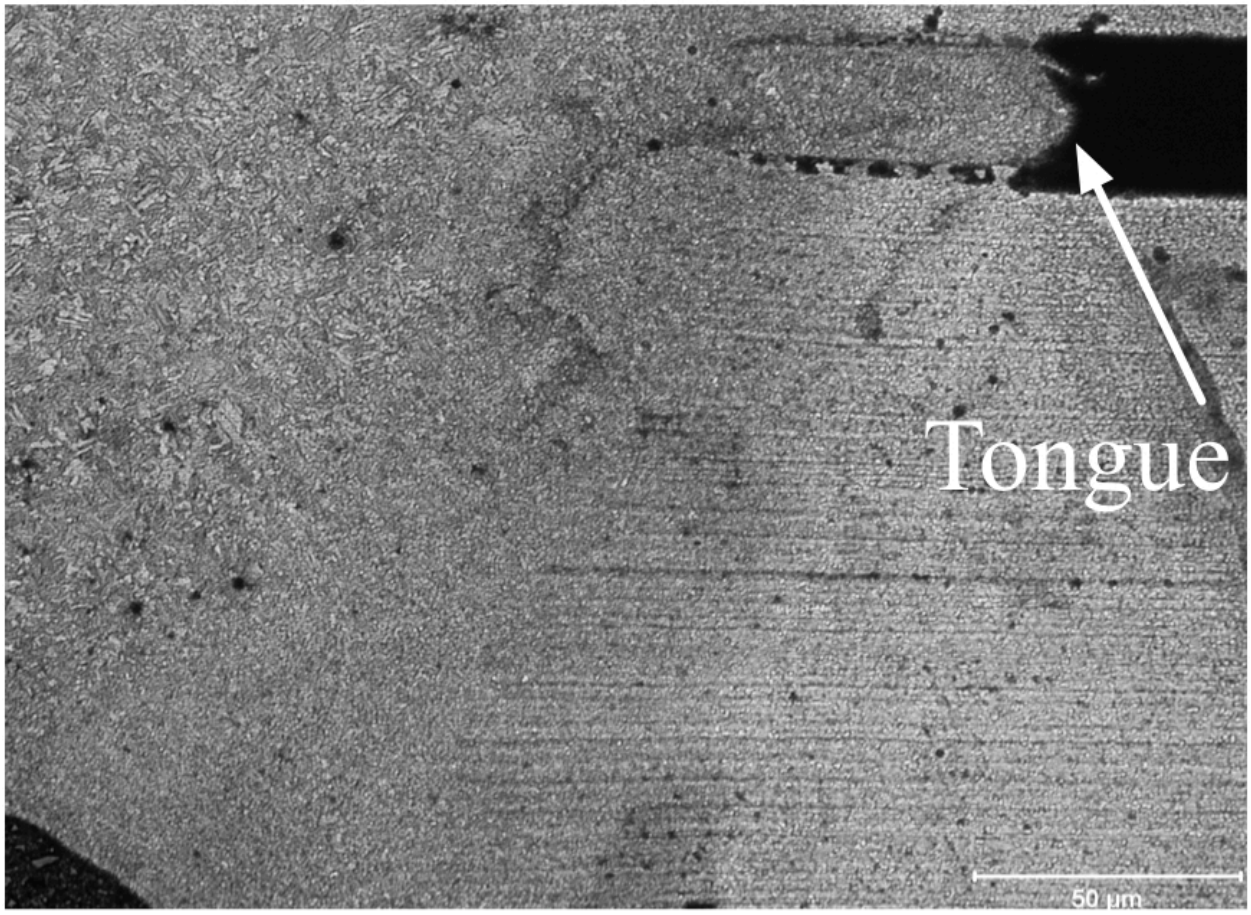

Figure 2.3 Image of tongue structure formed after spot welding

2.5 Spot Weld Heat Treatment

Heat treatment of metals is used to produce a favorable microstructure for a specific application. In the case of spot welded structures such as automotive body components, heat treatment of the entire structure is a cumbersome and often expensive procedure. One solution to these limitations that has been explored in the literature is an *in-situ* heat treatment often referred to as *in-situ* tempering. *In-situ* tempering of the steel may lead to specific beneficial microstructural changes within the spot weld joint.

The work of Chuko and Gould has indicated that tempering of spot welds can be performed by altering the welding procedure (*in-situ* tempering) (Chuko and Gould 2002). Their study found that the hardness of the weld could be reduced using a tempering step. By lowering the hardness of the weld, the susceptibility of the weld to hold time sensitivity can be lowered. Hold time sensitivity has been found to attribute at least in part to interfacial failure.

Existing models of spot weld fatigue life assume that the microstructure does not significantly effect the fatigue life of the welded joint, but it is rather dominated by geometry (Rathbun et al. 2003, Hilditch et al. 2007). The work of Chuko and Gould shows that several different HAZ hardness values are capable of being created using only *in-situ* tempering.

A recent study of TRIP spot welds joints also examined the benefits of traditional heat treatments on spot weld joints (Hilditch et al. 2007). Cross tension spot weld samples were subjected to a

pre-weld and post-weld heat treatment. It was found that tempering the spot welds above the temper embrittlement range resulted in increases in weld strength. The study also noted that some tempered samples failed due to interfacial failure. Some of the samples that were tempered and showed an increase in strength still exhibited interfacial failure. This would suggest that the tempering of the welds did not alleviate the welds susceptibility to interfacial failure.

2.6 Fracture Mechanics Approach to Spot Weld Joint Durability

Stress intensity solutions of spot weld joints has been studied extensively by several authors. Early studies estimated the stress intensity factors K_I and K_{II} at the faying surfaces of a single spot weld joint (Pook 1975). The solutions are displayed below:

$$K_I = \left[\frac{F}{r^{3/2}}\right]\left[0.341\left(\frac{r}{t}\right)^{0.397}\right], \tag{2.3}$$

$$K_{II} = \left[\frac{F}{r^{3/2}}\right]\left[0.282 + 0.162\left(\frac{r}{t}\right)^{0.710}\right], \tag{2.4}$$

where

K_I = Mode I stress intensity factor (N/mm$^{3/2}$),

K_{II} = Mode II stress intensity factor (N/mm$^{3/2}$),

F = Applied Force (N),

r = Nugget radius (mm),

t = Sheet thickness (mm).

A study also derived the stress intensity factor using local structural stresses for spot weld joints of equal thickness (Radaj et al., 1991, 1992). The solutions are shown below:

$$K_I = \left[0.58\sigma_b^{++} + 2.23\tau_{\perp}^{+-} \right]\sqrt{t}, \tag{2.5}$$

$$K_{II} = \left[0.50\sigma^{+-} + 0.50\sigma_b^{+-} + 0.55\tau_{\perp}^{++} \right]\sqrt{t}, \tag{2.6}$$

$$K_{III} = \left[1.41\tau_{\parallel}^{+-} \right]\sqrt{t}, \tag{2.7}$$

where

K_{III} = Mode III stress intensity factor (N/mm$^{3/2}$),

σ_b^{+-} = Antisymmetrical radial bending stress (N/mm^2),

σ_b^{++} = Symmetrical radial bending stress (N/mm^2),

σ^{+-} = Antisymmetrical radial membrane stress (N/mm^2),

$\tau_{\perp}^{++}$ = Symmetrical transverse shear stress (N/mm^2),

$\tau_{\perp}^{+-}$ = Antisymmetrical transverse shear stress (N/mm^2),

$\tau_{\parallel}^{+-}$ = Antisymmetrical longitudinal shear stress (N/mm^2),

The approach involving local structural stresses also included a calculation for an equivalent stress intensity factor which calculated the combined effect of the three individual stress intensity factors, as shown below:

$$K_{eq} = \sqrt{K_I^2 + K_{II}^2 + K_{III}^2}, \tag{2.8}$$

where

K_{eq} = Equivalent stress intensity factor.

Zhang later developed stress intensity factor calculations for tensile shear lap specimens and compared the results of his equation to that of previously developed equations (Zhang 1997, Zhang 1998, Zhang 2001). The equations he derived are shown below:

$$K_I = \frac{\sqrt{3}F}{2\pi b\sqrt{t}}, \tag{2.9}$$

$$K_{II} = \frac{2F}{\pi b\sqrt{t}}, \tag{2.10}$$

$$K_{III} = \frac{\sqrt{2}F}{\pi b\sqrt{t}}, \tag{2.11}$$

where

F = Applied Force (N),

b = Nugget diameter (mm),

t = sheet thickness (mm).

The solutions presented by Zhang were developed as closed form solutions for a circular rigid inclusion in a plate. These solutions are valid for thin sheets with the nugget diameter distinctly larger than the sheet thickness. A similar form of equivalent stress intensity may also be used in combination with this form of the stress intensity factor calculations.

Studies have also been conducted using finite element analysis (Pan et al. 2002). In this study shear lap specimen geometry was used to establish a critical local stress intensity factor. The crack shape used for this study was elliptical and and emanated from the main notch of the shear lap specimen.

A fracture mechanics study of the geometry produced in each of the weld configurations was applied to the fatigue data in the previously mentioned study by Rathbun et al. and suggests that for the low load, high cycle fatigue regime, the spot weld fatigue life is dominated by the geometry, with no significant effect by the microstructure, or material strength. The Rathbun et al. study suggests that during the weld process an initial "precrack" is imparted to the sample geometry. This initial "precrack" initiates the fatigue crack and the fatigue life of the specimen is spent entirely in the crack propagation phase.

During stable crack growth the stress intensity is described by a Paris law function, with material constants C and m. The Paris law of sub-critical crack growth is displayed below:

$$\frac{da}{dN} = C\Delta K^m \quad , \tag{6.3}$$

where

$$\frac{da}{dN} = \text{crack growth rate} \left(\frac{mm}{cycle} \right),$$

C = material constant,

m = material constant,

ΔK = Stress Intensity Range (MPa$\sqrt{}$m).

Barsom and Rolfe showed that these constants were only dependent on microstructure type, and independent of microstructure strength (Barsom and Rolfe, 1999). This behavior is similar to that observed for the high cycle fatigue testing in this study.

This study suggests that the local crack tip microstructure dominates the fatigue crack growth behavior of the steels. This study also implies that the sample geometry due to welding, dictates the fatigue behavior of the steels in the high cycle regime, at least to a larger extent than any other individual factor.

In summary, this literature review has indicated the following:

1. DP and TRIP steels are types of steels that are created using an intercritical heat treatment, with the TRIP steels also undergoing an isothermal transformation. These

steels are both continuous yielding and have unique work hardening properties that make them advantageous for use in sheet steel structures.

2. Several observations can be made about the spot weld geometry in relation to the fatigue life. A thicker sheet base material will increase the fatigue life of the joint. Increasing the nugget size and the base material strength tend to increase the fatigue life in the low cycle regime; however, the effect is negligible in the high cycle fatigue regime.

3. Interfacial failure of DP steel joints has been found to be related to welding parameters, and more prevalent in the low cycle fatigue regime as well as in joints using base material of higher strength. The interfacial failure of DP steels has been modeled by the empirical equation produced by Marya.

4. Interfacial failure of TRIP steels has also been found to be associated with welding parameters, including small nugget size with thicker sections. The occurrence of interfacial fracture of TRIP steels also increases in the low cycle regime.

5. *In-situ* weld tempering has been found to be capable of producing many different HAZ hardness values. Weld tempering has been used as a method to increase the strength of the spot weld joint; however, this has method will not completely alleviate the problem of interfacial failure.

6. Several fracture mechanics studies have been undertaken with relation to the spot weld geometry. Most notably the stress intensity factor solutions for the spot weld have been introduced by Zhang. Other studies indicate that the welding process imparts a "precrack" into the joint geometry and the entire fatigue life of the joint is effectively spent in crack propagation.

This review of the available literature guides the current study to compare the high cycle fatigue behavior of AHSS spot weld joints. Interfacial failure of TRIP 780 will be explored by varying the effect of squeeze force and current on the occurrence of interfacial failure during shear lap tensile tests. Altering the weld current and/or squeeze force will likely result in not only a change to the strength of the spot weld joint but also the occurrence of interfacial failure.

In this study the dependence of the microstructure on the high cycle fatigue life of the AHSS steels, specifically the TRIP steel will be investigated. The weld schedule will be altered to produce a spot weld in the shear lap configuration that achieves good strength, good fatigue life, and minimizes the occurrence of interfacial fracture. The results obtained from the fatigue testing performed can then be used in combination with a stress intensity solution in an attempt to normalize the results for the varying material geometries and forces used for the different materials. This study will show that a similar fatigue life is observed for all sets of data. Using a fracture mechanics approach to life prediction a conservative model for predicting the high cycle fatigue life of the spot weld joints will be developed.

Chapter 3

Base Material Examination

This chapter will discuss the steps undertaken to establish material properties and chemistry for the three types of steel utilized in this study, DP 980, DP 780, and TRIP 780. The sheet steel used for this study was graciously supplied by Arcelor Mittal Steel, East Chicago, Indiana. The three types of steel used for this study are as follows:

- DP 980
- DP 780
- TRIP 780

The letters reference the type of steel while the numbers associated with each steel are a reference to the tensile strength, in MPa, of the specific chemistry (i.e. DP 980 is a dual phase steel with a tensile strength of 980 MPa).

3.1 Chemical Analysis of Base Material

A chemical analysis of the steels was provided upon reception from the supplier; the major alloying elements of each chemistry for the steels are listed in Table III.1.

Table III.1. Major alloying elements of each chemistry, information provided with as-received material (Hou, 2008)

Material	Element (wt%)		
	C	Mn	Si
DP 980	0.10	2.14	0.68
DP 780	0.10	1.76	0.31
TRIP 780	0.21	1.74	0.06

3.2 Tensile Testing of Base Material

Tensile testing was performed on the as-received material to provide data regarding the monotonic material properties. This testing was conducted following the guidelines of ASTM E-8. Samples were machined from the as-received sheet steel; the geometry of the tensile samples is shown in Figure 3.1. Three samples of each base material were tested. A MTS servo-hydraulic test frame was used in combination with MTS Multitpurpose TestWare version 3.5B to perform the tensile tests. The accuracy of the load cell used for the tensile testing in this study is +/- 11 N. The bias of the load cell used for this study was computed to be less than 1%. The precision of the measured values is reported as the coefficient of variation in Table III.2.

Table III.2. Average tensile strength for each material tested

Material	Average UTS (MPa)	Coefficient of Variation
DP 980	1,046	2.9%
DP 780	803	0.1%
TRIP 780	806	1.7%

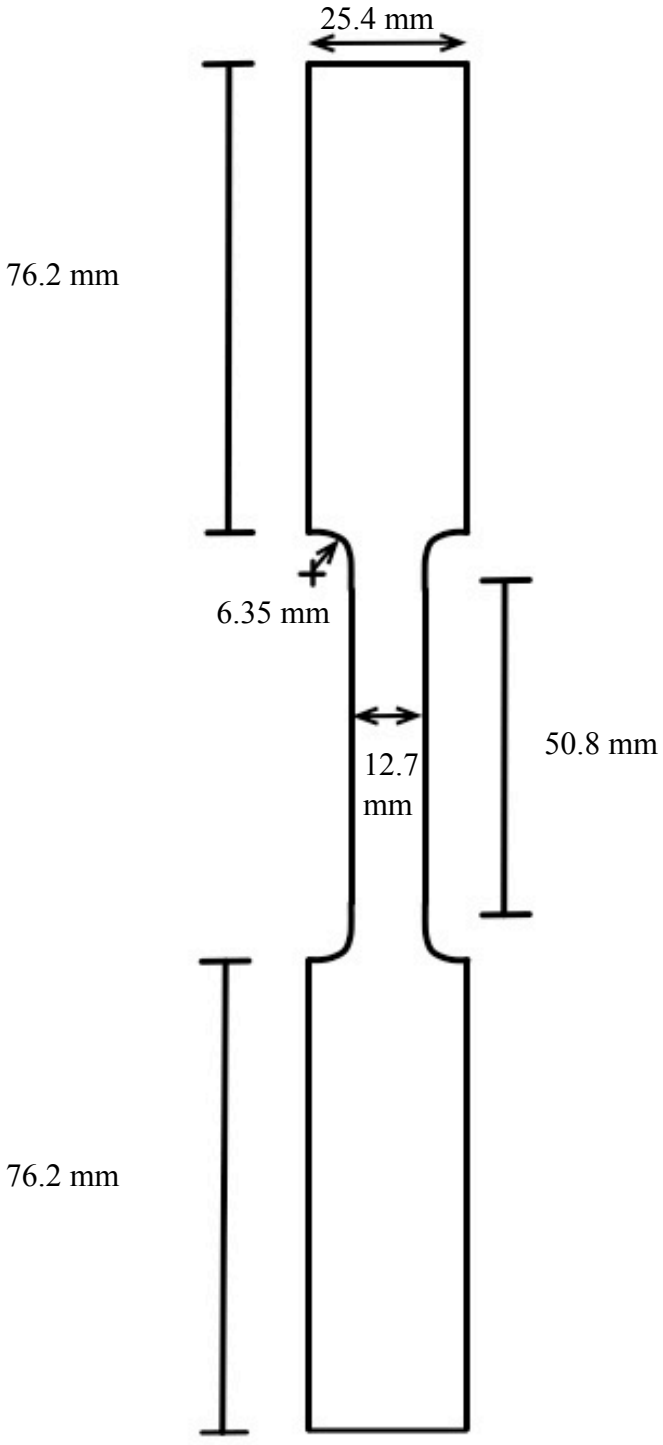

Figure 3.1 Tensile sample geometry

3.3 Fatigue Testing of Base Material

Fatigue testing of each of the base material chemistries was performed to characterize the nominal fatigue life of the steel. An MTS servo-hydraulic piston was utilized in coordination with a specially fabricated test frame to test the steel samples.

Prior to beginning the fatigue testing the test frame crosshead and grip assembly was aligned using a strain gaged sample. Twelve separate strain gages were affixed to a dog bone sample and monitored using Vishay P3 strain indicators. The frame and grip assembly was continually adjusted in an attempt to drive all of the strain readings to a similar value. This adjustment was repeated until all strain gages on the test sample were within an acceptable range of strain, approximately +/- 25 με, under a load of approximately 11,125 N (approximately half of the capacity of the frame). An image of the experimental setup can be found in Figure 3.2. The accuracy of the load cell used for the fatigue testing in this study is +/- 11 N. The bias of the load cell used for this study was computed to be less than 1%.

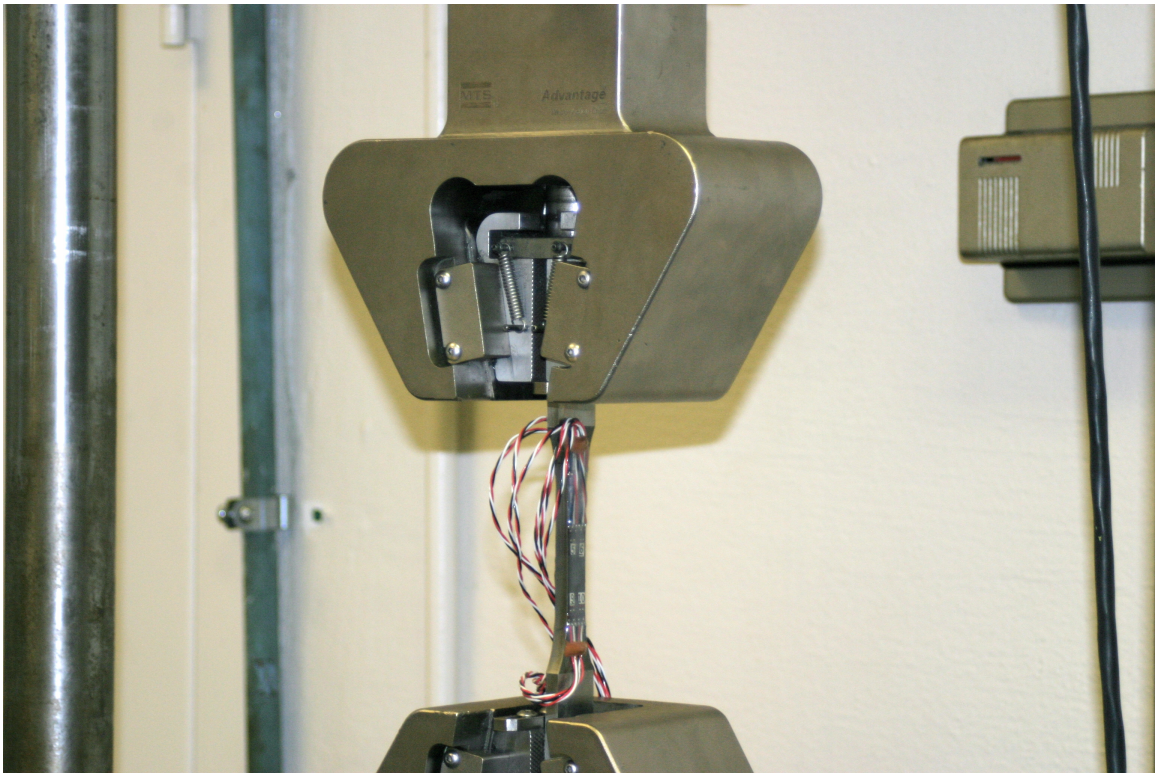

Figure 3.2 Photograph displaying strain gaged sample used for alignment of test frame

Each fatigue sample was machined in accordance to ASTM E466 Standard Practice for Conducting Constant Amplitude Axial Fatigue Tests of Metallic Specimens (ASTM E466). An example of the specimen geometry is shown in Figure 3.3. The samples were also ground to a 600 grit finish in the area of the reduced cross section to mitigate the effect of surface scratches. The testing procedure utilized was also in accordance with ASTM E466.

An MTS 407 controller was used to program a sinusoidal wave function for controlling the constant amplitude load signal. All calculations made with respect to calculating the loads used for the fatigue testing were made based on the aforementioned uniaxial tensile test data. The fatigue testing was conducted using stress based approximations of 90%, 80%, 70%, 65%, and 60% of the ultimate strength of the material. All fatigue testing was performed with an R-Ratio of 0.1 (R is the ratio of the maximum applied load to the minimum applied load) on servo-hydraulic testing machines in load control and a frequency of approximately 10 Hz. Three samples of each chemistry were tested at each load range, for a total of 15 samples. ASTM E739 was used as a guideline for choosing the sample population (ASTM E739). Failure of the samples was judged to be complete fracture of the specimen. An image of the fatigue testing apparatus is displayed as Figure 3.4.

Following the fatigue testing the results were plotted on a log - log coordinate system to develop conventional stress range proportional to the UTS versus cycles to failure plots (S-N curves) for each material. Figures 3.5 - 3.7 display the stress range versus cycles results of the fatigue testing for the DP 980, DP, 780 and TRIP 780 materials, respectively.

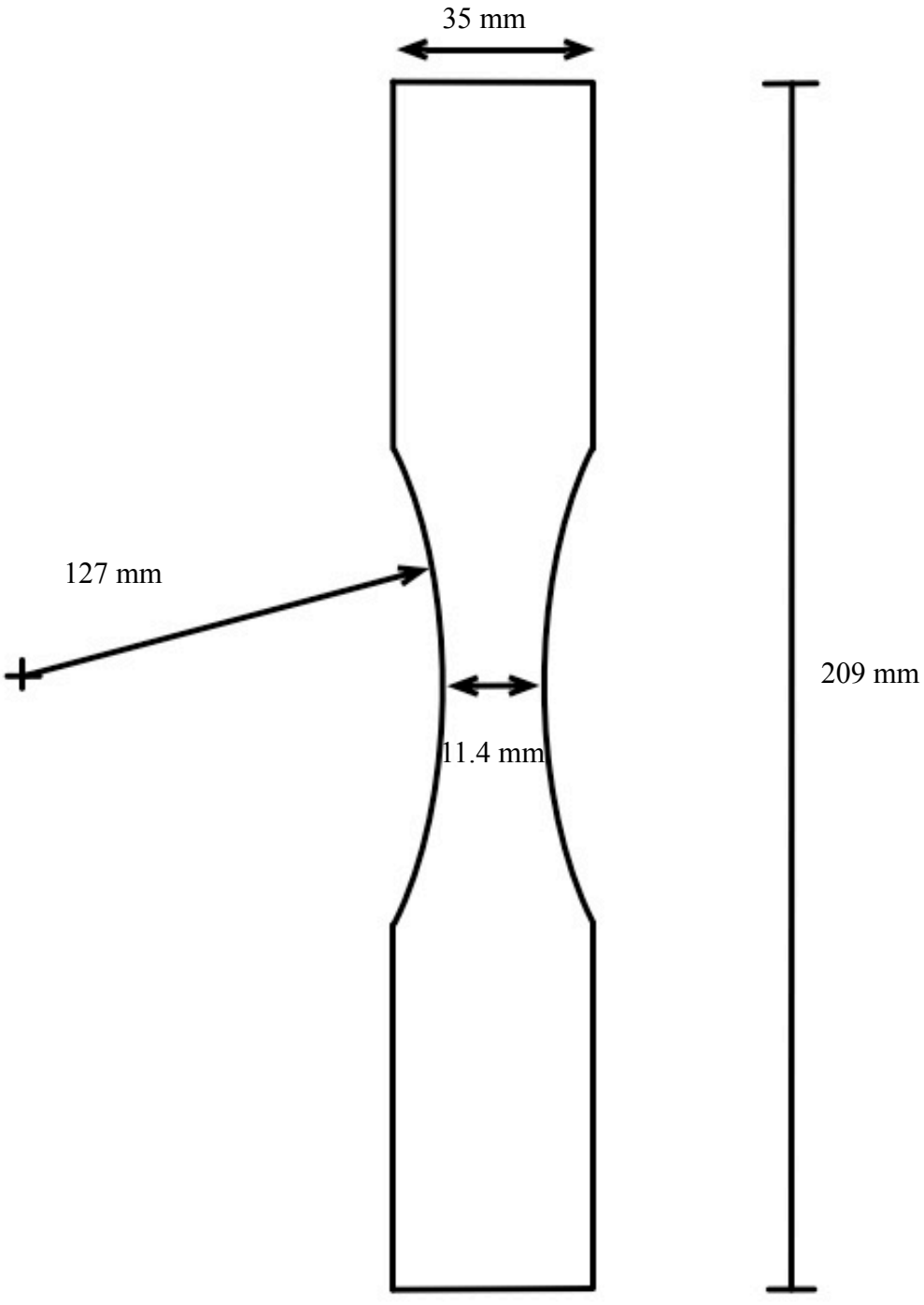

Figure 3.3 Fatigue specimen geometry

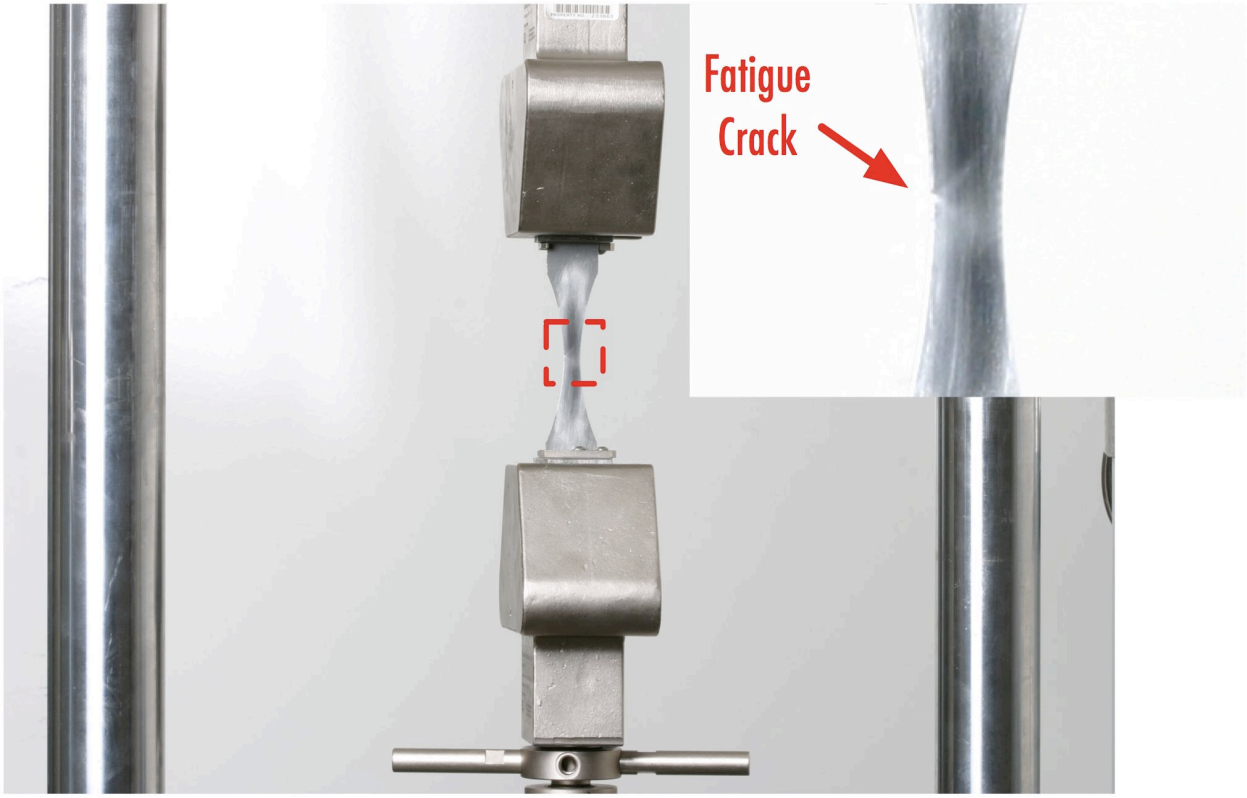

Figure 3.4 Photograph displaying sample during fatigue test

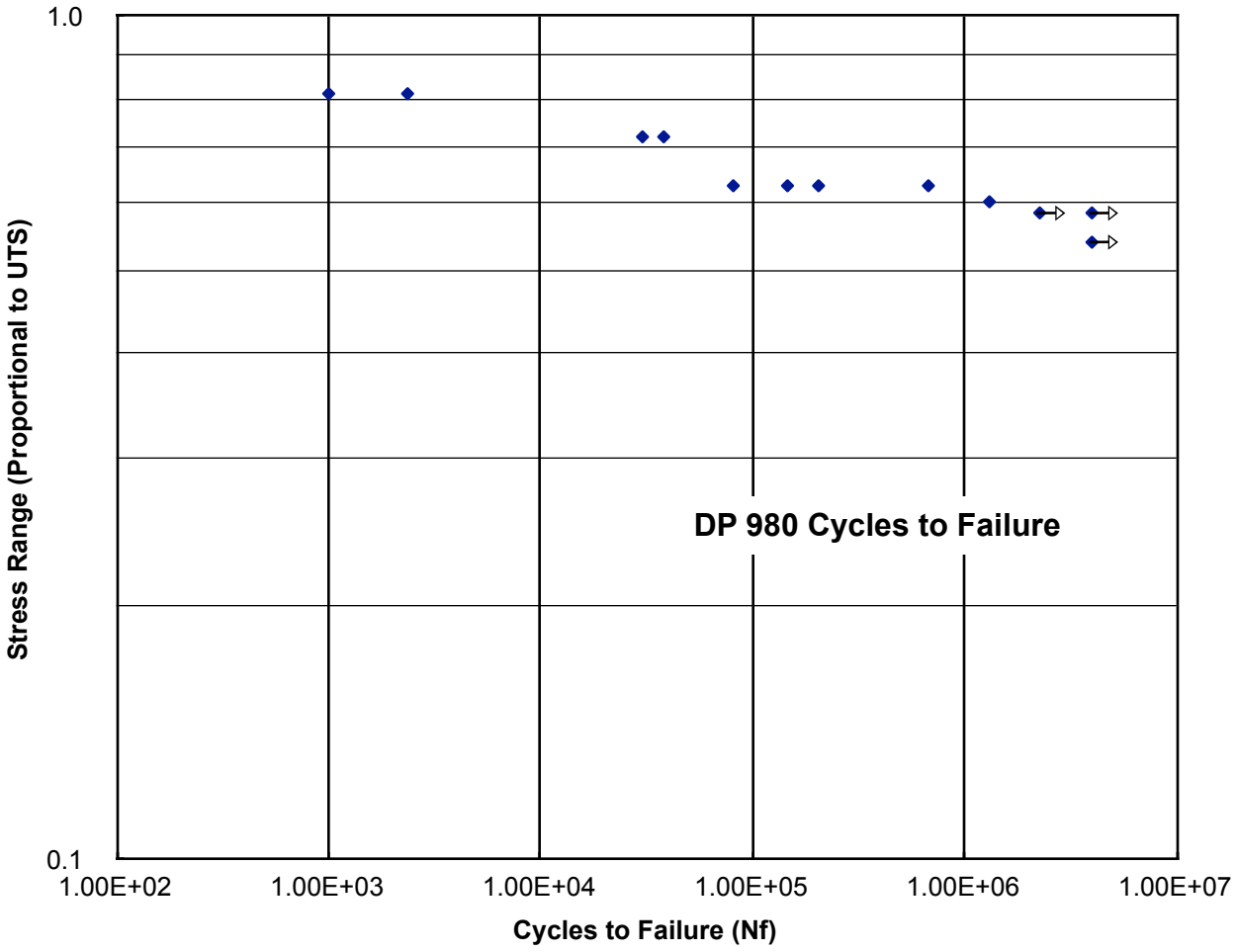

Figure 3.5 S-N curve for DP 980

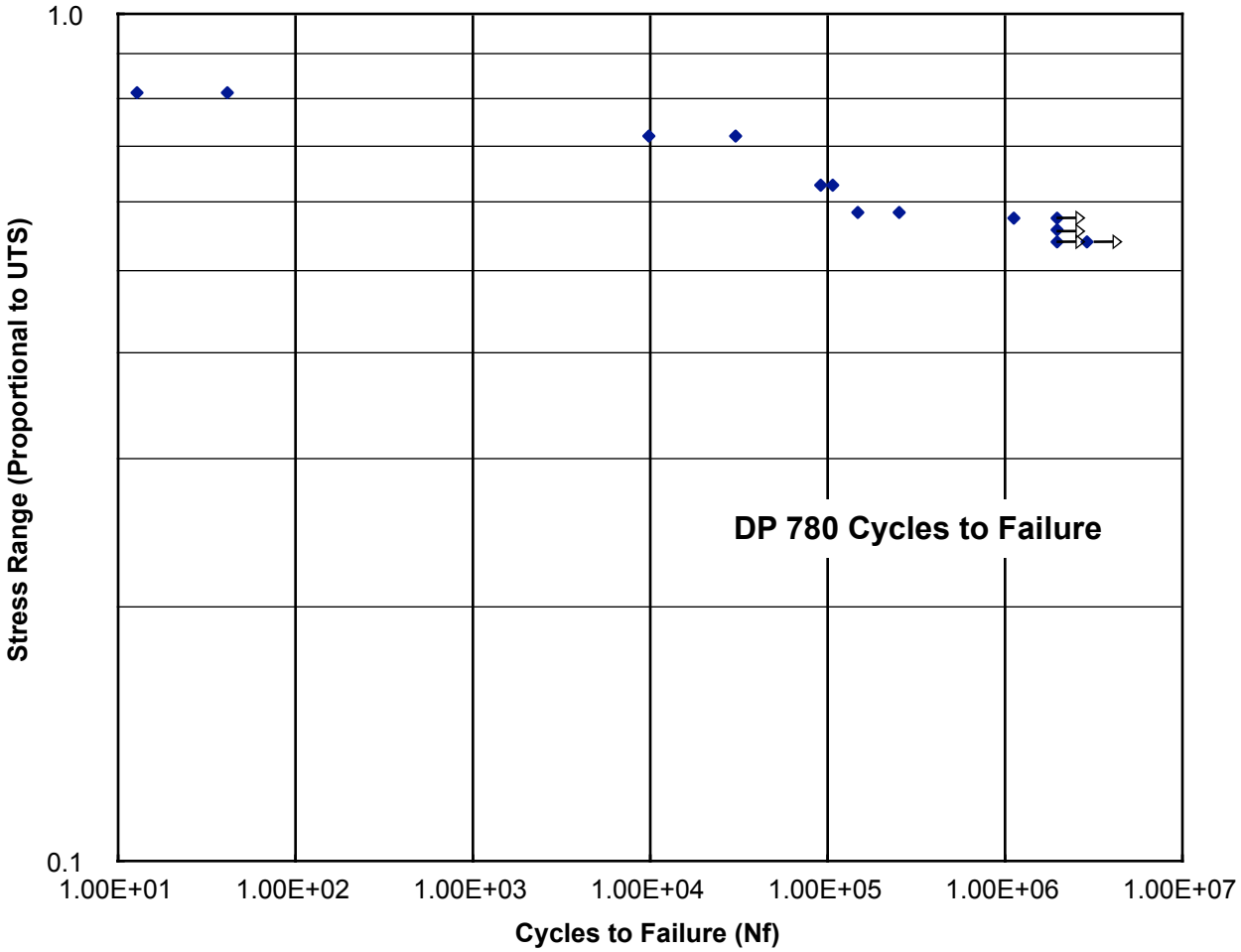

Figure 3.6 S-N curve for DP 780

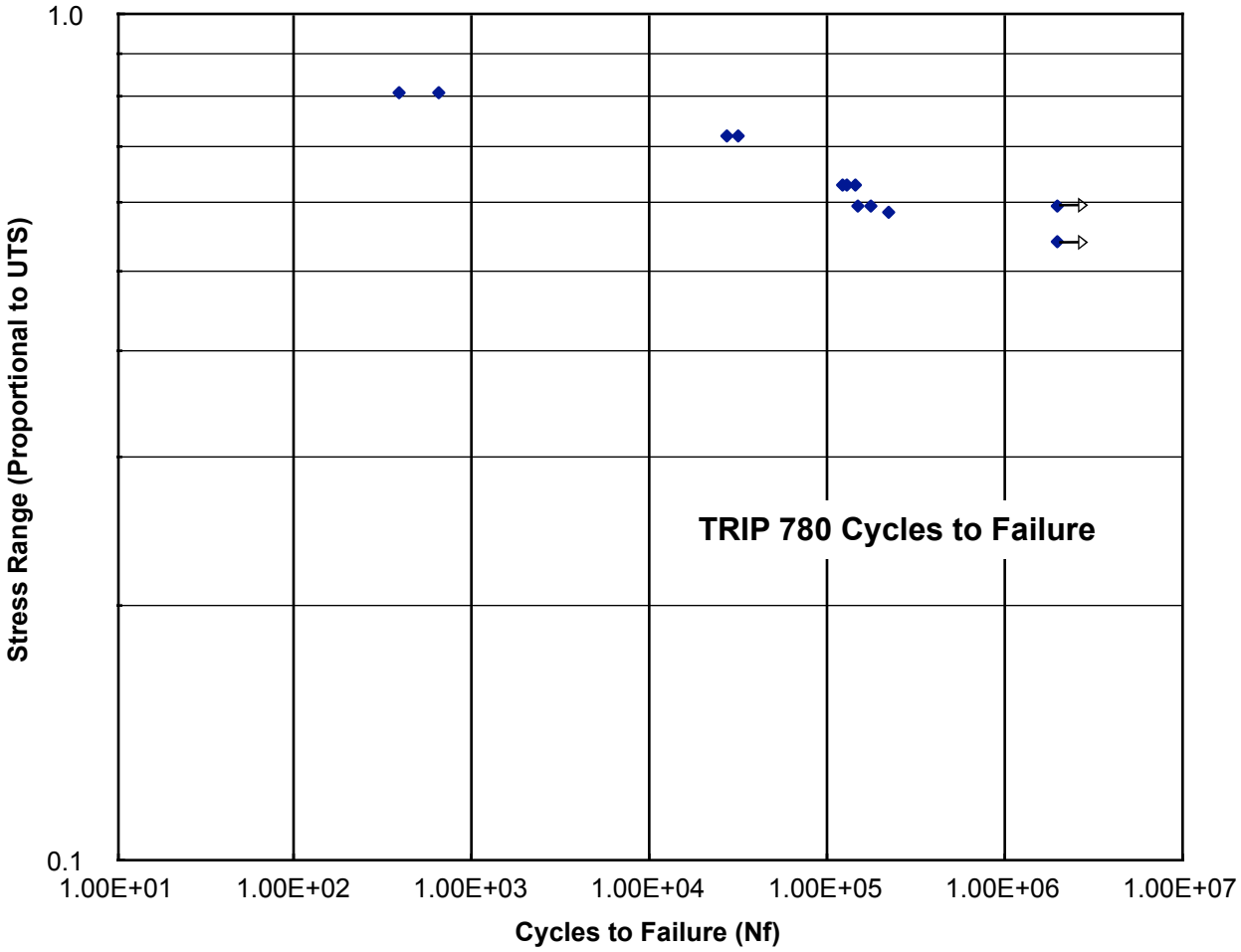

Figure 3.7 S-N curve for TRIP 780

3.4 Metallographic Inspection of Base Material

A sample of each type of steel was sectioned to produce metallographic specimens. All specimens were sectioned transverse to the rolling direction of the steel. The samples were prepared using a Struers LaboPress-3 hot mounting press; the samples were mounted in black phenolic. The samples were mounted to allow the transverse (through thickness) direction to be examined. An Allied M-Prep 3 polisher was used to grind and polish the samples. The samples were prepared following standard metallographic procedures outlined in ASTM E3 Standard Guide for Preparation of Metallographic Specimens (ASTM E3).

After preparation the samples were examined using a Nikon inverted light microscope. Prior to inspection the samples were etched using a 4% Nital solution (ASM Handbook Volume 9). A representative micrograph of each chemistry is displayed in Figures 3.8 - 3.10.

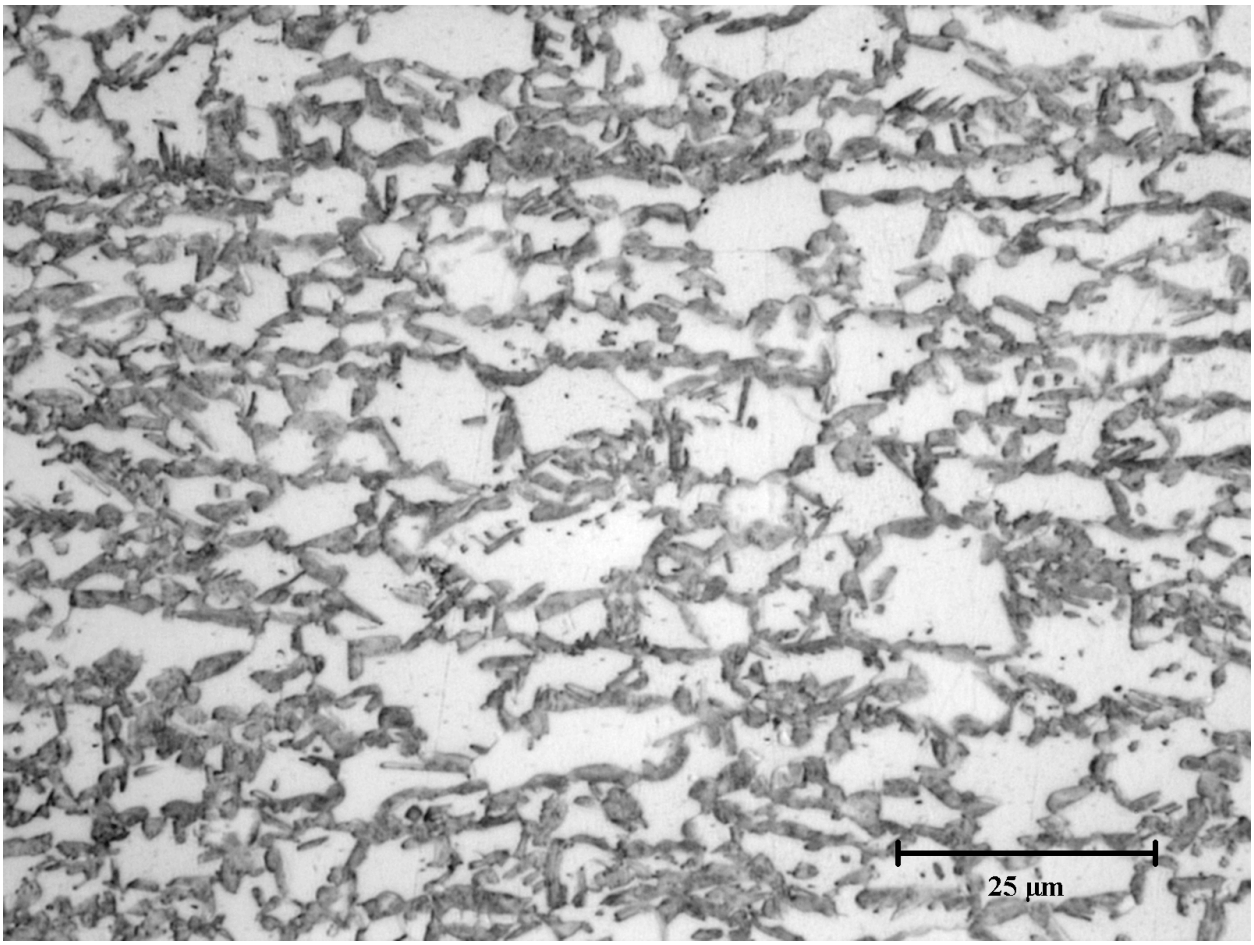

Figure 3.8 Image of DP 980 base material, Etchant 4% Nital

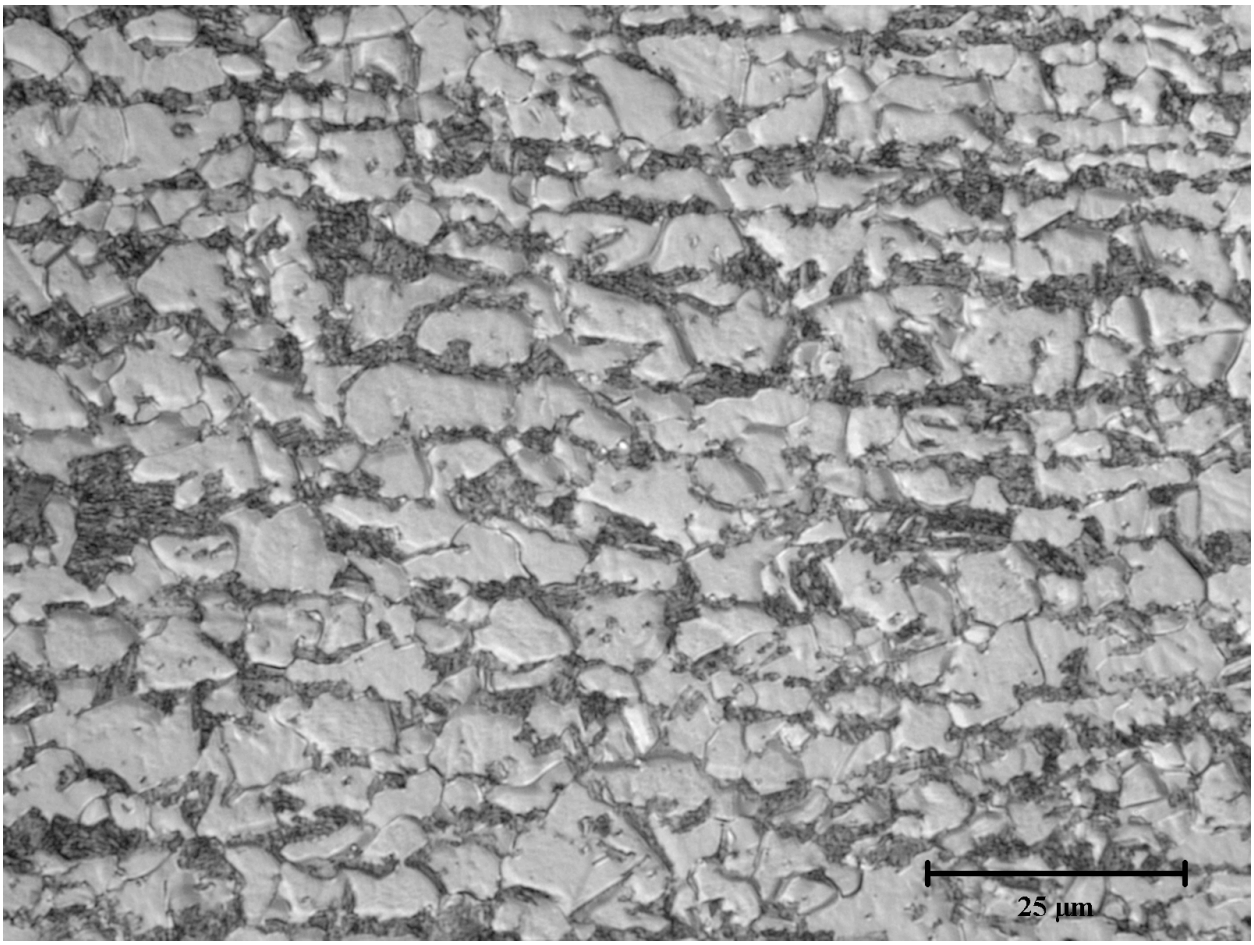

Figure 3.9 Image of DP 780 base material, Etchant 4% Nital

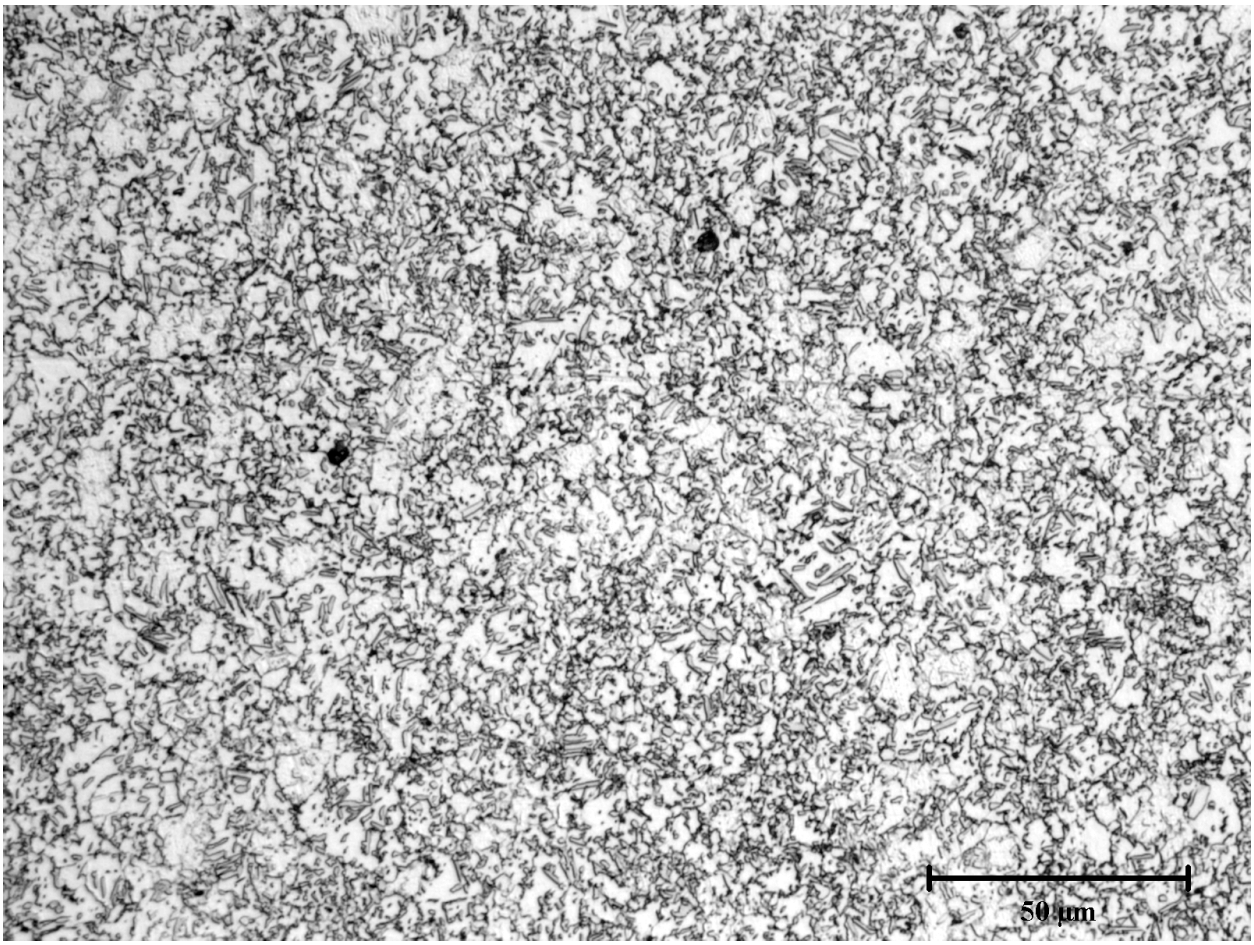

Figure 3.10 Image of TRIP 780 base material, Etchant 4% Nital

Figure 3.8 displays the microstructure of the DP 980 material. It is apparent that the steel consists primarily of martensite in ferrite matrix. Figure 3.9 displays the microstructure of the DP 780 material which is also comprised primarily of martensite in ferrite matrix. The martensite appears to be dispersed more finely and with greater uniformity in the DP 980 as opposed to the DP 780 material; this would contribute to the higher tensile strength exhibited by the DP 980 material.

Figure 3.10 displays the microstructure of the TRIP 780 material. This material consisted primarily of bainite and retained austenite in a ferrite matrix.

Chapter 4

Development of Spot Weld Specimen

This chapter will discuss the steps performed to establish suitable specimen geometry and welding schedule for the subject materials.

4.1 Overview of Spot Weld Joint

The basic process to produce a spot weld is to overlap two pieces of sheet material and bring electrodes into contact with the sheets. As a large current flows through the electrodes, the large electrical resistance at the sheet interface creates a molten metal zone that will become the weld nugget. This process is shown schematically in Figure 4.1, and an example of the resulting welded joint is shown in Figure 4.2.

The initial portion of this investigation will focus on identifying potential weld schedule parameters that will result in a variety of weld strengths and HAZ microstructures. The weld parameters used are based upon information in the literature as well as some alternative welding procedures. Typical weld parameters include the electrode force or tip pressure, current (known as heat), and weld time. Additionally, water cooled electrodes can be used to control the quenching rate, and the hold or squeeze time of the electrodes after the weld can affect weld

strength and microstructure. Approximately 10 conditions were explored with all weld schedules and quenching parameters resulting in differing HAZ microstructures, hardness, and strength for the TRIP steels. Several of these variations of heat treatment and their respective effects on the welds strength, HAZ hardness, failure mode, etc. have been discussed in previous chapters.

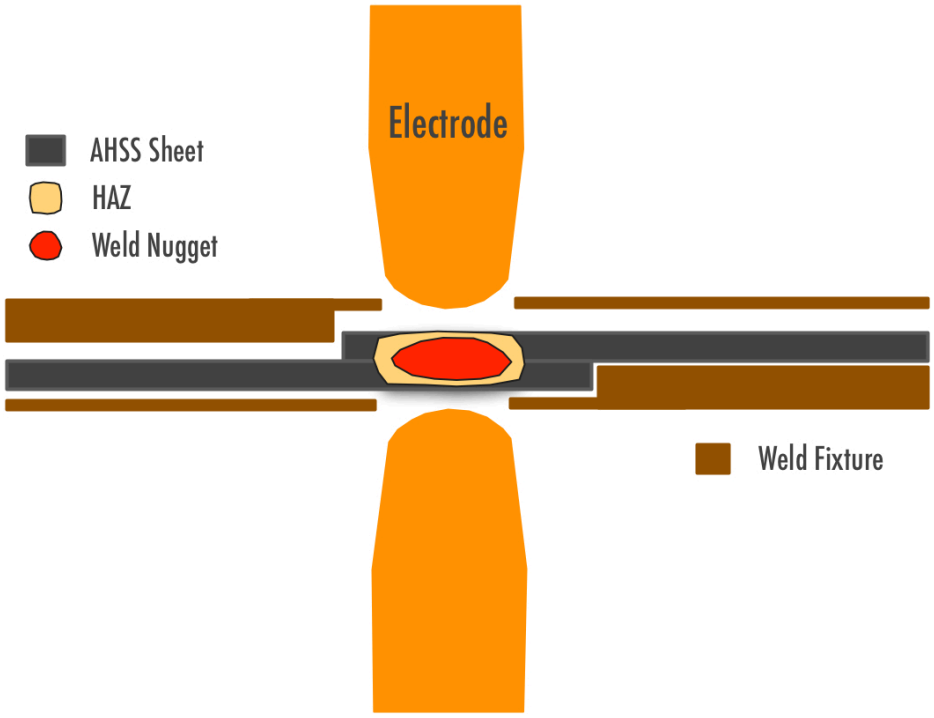

Figure 4.1: Spot weld lap joint schematic

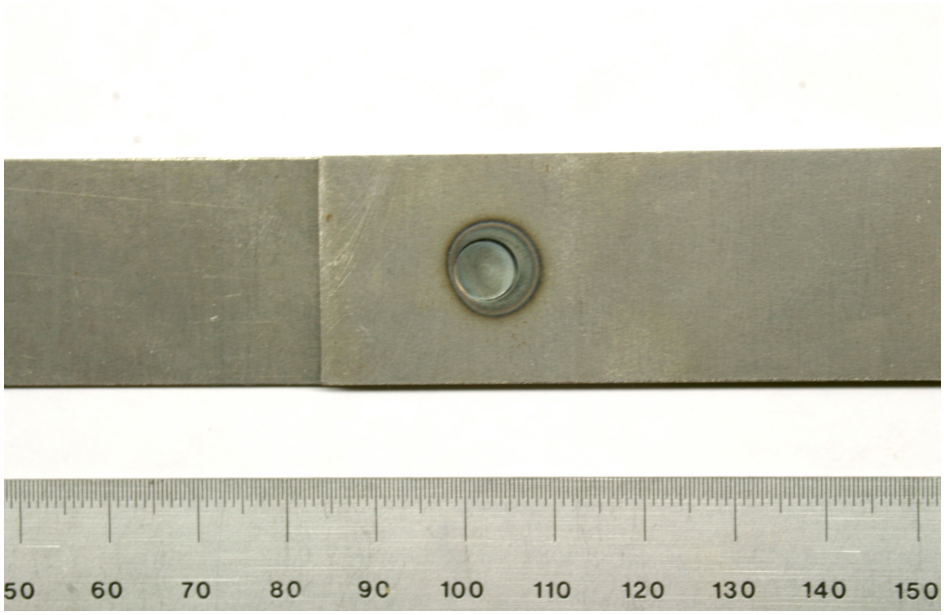

Figure 4.2: Representative spot weld (scale in mm)

4.2 Tensile Shear Lap Specimen

All welds produced for this study were single weld tensile shear lap specimens. The shear lap specimen is made by overlapping two coupons of the material and performing a spot weld on the section of the overlap. The dimensions of the coupon used for this study is shown in Figure 4.3 and follows the AWS test specification D8.9 "Recommended practices for test methods for evaluating the resistance spot welding behavior of automotive sheet steel materials" (AWS D8.9 2002). A shear lap specimen following the weld process is shown in Figure 4.4. The shear lap specimens defined in this section were used for both weld strength testing and fatigue testing of the weld joint. Prior to welding the shear lap joint all coupons were cleaned and wiped to remove surface debris as well as surface oils.

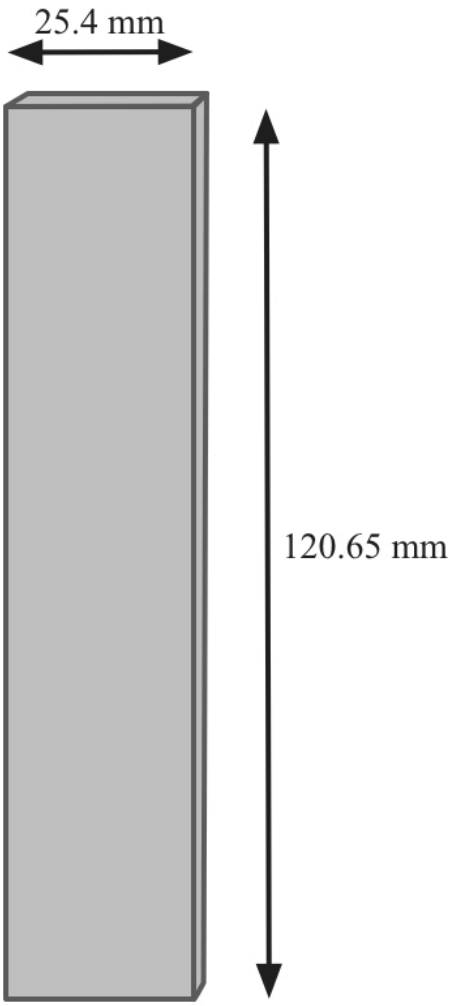

Figure 4.3 Dimensions of weld coupon, thickness is determined by as-received sheet

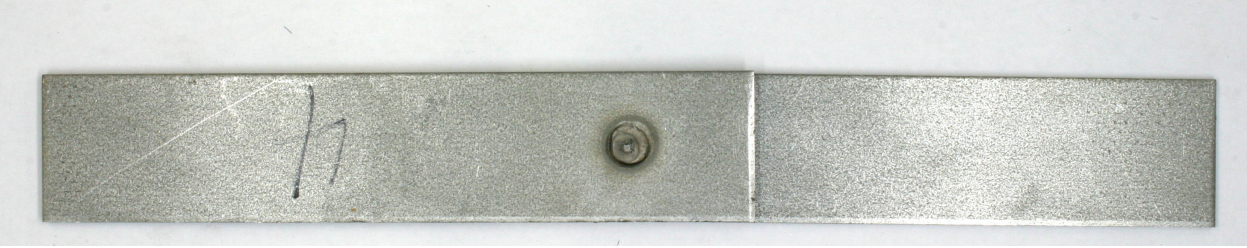

Figure 4.4 Shear lap specimen

4.3 Development of Weld Schedule

Weld schedules used for the AHSS were developed by first considering weld schedules found in the literature (Matlock 2003, Yan 2001, Kang 1997) and from the steel supplier. The goal of the weld schedule was to produce adequate strength for the joint while maintaining a consistent failure mode, namely a method to avoid interfacial failure of the steel, specifically with respect to the TRIP steel.

All spot welds produced in this study were made using a Thompson Standard Press-Type Resistance Welder. The electrodes used for all spot welds had a nominal diameter of 7.25 mm. Figure 4.5 displays an image of the resistance spot welder used for this study. The shear lap specimens created for this study were placed into a welding fixture fabricated for this welder for the express purpose of producing shear lap specimens and to insure manufacturing repeatability. Figure 4.5 displays a photograph of the weld fixture in place on the test frame and a zoomed view of the section of the fixture designed to hold the workpiece.

Several of the known weld schedules were used to develop a set of parameters used in the final weld schedule for all materials. Many parameters used in the automated welding process were not altered when considering a weld procedure and values available in the literature were used. The main parameters varied for this study included, weld force, average weld current, and the number of weld pulses performed.

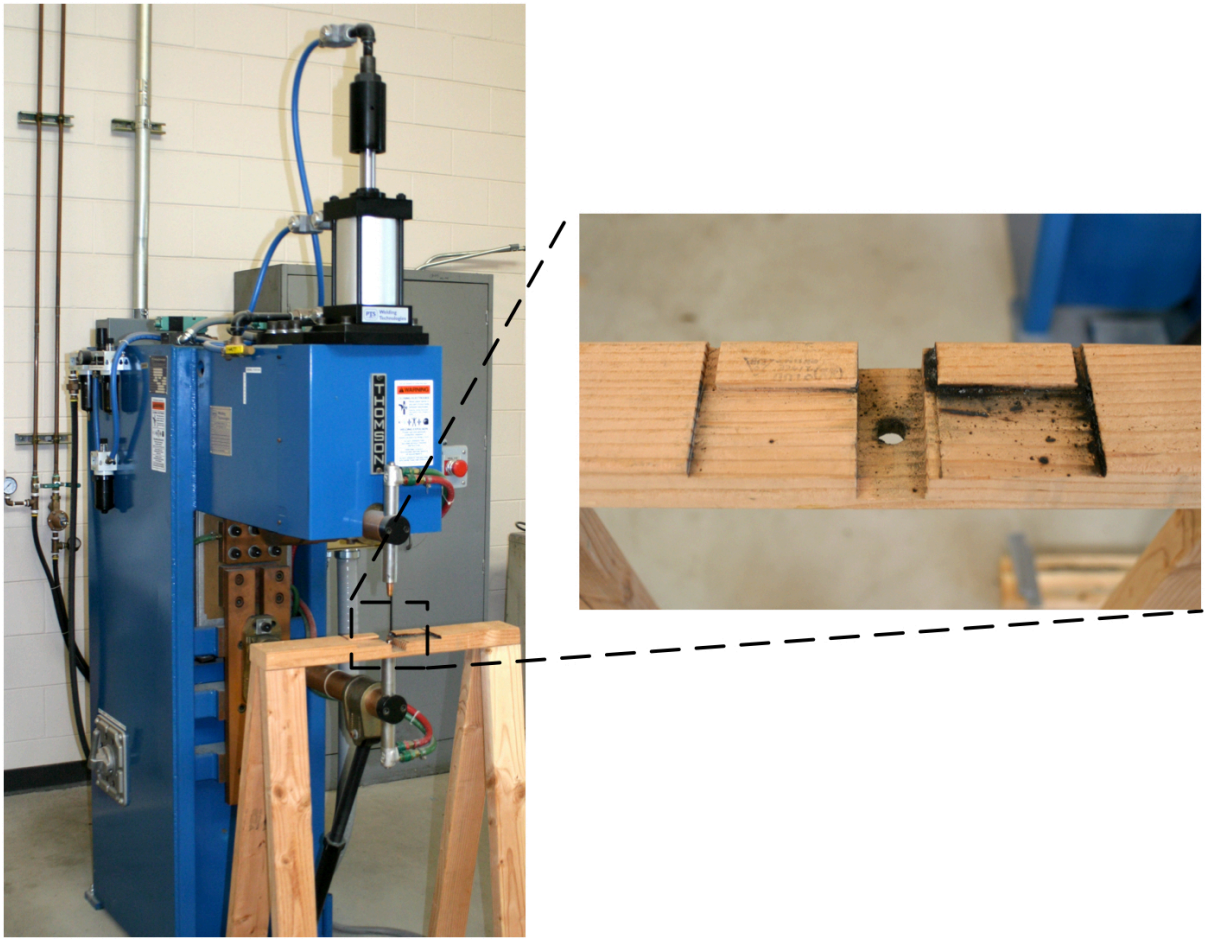

Figure 4.5 Photograph of the weld fixture in place on the test frame in addition to a zoomed view of the section of the fixture designed to hold the workpiece

To determine the effectiveness of the welding procedure, tensile shear specimens were created and a weld strength test was performed. The weld strength test is performed in a similar manner as a uniaxial tensile test; however, the test specimen has the geometry of the shear lap specimen rather than a standard "dogbone" type specimen. A 44 kN capacity screw driven Tinius Olsen frame was used to perform the weld strength tests. For the weld strength test the load applied to the sample was increased until failure of the weld joint. Failure of the weld joint was determined to be complete separation of the weld joint or the inability of the joint to support 30% of the maximum test load. The load applied to the sample increases as a function of the test frame crosshead travel; the rate of travel used for all weld strength tests was 2.54 mm/min.

For the DP steels several known weld schedules were found in the literature and used as a basis for the weld schedule outlined in this study. The average nugget diameter produced for the DP 980 and the DP 780 steel was approximately 8 mm. The values for the nugget diameter were determined from measurements conducted during the metallographic examination which is detailed in Chapter 5, a total of 3 samples for each chemistry were measured. For the DP 980 samples the average current used ranged from 9.5 - 10.4 kA. For the DP 780 samples the average current used ranged from 9.2 - 9.6 kA. The remaining weld schedule used for the dual phase steels is further outlined in Table IV.1.

The weld schedule for the TRIP steel was not found directly from the literature. Information regarding TRIP steels of differing chemistry were found; however, a weld schedule for a TRIP steel of this exact type could not be found. The average weld nugget size produced for the TRIP

steel was 8 mm. The average current used to join the TRIP steel ranged from 8.1 - 8.5 kA. The complete weld schedule used is outlined in Table IV.1, with the weld current omitted as this has been discussed above and will be discussed in detail in the remainder of this chapter.

Table IV.1. Table outlining weld schedules used for the three materials

	Force (N)	Squeeze (cycles)	Weld (cycles)	Cool (cycles)	Off (cycles)	Hold (cycles)
DP 980	5000	90	20	50	50	80
DP 780	6000	90	20	50	50	80
TRIP 780	5000	90	20	50	50	80

4.4 Evaluation of TRIP Weld schedule

Several iterations of the TRIP steel weld schedule were attempted in an effort to avoid interfacial failure under static loading conditions. Interfacial failure of the weld specimen is a failure mode that occurs when the weld specimen fractures completely through the weld nugget, that is to say the fracture does not travel through the base material. Interfacial failure of a shear lap specimen is often characterized by cracking or fracture of the weld specimen in the direction normal to the applied force.

As the name indicates interfacial failure occurs at the interface of the two overlapping sheets, or coupons in the case of the shear lap specimen. Interfacial failure of spot welds is typically associated with a lack of deformation of the joint prior to failure. One of the advantages to using steel, specifically advanced high strength steel, is the excellent work hardening properties of the material, which occur during plastic deformation. Interfacial failures occur through the weld joint at relatively low strains for the structure, which can have a detrimental effect on the structures ability to deform while still supporting load.

In order to determine a weld schedule for the TRIP steel the weld force and the average weld current were varied to produce several different sample sets of shear lap specimens for weld strength tests. Weld samples were created using a weld force ranging from 3500 N - 6000 N and average weld current values of 6.5 kA - 10 kA. Weld strength tests were performed for each shear lap specimen and the resulting tensile strength was recorded. The results of the weld

strength tests as well as the fracture mode recorded for each specimen are displayed in Figure 4.6 and 4.7. Figure 4.6 displays the tensile strength of the spot weld versus the average weld current of the spot weld. Figure 4.7 displays the tensile strength of the spot weld versus the weld force.

Four conclusions can be drawn form the observed data:

1) The weld force used to produce a spot weld in the range of 3500 N - 6000 N does not have an effect on the fracture mode of the specimen if the average current is constant.

2) The average current used to produce a spot weld does effect the fracture mode of the spot weld for several forces. Welds produced with an average weld current of approximately 8 kA, did not experience interfacial failure. Welds produced with an average current in the range between 6.3 kA - 6.7 kA only experienced interfacial failure. Welds produced with an average current in the range 9.3 - 9.9 kA experienced both interfacial failure and nugget pullout.

3) The tensile strength of spot welds that did not experience interfacial failure were not as large as the tensile strengths achieved by some of the welds that did experience both button pullout and interfacial failure.

4) Interfacial failure of spot welded TRIP 780 can be mitigated using a certain range of currents when welding. This appears to come as a tradeoff for sacrificing strength of the joint. Higher values of weld strength were obtainable; however, welds that failed with higher strengths also experienced interfacial failure.

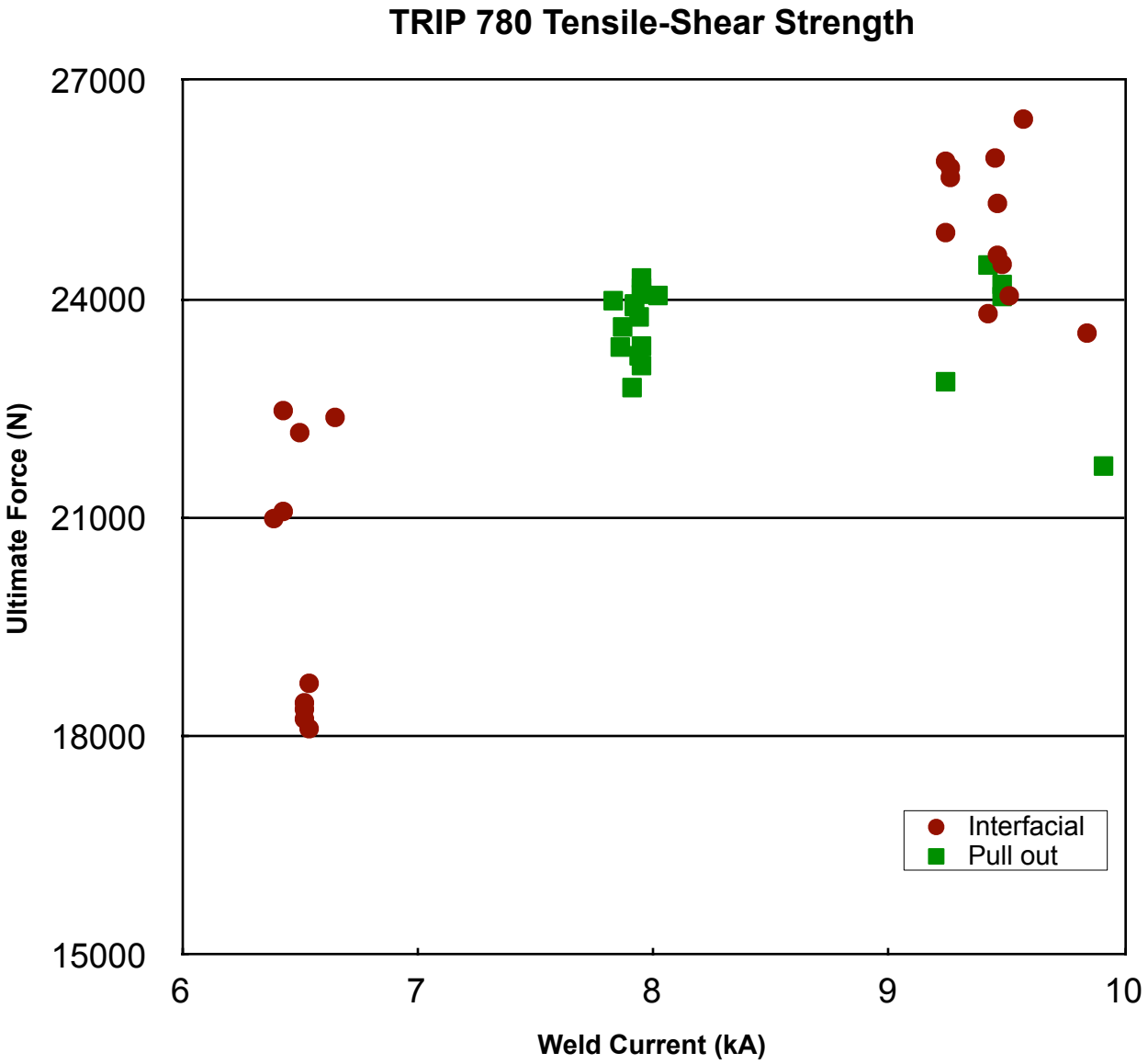

Figure 4.6 Graph displaying the tensile strength of the spot weld versus the average weld current of the spot weld, failure mode also designated

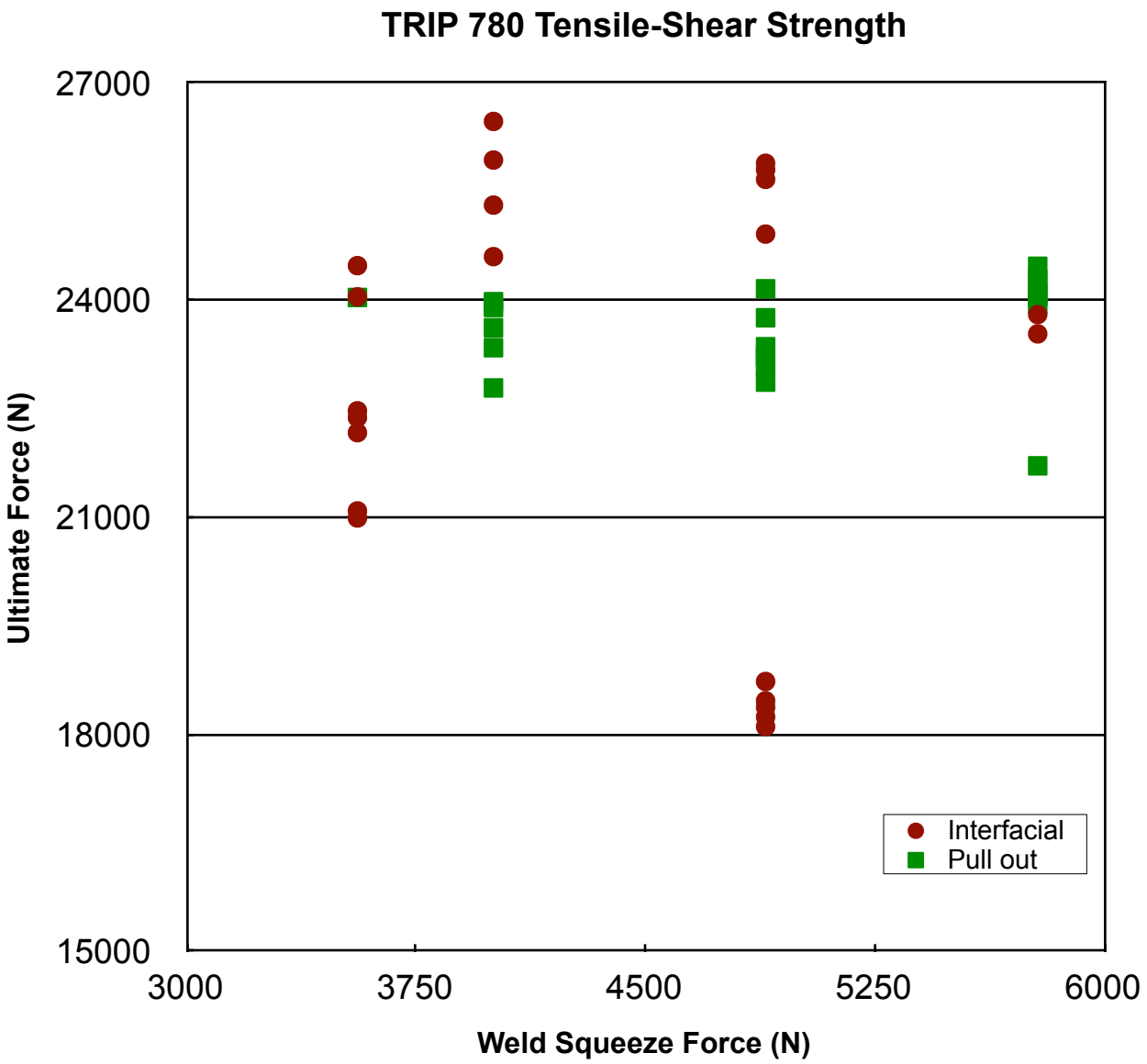

Figure 4.7 Graph displaying the tensile strength of the spot weld versus the weld squeeze force of the spot weld, failure mode also designated

4.5 Fatigue Testing of Spot Welded Joints

Two welding processes for each of the three material types were used during the fatigue testing of the spot welded joints, the welding process and the number of samples tested are described in this section.

Past studies had indicated that interfacial failure was possible in high strength steels in the high cycle fatigue regime. In order to explore the effect of in-situ tempering of the steel with respect to the high cycle fatigue properties two sets of fatigue samples were made for each chemistry of steel, for a total of six sample sets. The weld schedule defined previously for each chemistry was followed for the fatigue specimens; however, one sample set was welded using one pulse of the outlined schedule, while the second sample set was welded using three pulses of the outlined schedule.

The spot welded samples produced for the fatigue testing were welded using the same pedestal spot welder that has been defined earlier in this study and with the same mounting fixture to produce shear lap joints. Fifteen shear lap specimens were produced for each sample set to be tested. Each of the lap joints created was cleaned according to the process outlined previously in this chapter.

The same test frame and fixture as defined earlier in Chapter III, were again used in combination with an MTS 407 controller to program a sinusoidal wave function for controlling the constant

amplitude load signal. All calculations made with respect to the loading used for the fatigue testing were made based on the aforementioned tensile shear lap test data. The fatigue testing was conducted using calculations of 40%, 30%, 25%, 20%, and 15% of maximum stress proportional to the ultimate strength of the weld joint. All fatigue testing was performed with an R-Ratio of 0.1 on servo-hydraulic testing machines in load control and a frequency of approximately 3 Hz. Three samples of each chemistry and of each weld schedule were tested at each load range for a total of 30 samples for each chemistry. ASTM E739 was used as a guideline for choosing the sample population (ASTM E739). Failure of the samples was judged to be complete fracture of the specimen, or a drop in the applied load amplitude of 30%.

Following the fatigue testing the results were plotted on a log - log coordinate system to develop conventional stress range versus Cycles to failure plots (S-N curves) for each material. Figures 4.8 - 4.13 display the results of the fatigue testing for the 2 weld schedules for each chemistry. The fracture mode of the shear lap specimens was also observed with any interfacial failures being recorded.

Figure 4.8 displays a graph that depicts the fatigue life for shear lap spot welded DP 980 using 1 pulse, plotting the stress range versus the cycles to failure of the joint. Figure 4.9 displays a graph that depicts the fatigue life for shear lap spot welded DP 980 using 3 pulses, plotting the stress range versus the cycles to failure of the joint. Figure 4.10 displays a graph that depicts the fatigue life for shear lap spot welded DP 780 using 1 pulse, plotting the stress range versus the cycles to failure of the joint. Figure 4.11 displays a graph that depicts the fatigue life for shear

lap spot welded DP 780 using 3 pulses, plotting the stress range versus the cycles to failure of the joint. Figure 4.12 displays a graph that depicts the fatigue life for shear lap spot welded TRIP 780 using 1 pulse, plotting the stress range versus the cycles to failure of the joint. Figure 4.13 displays a graph that depicts the fatigue life for shear lap spot welded TRIP 780 using 3 pulses, plotting the stress range versus the cycles to failure of the joint.

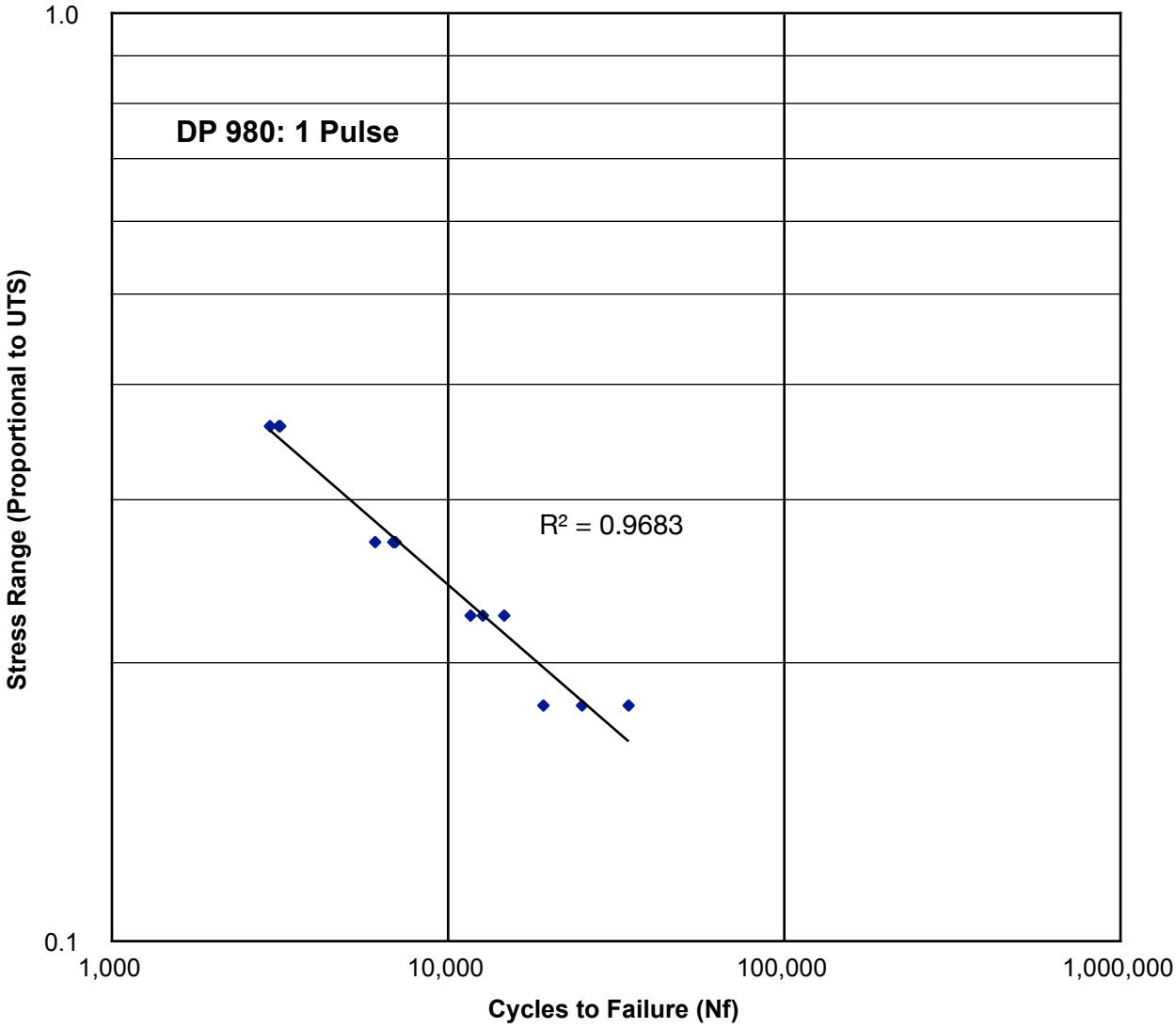

Figure 4.8 Fatigue life diagram for shear lap spot welded DP 980 using 1 pulse

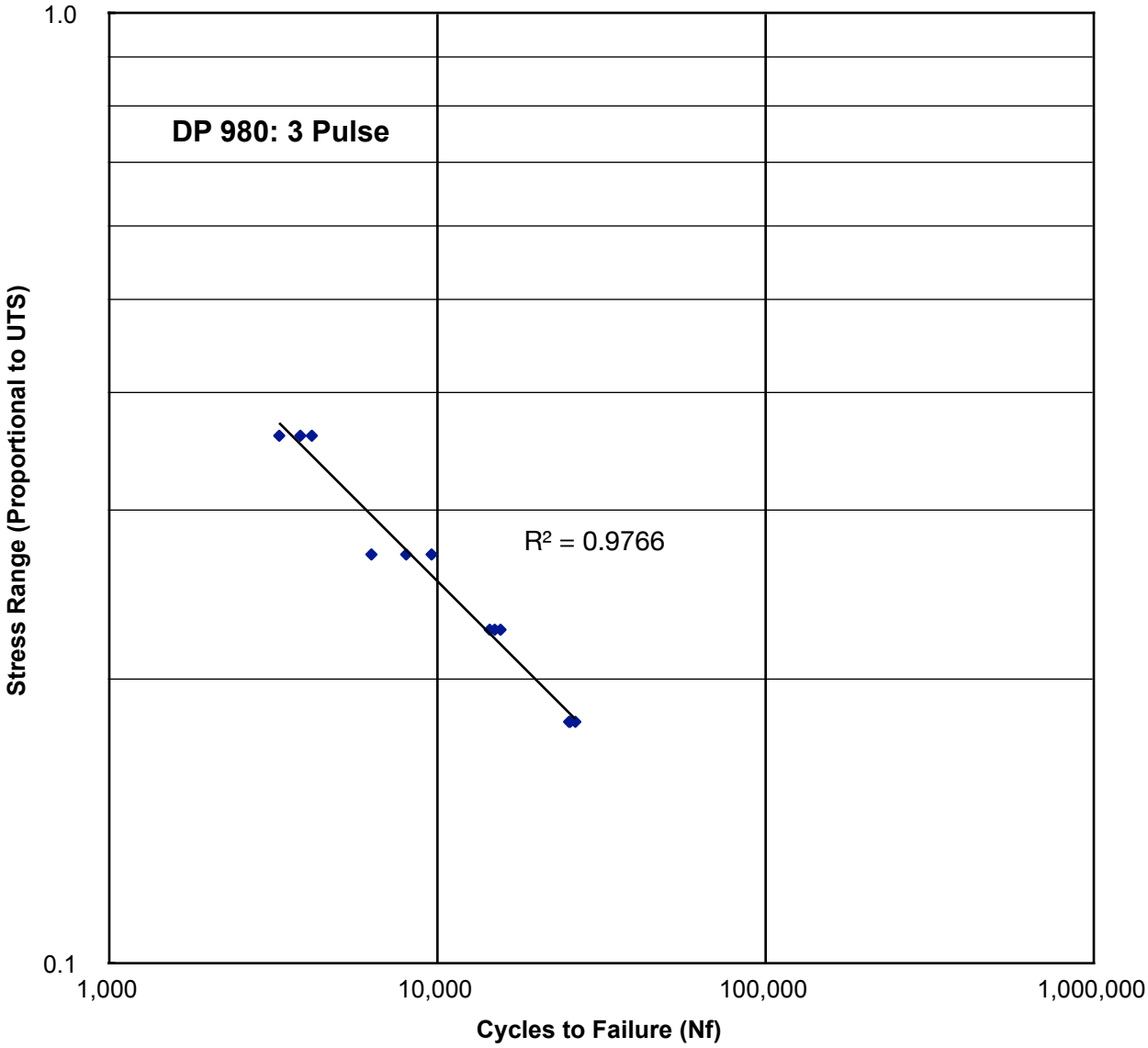

Figure 4.9 Fatigue life diagram for shear lap spot welded DP 980 using 3 pulses

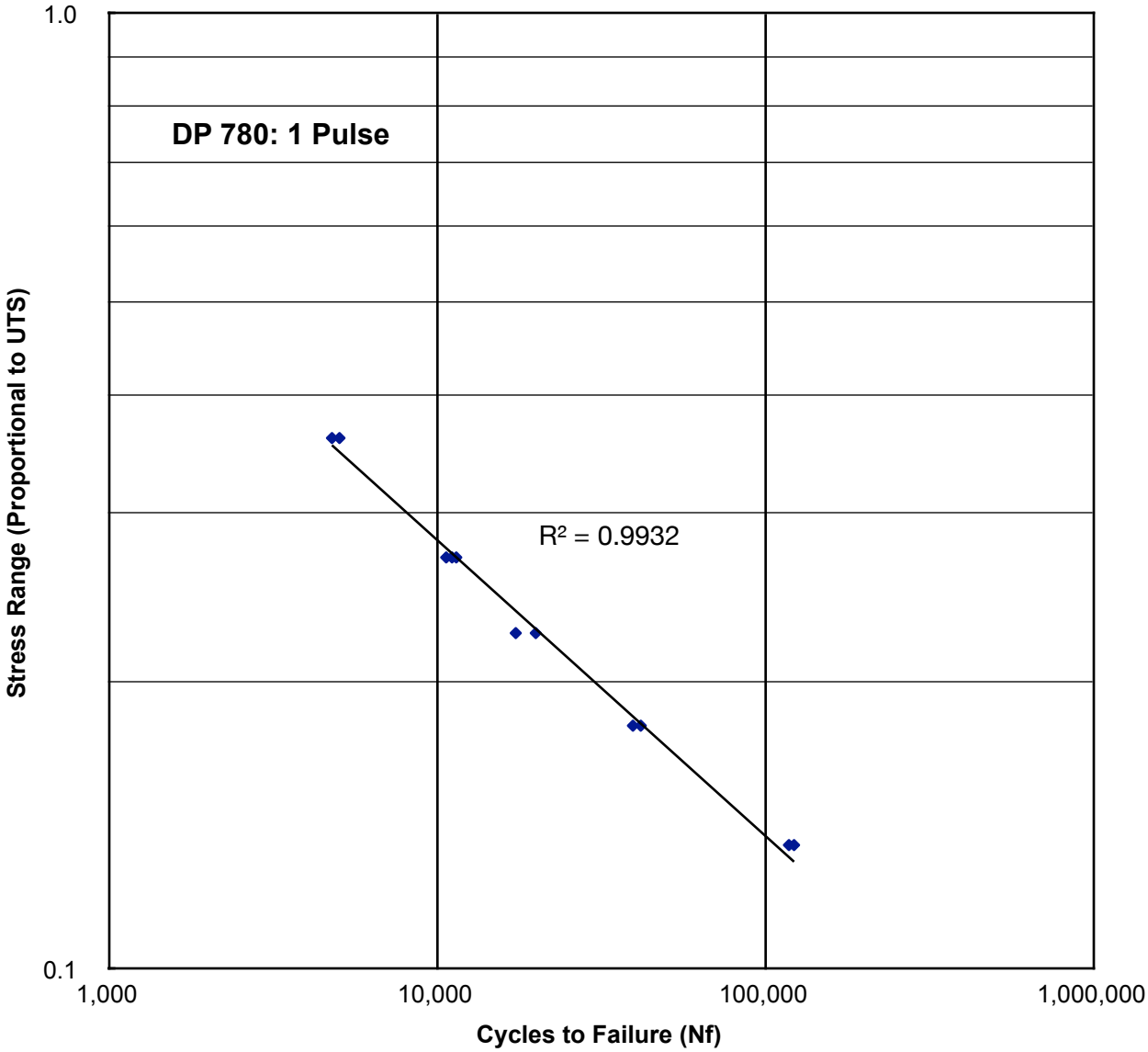

Figure 4.10 Fatigue life diagram for shear lap spot welded DP 780 using 1 pulse

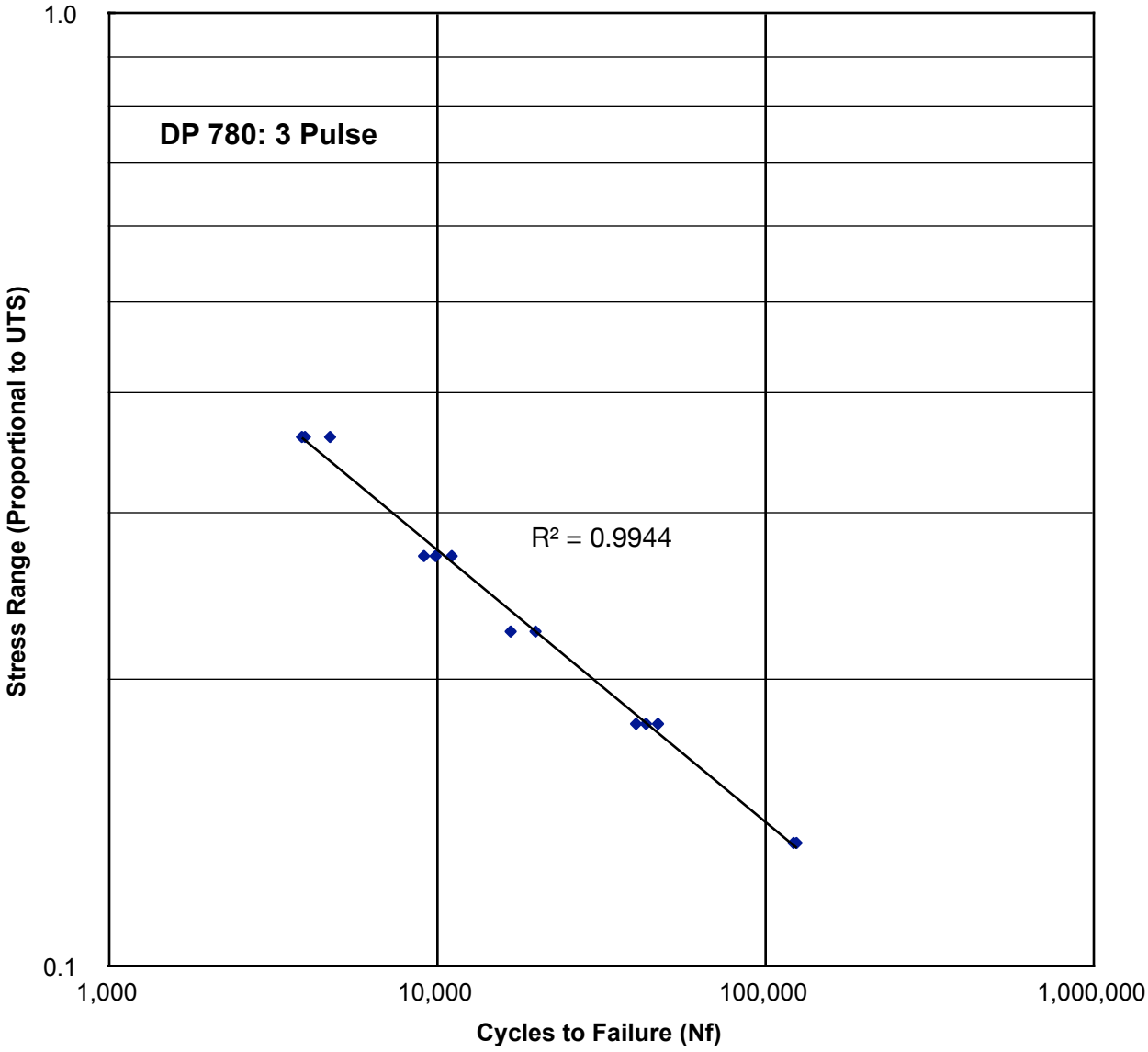

Figure 4.11 Fatigue life diagram for shear lap spot welded DP 780 using 3 pulses

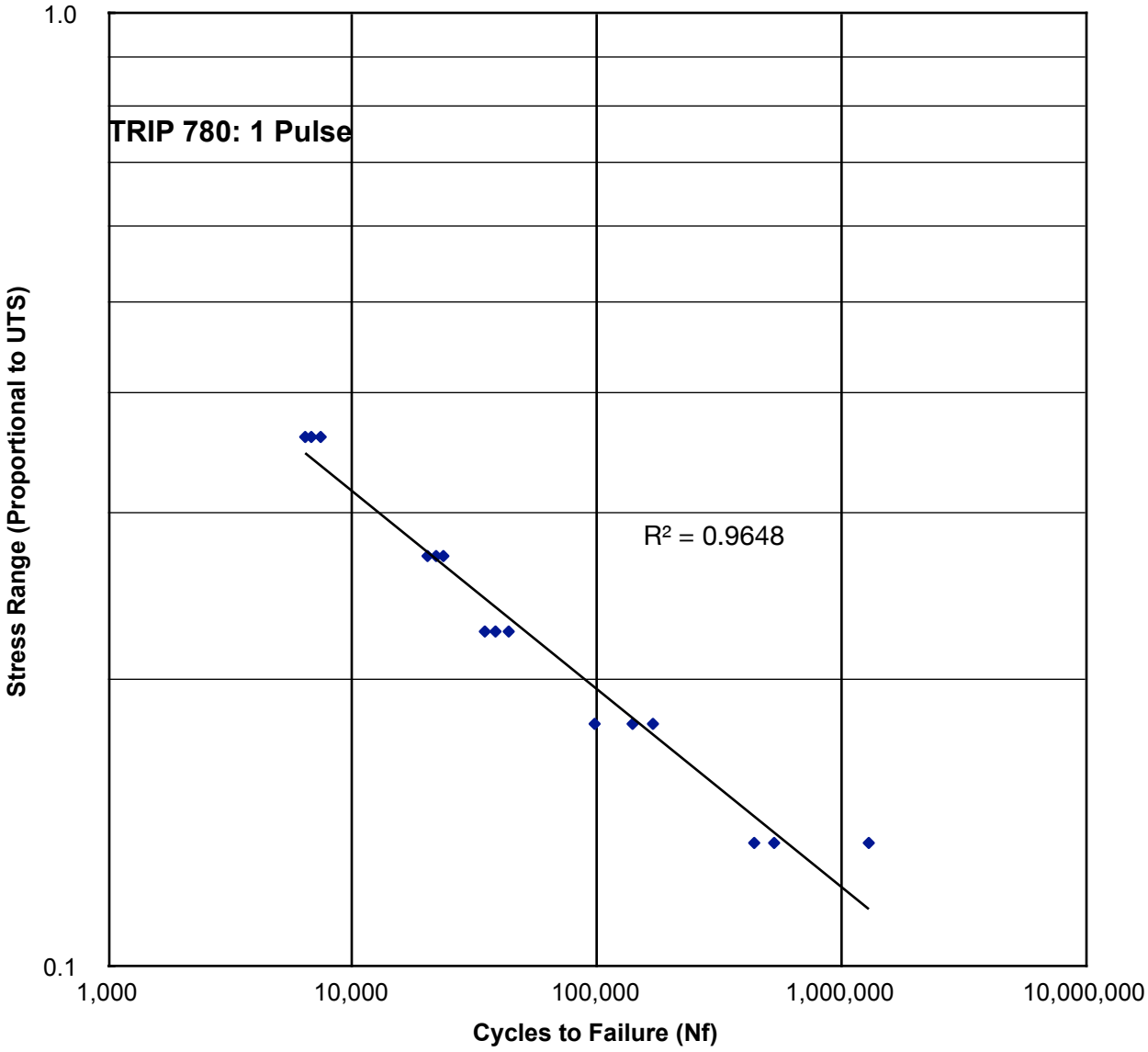

Figure 4.12 Fatigue life diagram for shear lap spot welded TRIP 780 using 1 pulse

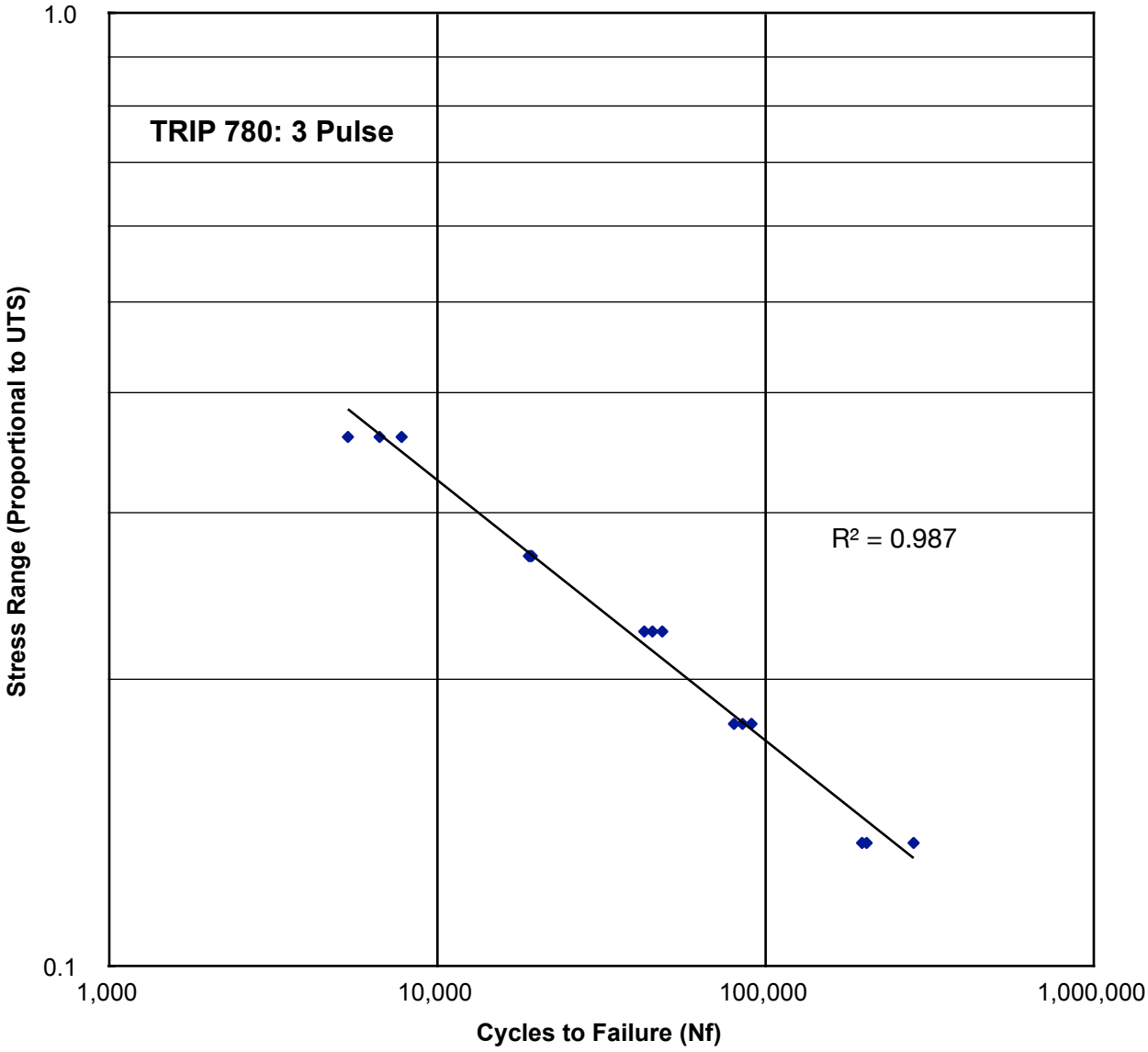

Figure 4.13 Fatigue life diagram for shear lap spot welded TRIP 780 using 3 pulses

The results of this data were also plotted by material type to compare the relative performance of each weld schedule on the high cycle fatigue life. Figure 4.14 displays a graph that depicts the fatigue life for shear lap spot welded DP 980 plotting the applied maximum stress versus the cycles to failure of the joint. Figure 4.15 displays a graph that depicts the fatigue life for shear lap spot welded DP 780, plotting the applied maximum stress versus the cycles to failure of the joint. Figure 4.16 displays a graph that depicts the fatigue life for shear lap spot welded TRIP 780, plotting the applied maximum stress versus the cycles to failure of the joint.

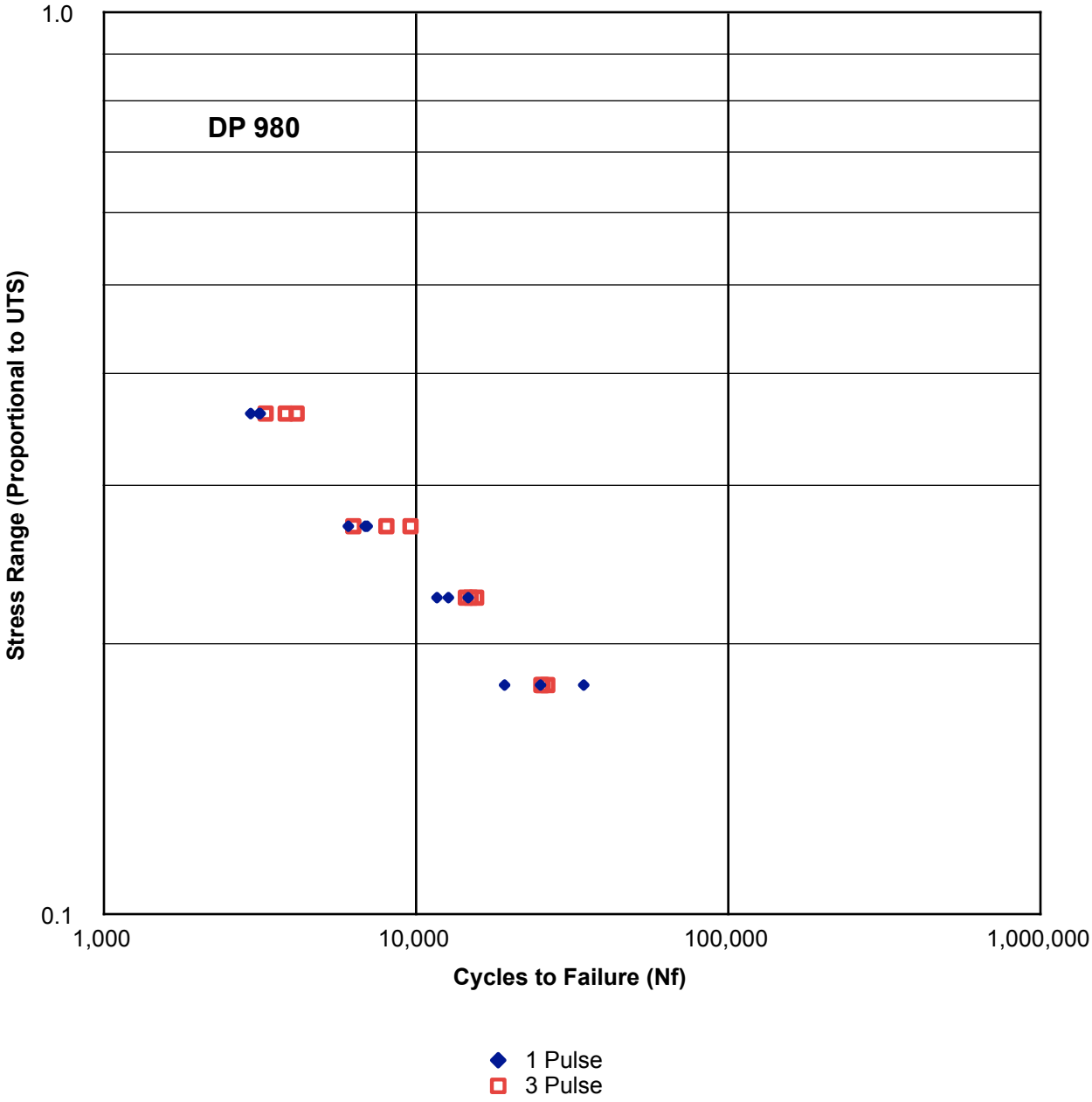

Figure 4.14 Fatigue life diagram for shear lap spot welded DP 980

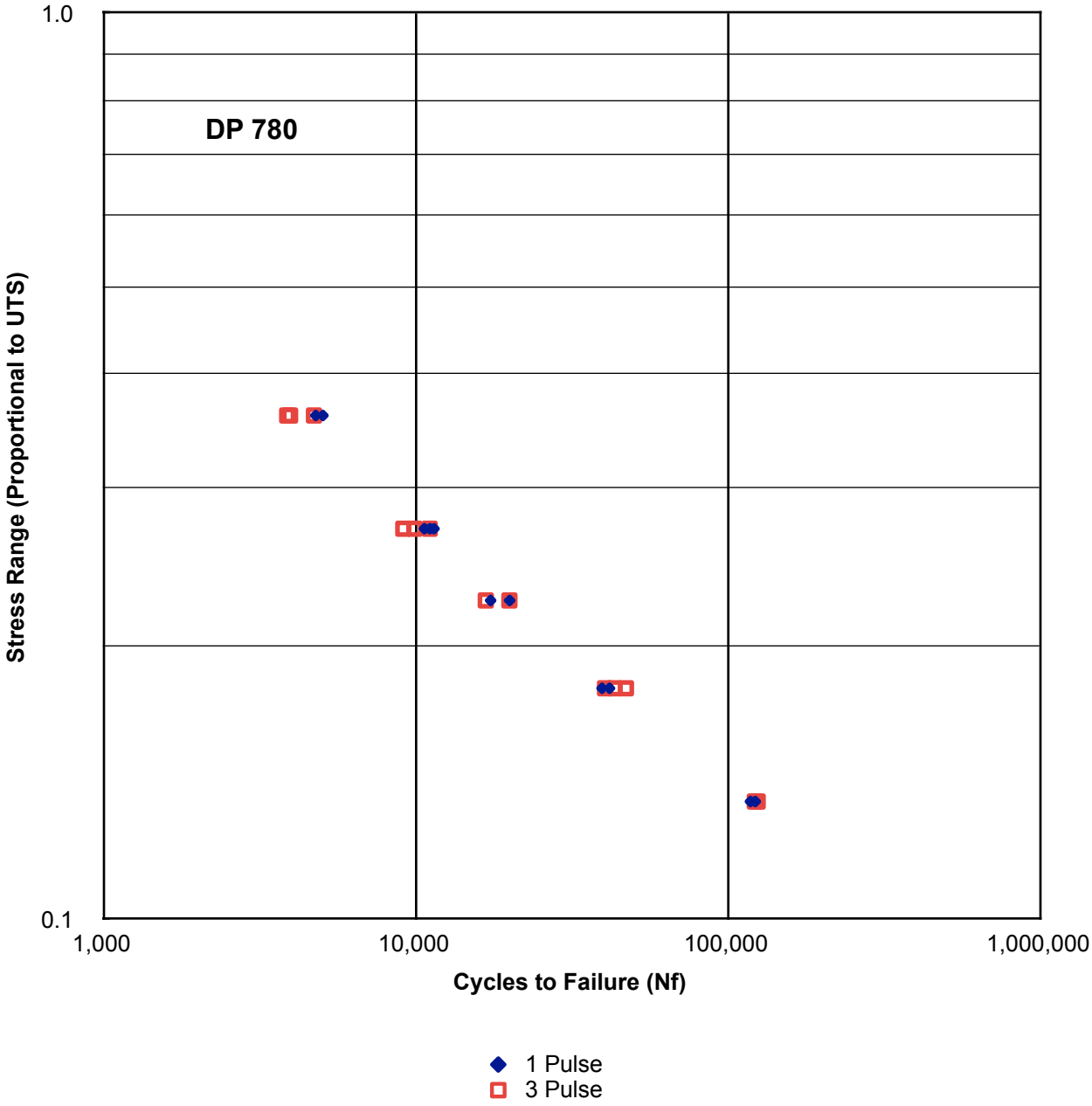

Figure 4.15 Fatigue life diagram for shear lap spot welded DP 780

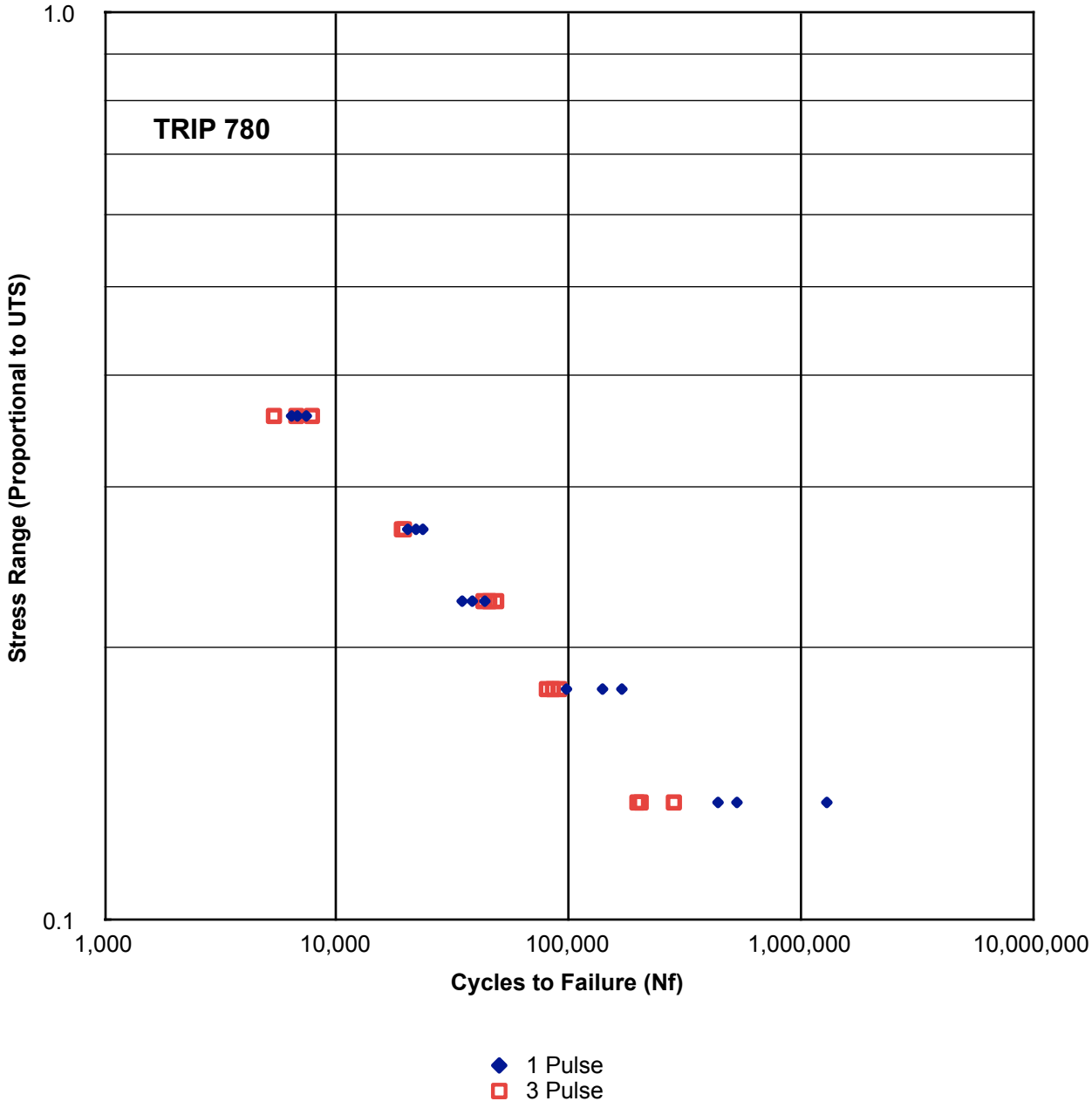

Figure 4.16 Fatigue life diagram for shear lap spot welded TRIP 780

Four conclusions can be drawn from the observed data:

1) The effect of multiple pulse welding on the high cycle fatigue life of the steels is negligible. The largest discrepancy between fatigue life occurred for the TRIP 780 steel for the lowest tested stress range. At this range the average life differed by a factor of 3 with the 1 pulse schedule yielding a larger fatigue life. The remainder of the samples differed by a factor of 2 or less with the results often within 10%, specifically for samples with fatigue lives in the range 10^4 and 10^5. All three steel types exhibited similar cycles to failure at the tested loads for each weld schedule.

2) Following the above conclusion, all three of the steels behaved similarly relative to the differing weld schedules, suggesting that the high cycle fatigue life of the spot weld joint may be dictated by the joint geometry rather than the material properties.

3) No interfacial failures were observed for the fatigue tested specimens for either weld schedule in any of the materials. This data is consistent with the observed behavior in the literature in the low fatigue load regime.

4) In combination with the data collected previously, it is apparent that a weld schedule can be created to eliminate interfacial failure in both the fatigue regime of 10^4 and above cycles to failure as well as the overload condition for shear lap spot welded TRIP 780.

Chapter 5

Examination of Spot Weld Joint Material

This chapter will discuss the steps undertaken to characterize the spot weld microstructure as well as the associated weld properties in relation to the joints used for the fatigue study.

5.1 Metallographic Inspection of the Spot Weld Joint

A untested shear lap specimen for each of the chemistries and weld schedule used in the fatigue study defined previously was used to procure samples for metallographic examination. The shear lap specimens were sectioned in order to obtain two metallographic samples from each shear lap specimen. A sectioning diagram is displayed in Figure 5.1. The arrows on the sectioning diagram indicate the plane of material that was viewed with each sample being prepared in a direction transverse to the thickness of the sheet.

The shear lap specimens were sectioned using a Struers cutoff wheel. The samples were mounted and prepared using the same methods outlined previously in Chapter 3. After preparation the samples were viewed using a Nikon inverted light microscope. The samples were observed both in the as-polished condition and also after etching.

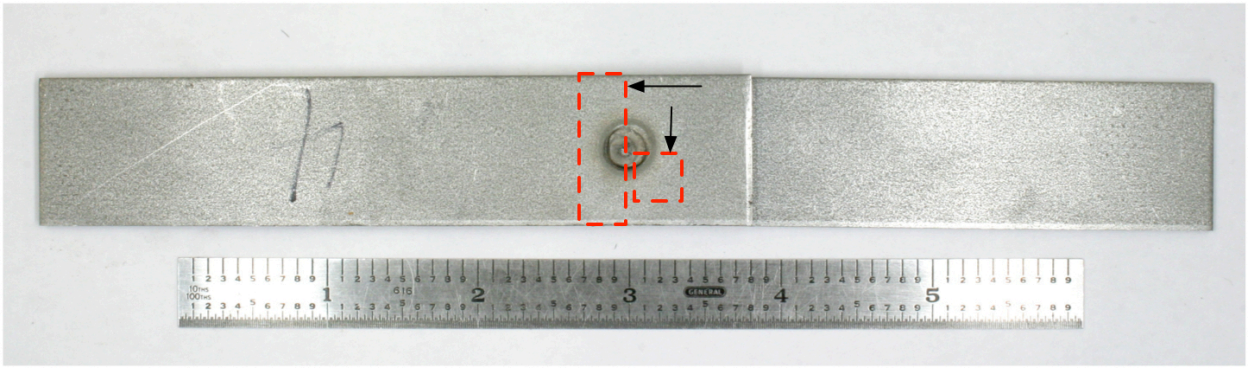

Figure 5.1 Sectioning diagram displaying samples used for metallographic inspection

5.2 Spot Weld Geometry

The as-polished metallographic samples were observed to identify the geometry of the interface of the spot weld samples. Images of the weld interface were recorded at 50X and 500X. Figure 5.2 displays a representative image of the geometry inherent to the spot weld interface.

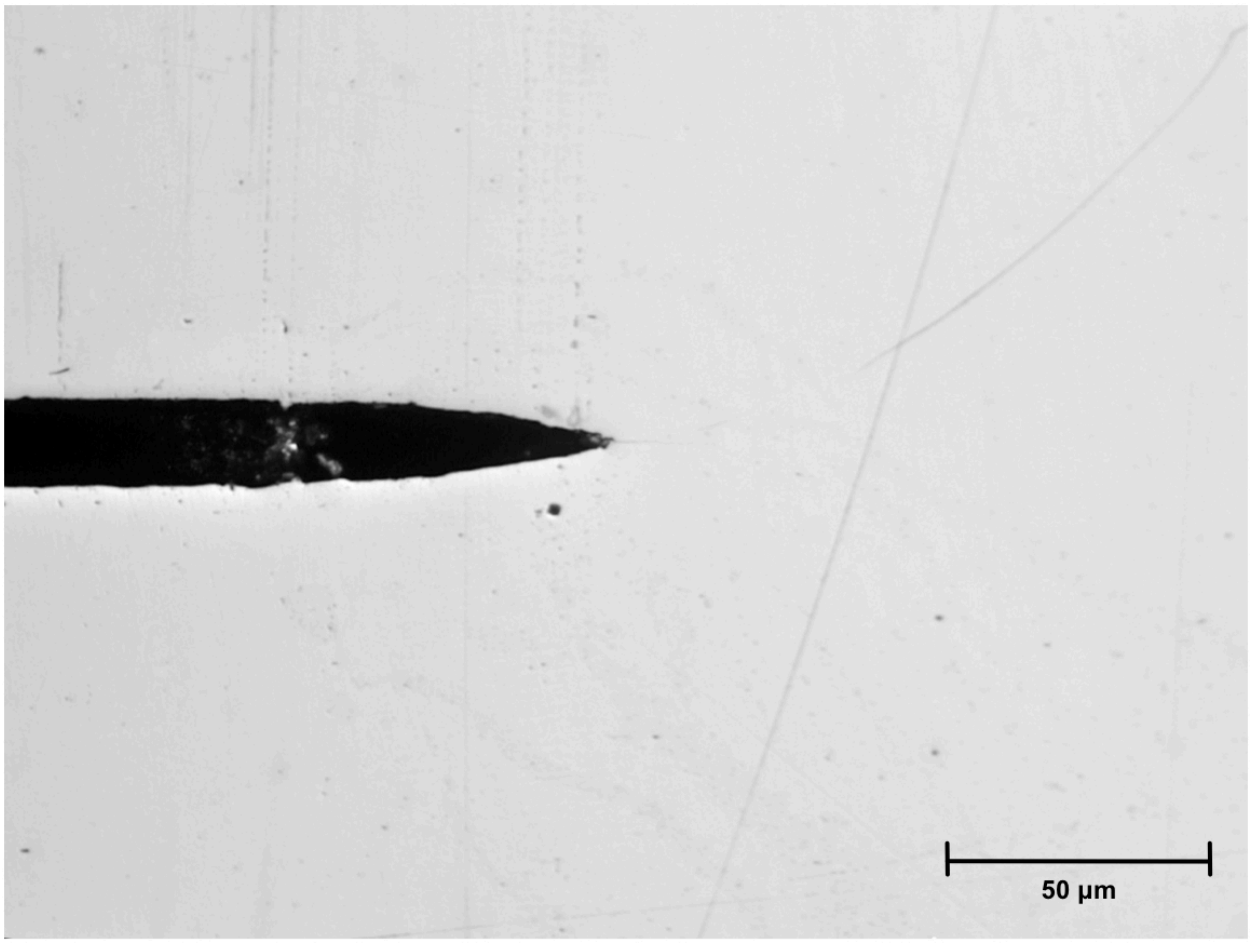

Figure 5.2 Image of as-polished shear lap joint

5.3 Examination of Spot Weld Microstructure

The metallographic samples were etched following inspection in the as-polished condition. The DP steels were etched using a solution of 3% Nital for approximately 5 seconds. The TRIP steel samples were etched using a two step process. The first step was applying a 3% Nital solution for approximately 5 seconds. The second step in the etching process consisted of applying sodium metabisulfate for approximately 30 seconds. The samples were again examined using an inverted light microscope with images recorded at various magnifications and locations.

Figure 5.3 displays a representative image of the HAZ microstructure of a spot weld consisting of DP 980 welded with 1 pulse. Figure 5.4 displays a representative image of the HAZ microstructure of a spot weld consisting of DP 980 welded with 3 pulses. Figure 5.5 displays a representative image of the HAZ microstructure of a spot weld consisting of DP 780 welded with 1 pulse. Figure 5.6 displays a representative image of the HAZ microstructure of a spot weld consisting of DP 780 welded with 3 pulses. Figure 5.7 displays a representative image of the HAZ microstructure of a spot weld consisting of TRIP 780 welded with 1 pulse. Figure 5.8 displays a representative image of the HAZ microstructure of a spot weld consisting of TRIP 780 welded with 3 pulses.

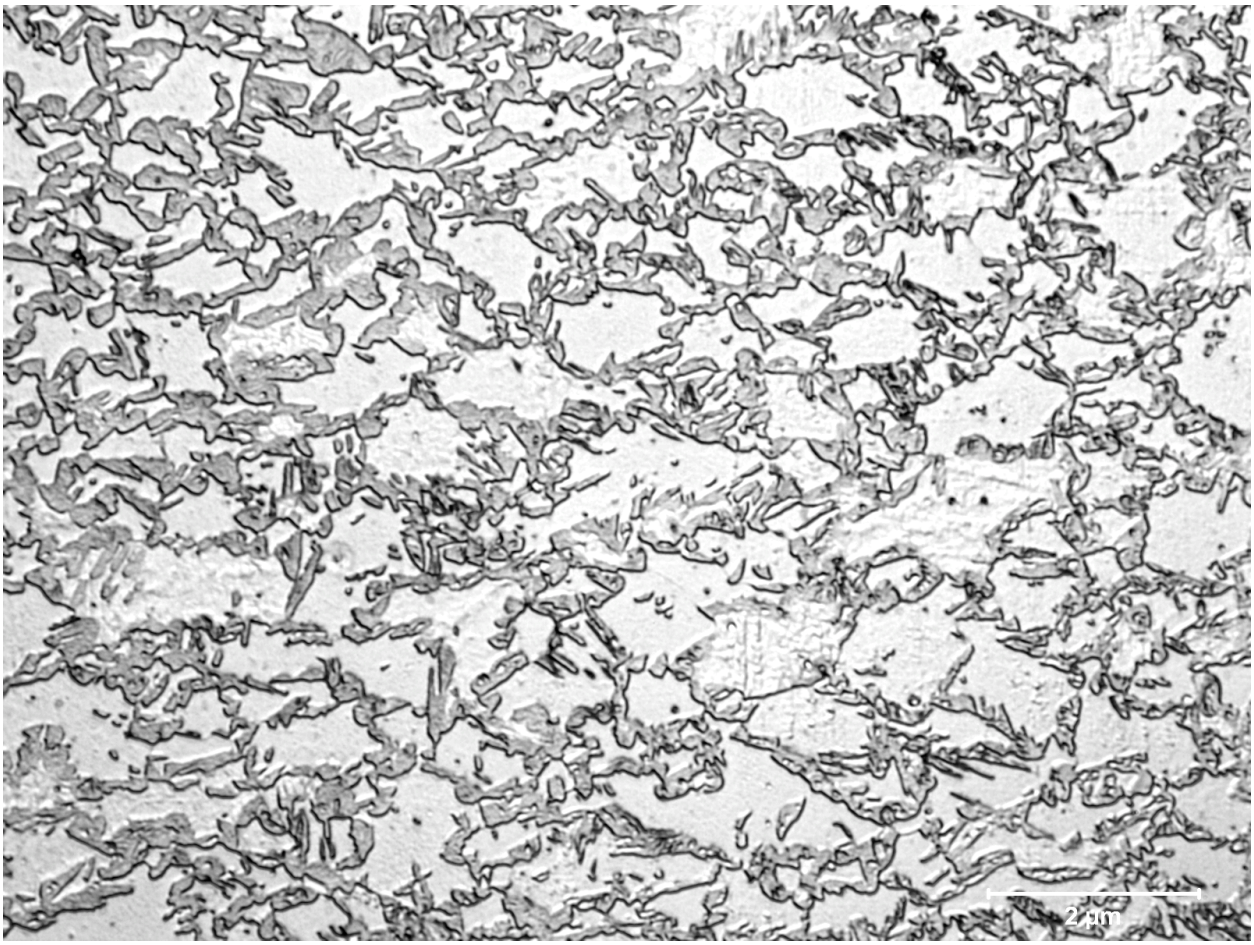

Figure 5.3 Image of DP 980 HAZ microstructure welded with 1 pulse, Etchant 3% Nital

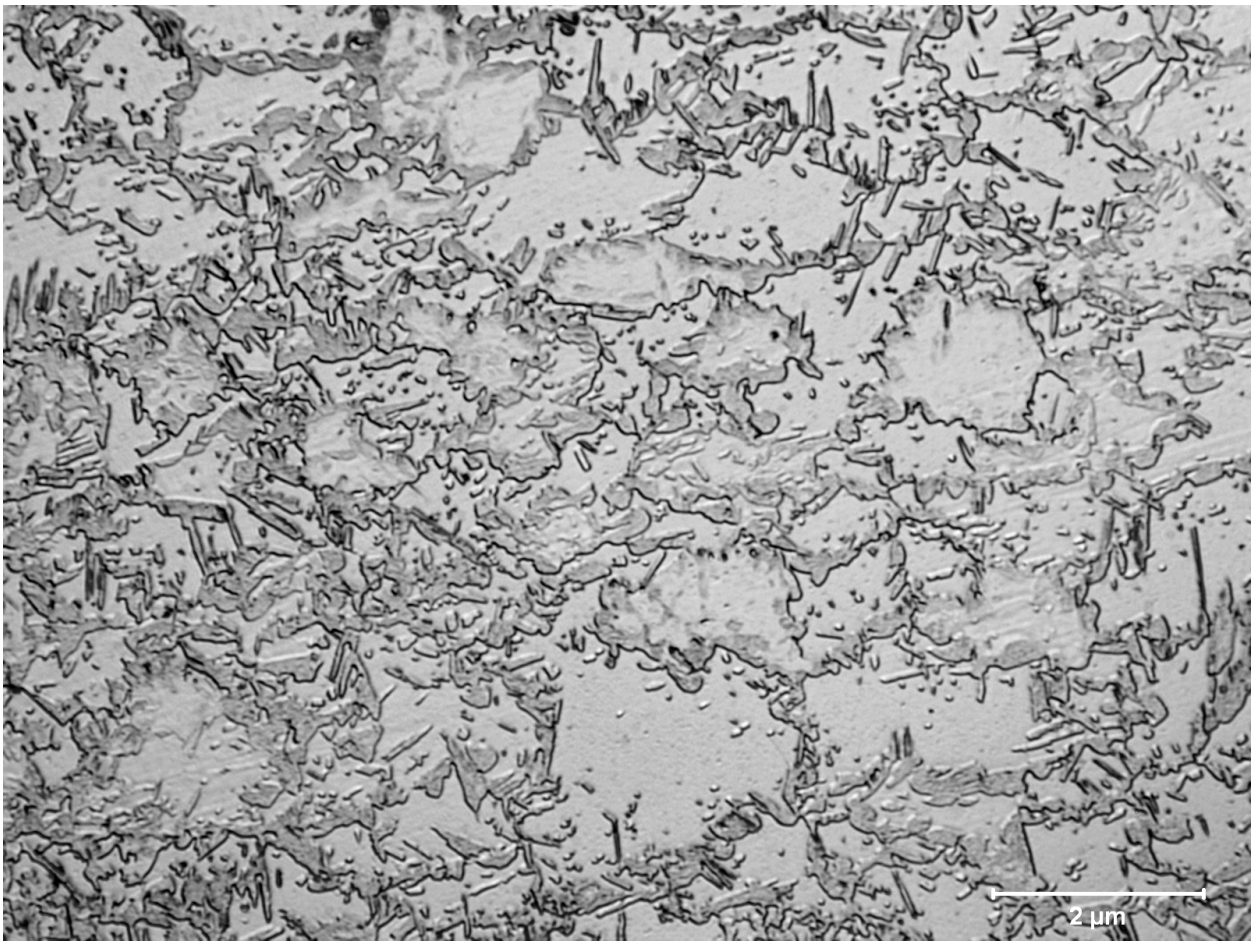

Figure 5.4 Image of DP 980 HAZ microstructure welded with 3 Pulses, Etchant 3% Nital

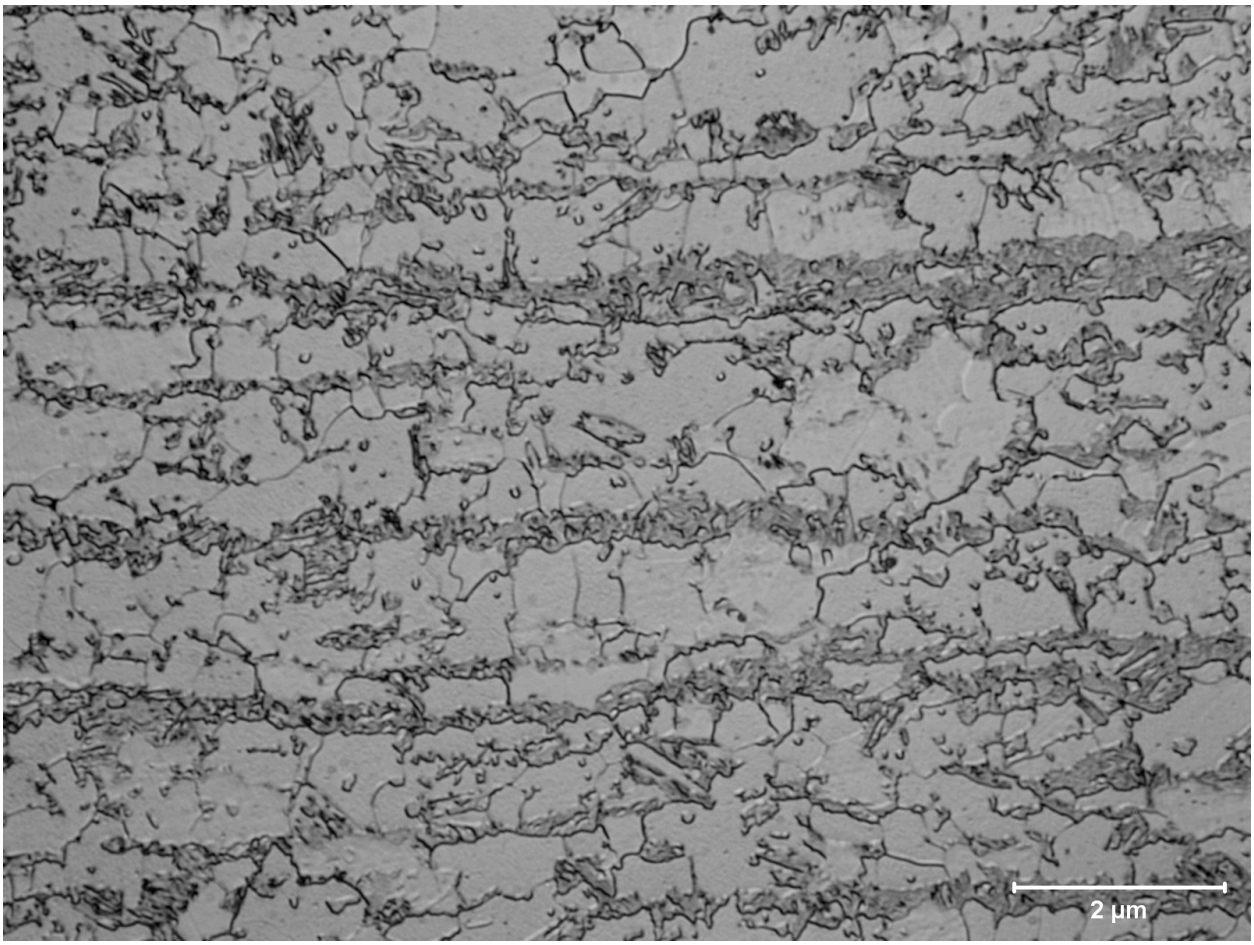

Figure 5.5 Image of DP 780 HAZ microstructure welded with 1 Pulse, Etchant 3% Nital

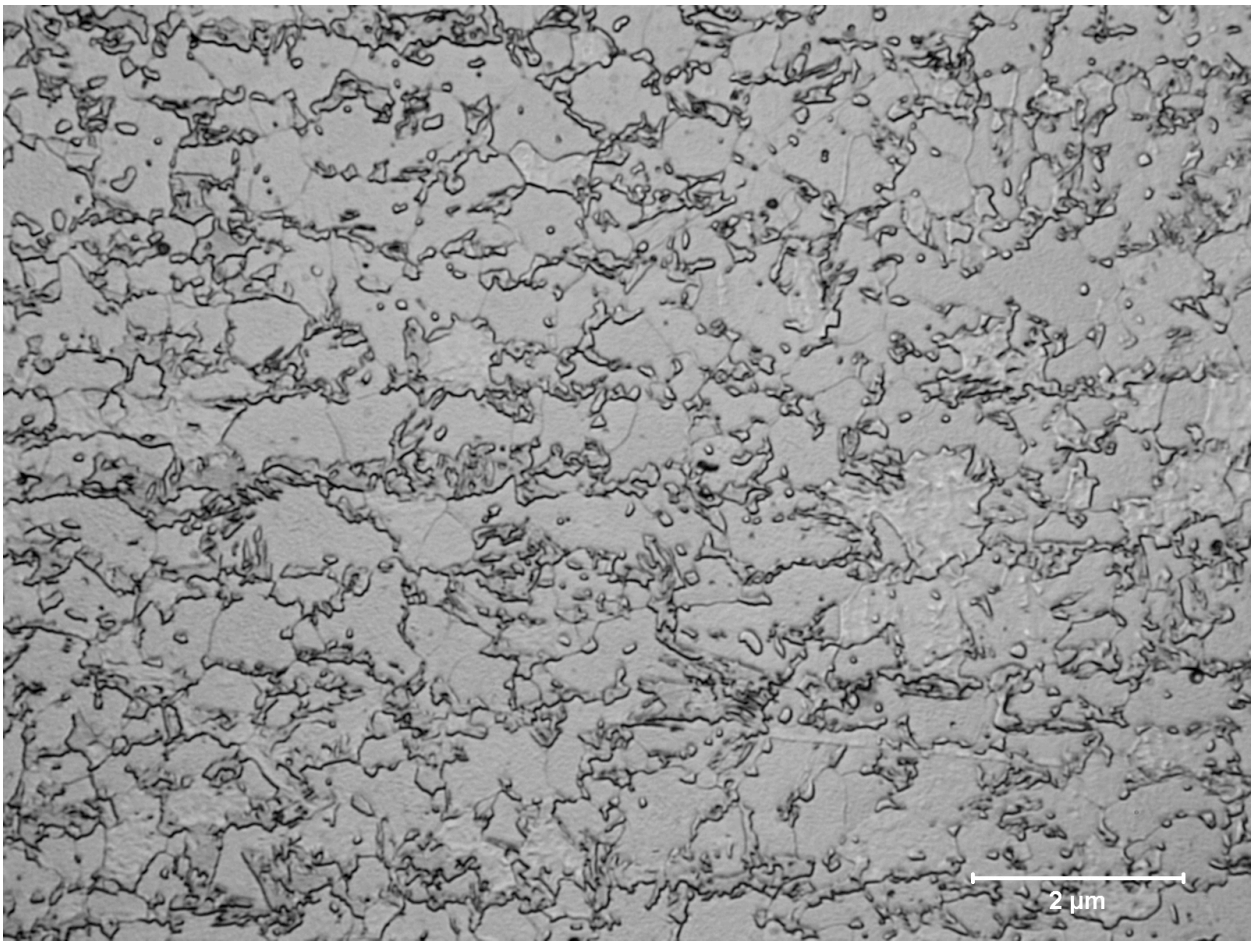

Figure 5.6 Image of DP 780 HAZ microstructure welded with 3 Pulses, Etchant 3% Nital

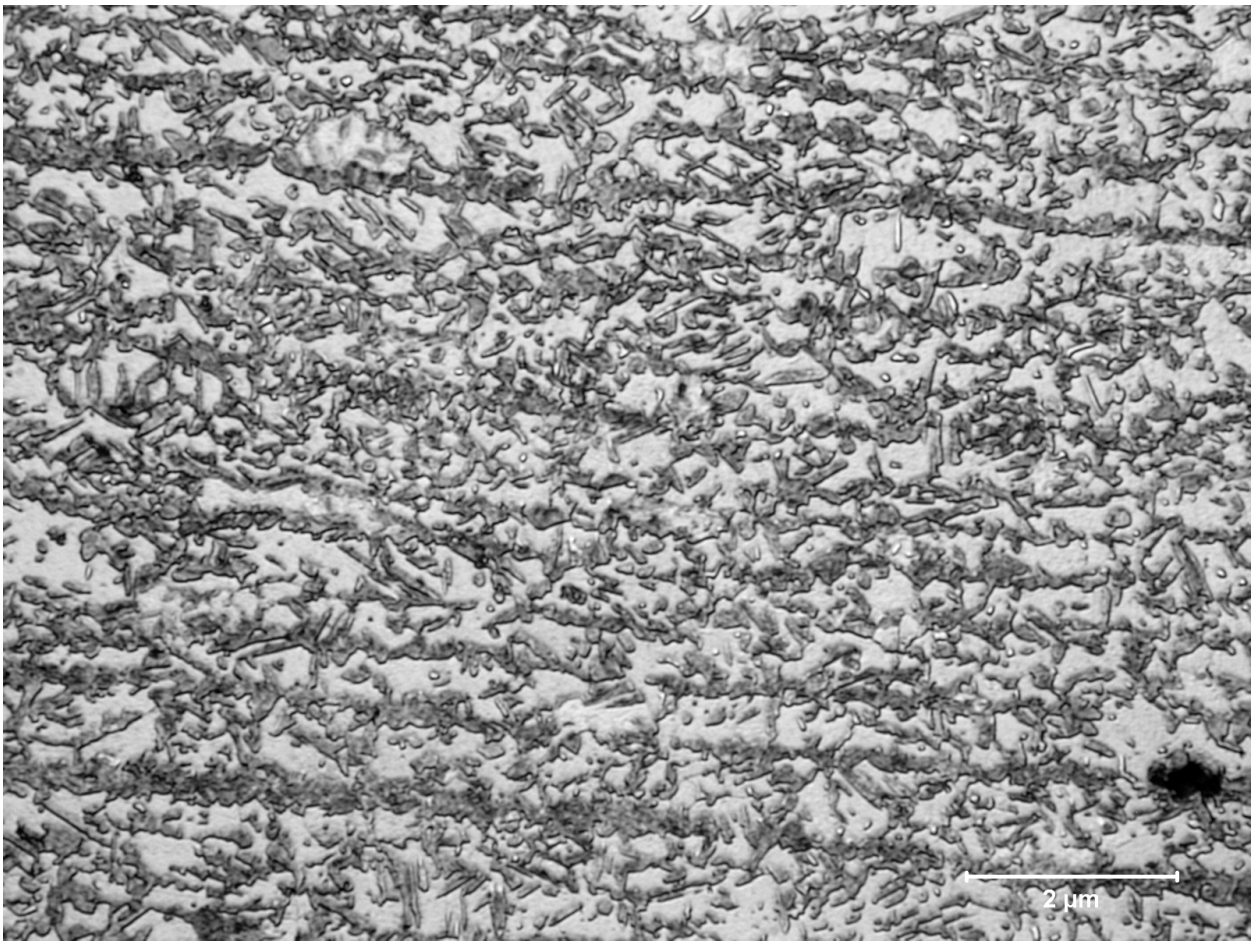

Figure 5.7 Image of TRIP 780 HAZ microstructure welded with 1 Pulse, Etchant Sodium Metabisulfate

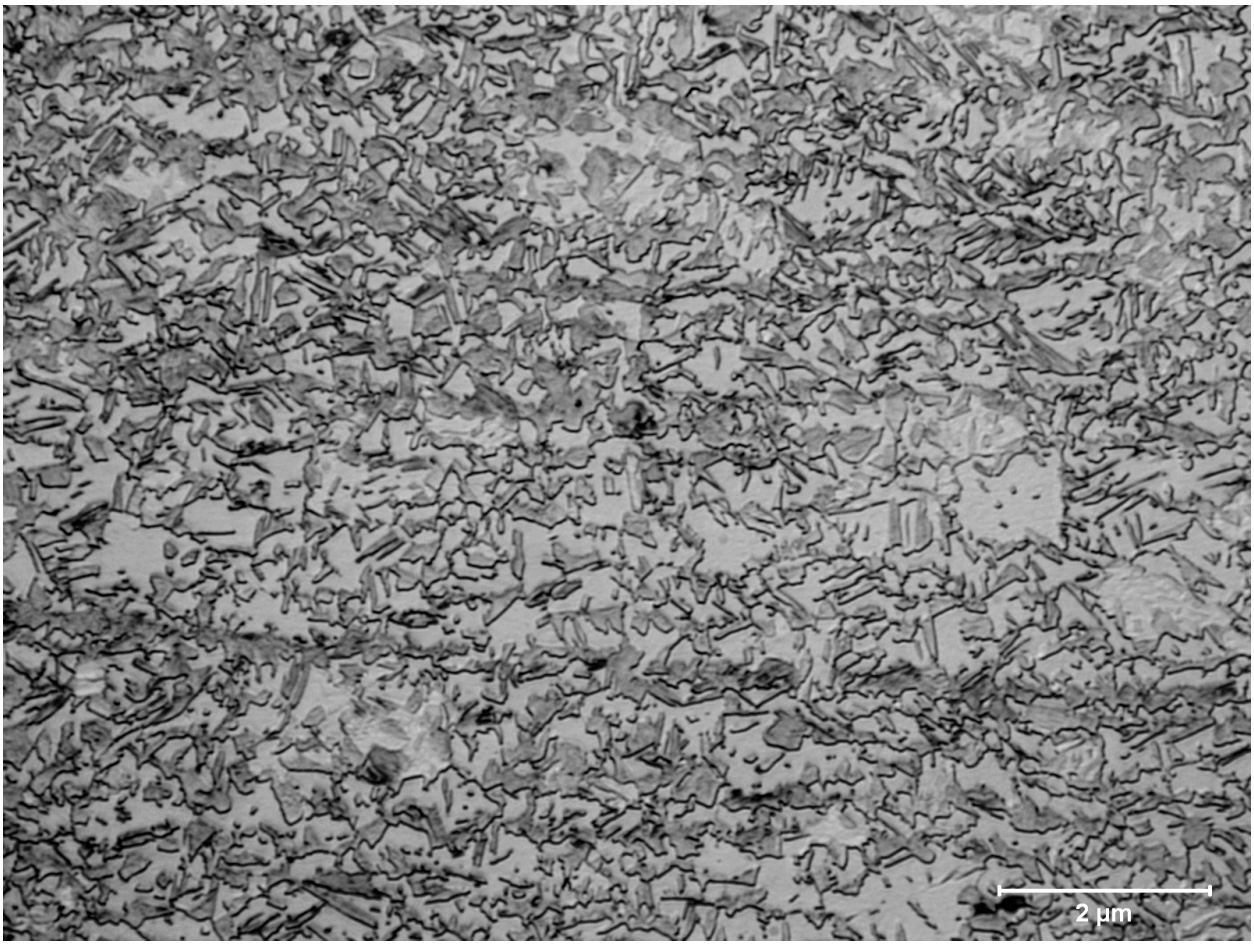

Figure 5.8 Image of TRIP 780 HAZ microstructure welded with 3 Pulses, Etchant Sodium Metabisulfate

5.4 Microhardness of Spot Weld

Following metallographic inspection of the metallographic samples, microhardness traverses were performed to quantify the hardness of the weld joint. A Knoop indenter was used with a 500 gram load and a dwell time of 10 seconds. The traverses were performed on the metallographic sample that encompassed an entire transverse section of the weld. Figure 5.9 displays a metallographic mount annotated to show the hardness traverse. The traverses were conducted with an indenter spacing of 0.127 mm. Hardness measurements were conducted and the hardness values were converted to a value on the Rockwell C scale (HRC). The length of the indent, the Knoop hardness, and the converted HRC value were recorded.

Figure 5.10 displays a plot of the hardness of a weld as a function of position for the DP 980 welded with the 1 pulse schedule. Figure 5.11 displays a plot of the hardness of a weld as a function of position for the DP 980 welded with the 3 pulse schedule. Figure 5.12 displays a plot of the hardness of a weld as a function of position for the DP 780 welded with the 1 pulse schedule. Figure 5.13 displays a plot of the hardness of a weld as a function of position for the DP 780 welded with the 3 pulse schedule. Figure 5.14 displays a plot of the hardness of a weld as a function of position for the TRIP 780 welded with the 1 pulse schedule. Figure 5.15 displays a plot of the hardness of a weld as a function of position for the TRIP 780 welded with the 3 pulse schedule.

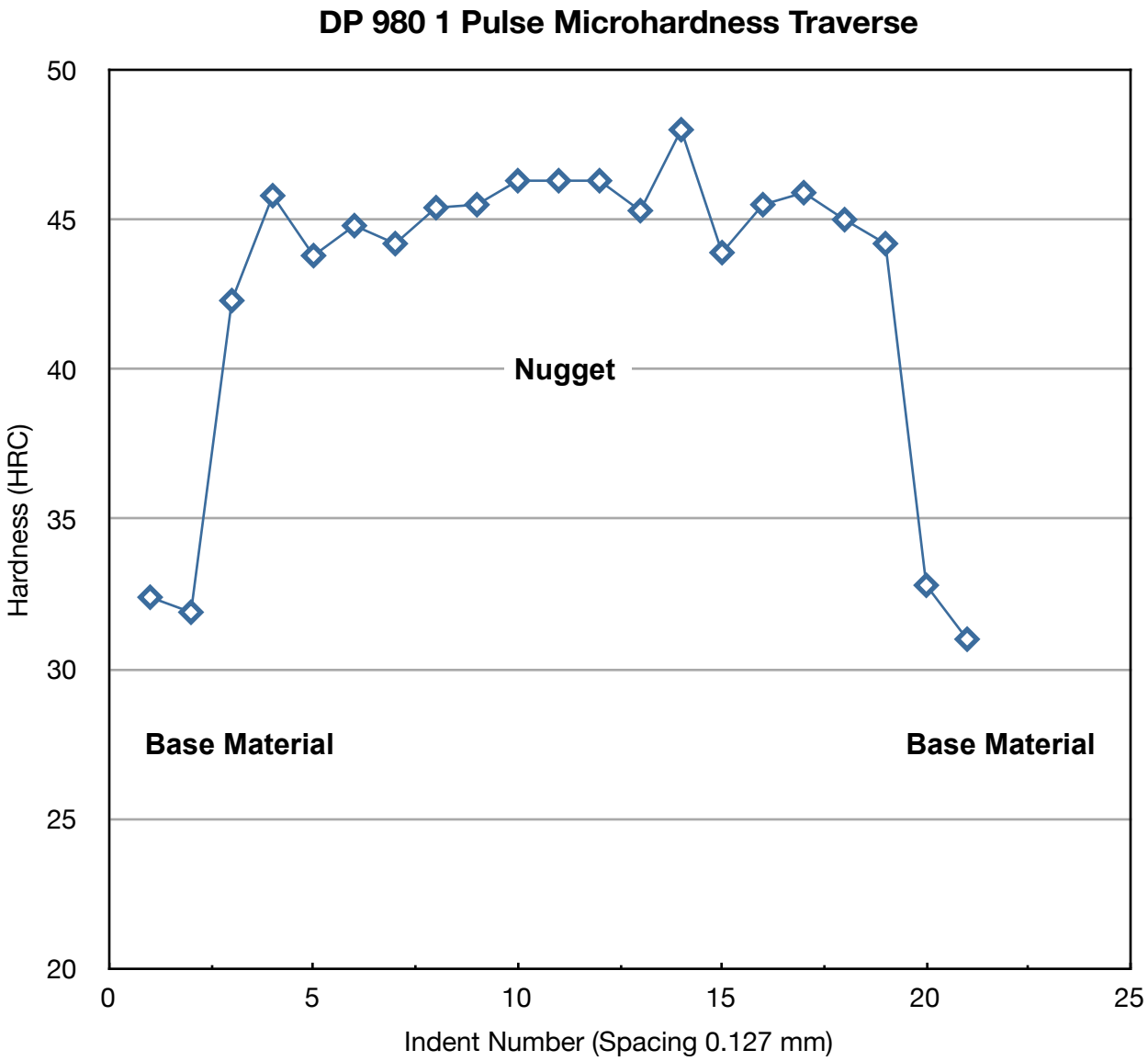

Figure 5.10 Plot of the hardness of a weld as a function of position for the DP 980 welded with the 1 pulse

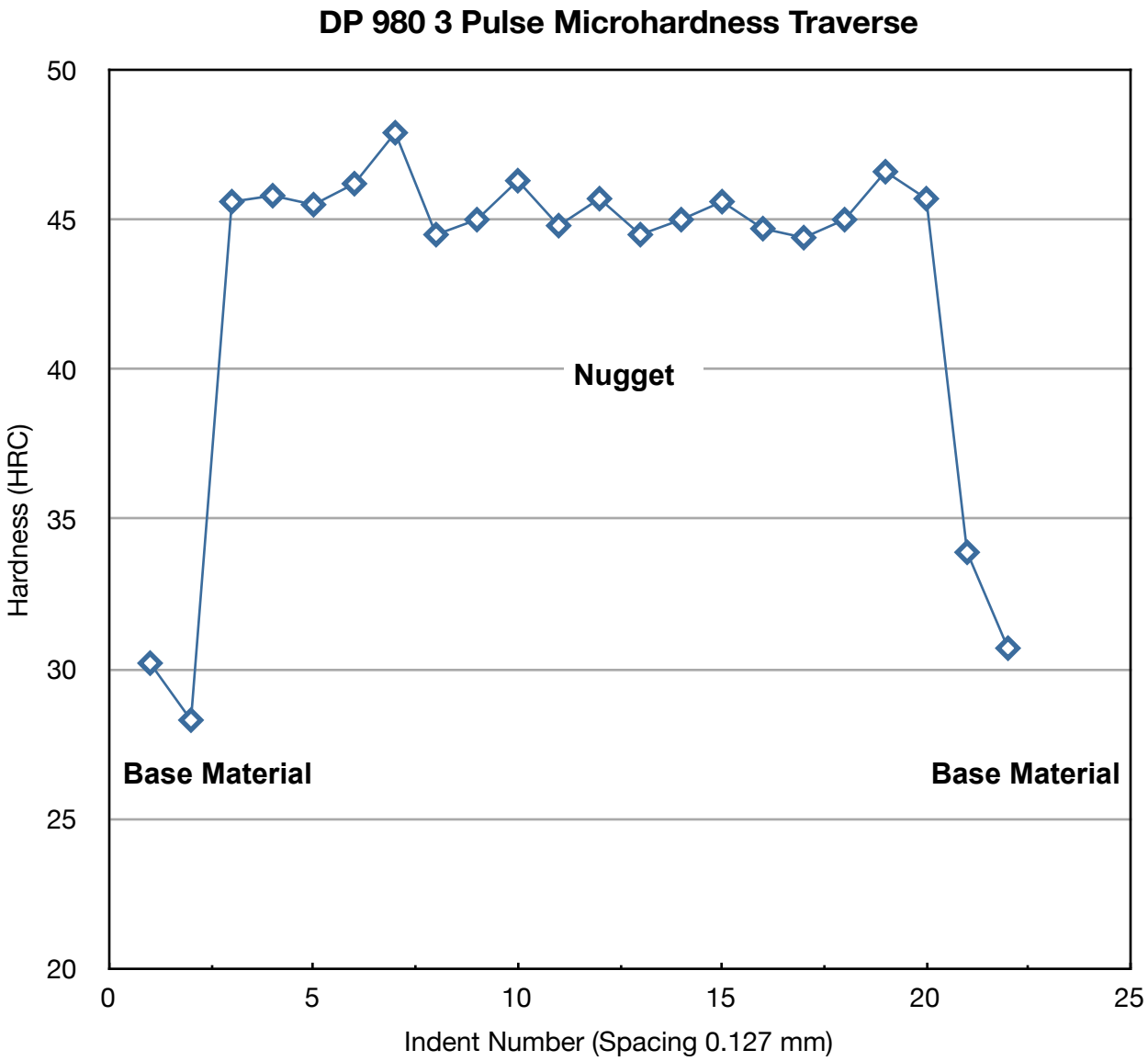

Figure 5.11 Plot of the hardness of a weld as a function of position for the DP 980 welded with the 3 pulses

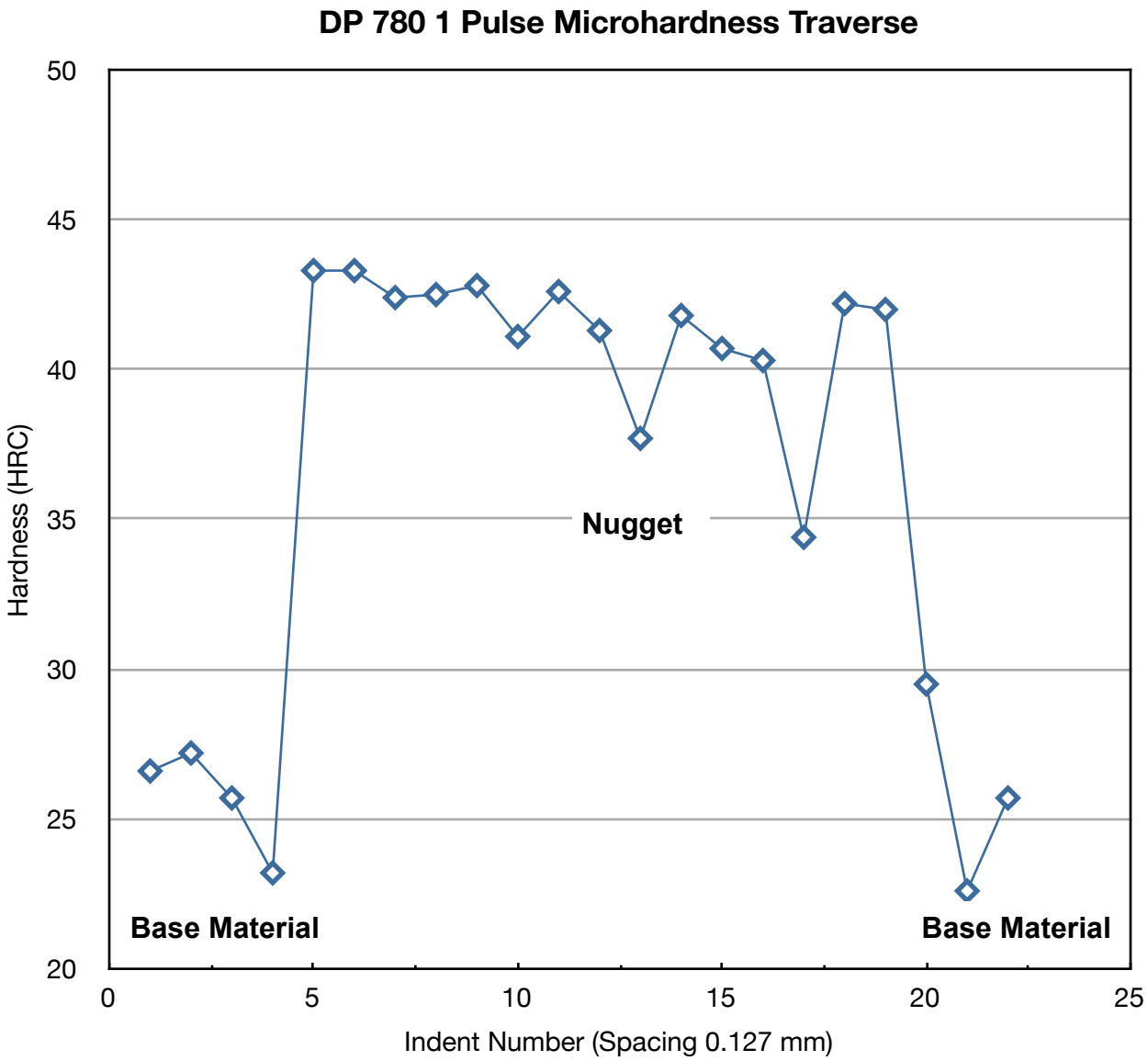

Figure 5.12 Plot of the hardness of a weld as a function of position for the DP 780 welded with the 1 pulse

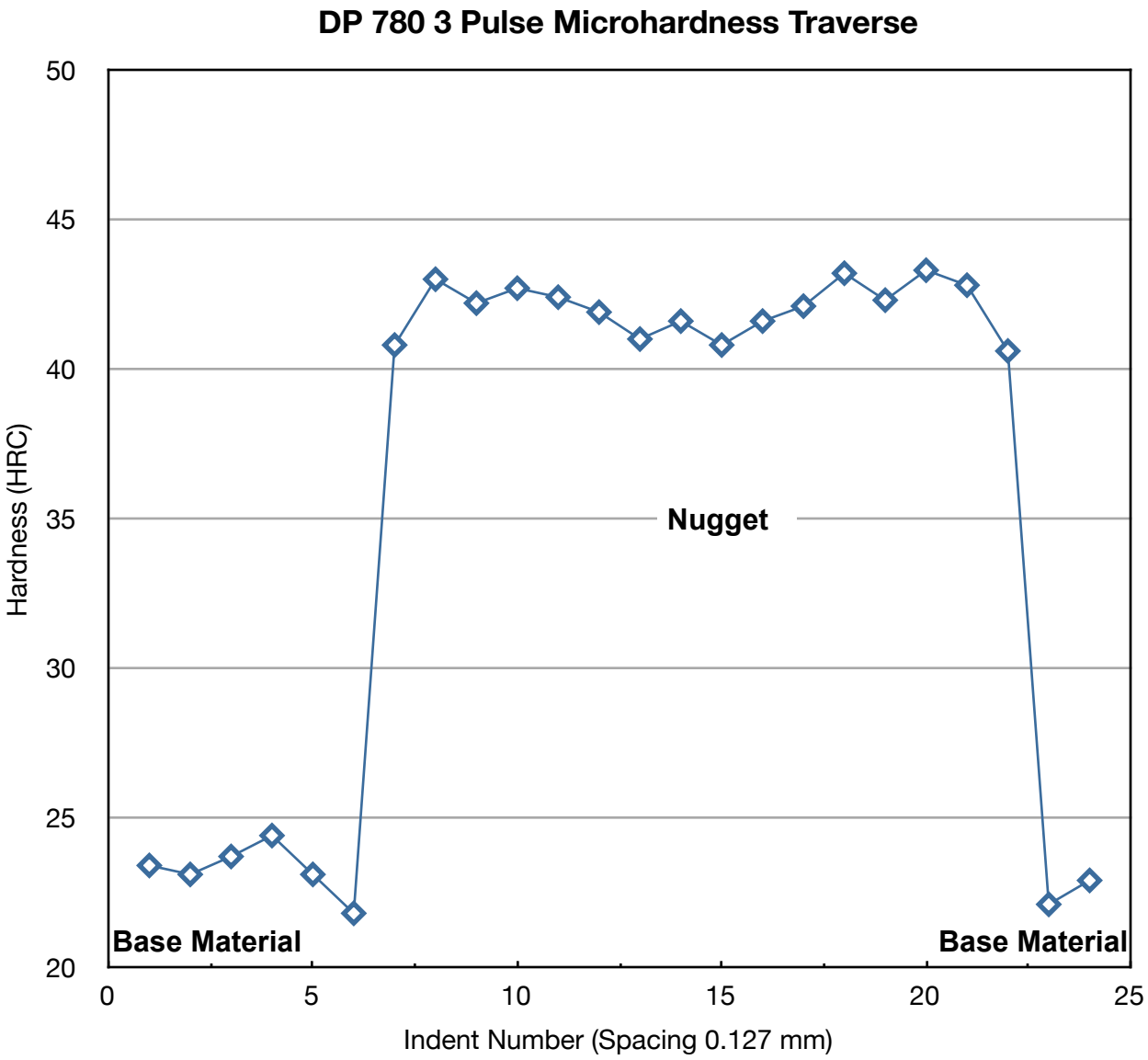

Figure 5.13 Plot of the hardness of a weld as a function of position for the DP 780 welded with the 3 pulses

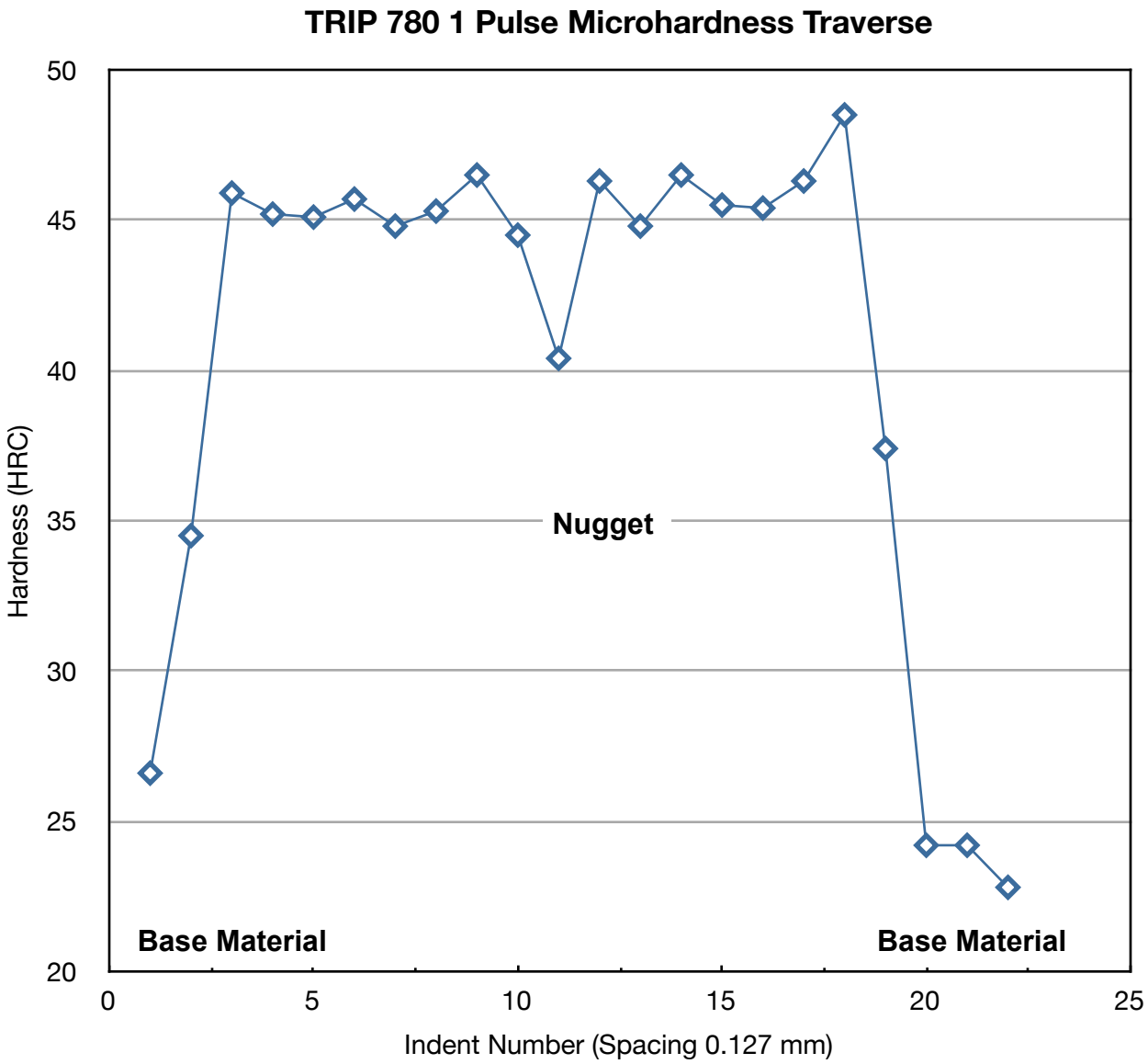

Figure 5.14 Plot of the hardness of a weld as a function of position for the TRIP 780 welded with the 1 pulse

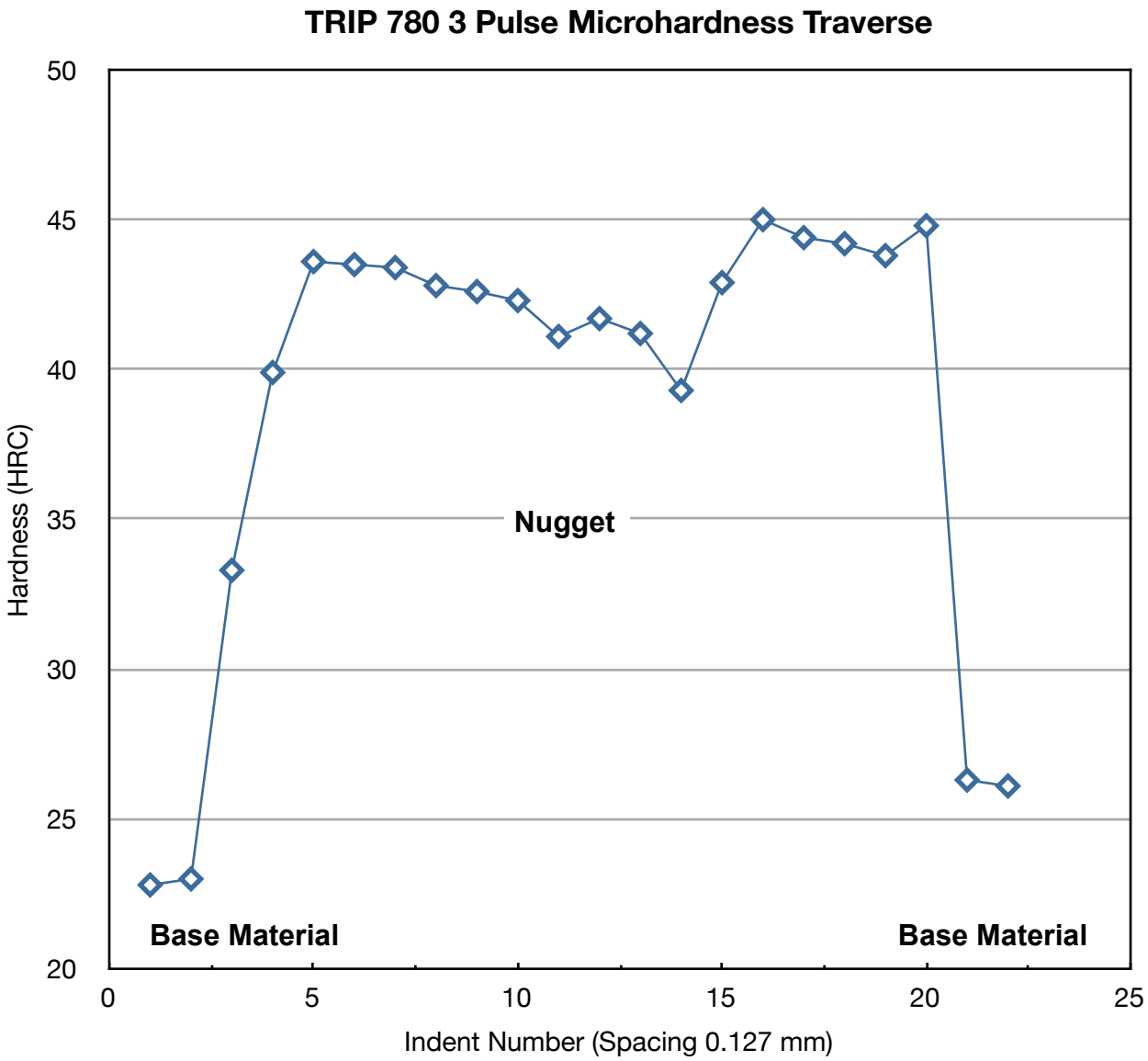

Figure 5.15 Plot of the hardness of a weld as a function of position for the TRIP 780 welded with the 3 pulses

The information collected from the metallurgical examination was used to compare to the model and proposed by Marya et al., Chapter 2 equation 2.2 Based on the hardness values recorded, the Marya et al. model predicts the failure force of the shear lap specimens for the weld schedule to be 22.5 kN. This model proves to be a good estimate of the recorded failure strength for the samples that failed via pullout, the observed failure forces ranged from approximately 21.7 kN - 24.5 kN. It is worth noting that the failure force for the samples that experienced interfacial failure did exceed 26 kN in some cases.

5.5 Fractography of Spot Weld

Several of the shear lap specimens used in the previously mentioned tensile strength testing were further examined using light microscopy in an effort to better document the fracture surface. A representative sample was chosen from each of the three tiers of average weld current. The samples were examined using a Nikon binocular light microscope. Figure 5.16 displays the fracture surface of a sample welded with an average current of approximately 6.5 kA and a weld force of 3600 N. Figure 5.17 displays the fracture surface of a sample welded with an average current of approximately 8 kA and a weld force of 5800 N. Figure 5.18 displays the fracture surface of a sample welded with an average current of 9.5 kA and a weld force of 5800 N.

Two full interfacial failures were chosen and one pullout failure was also examined. Figure 5.16 displays a full interfacial failure of a TRIP steel with a relatively low weld current and low weld force. Limited weld porosity is observed and some weld cracking can be observed in the nugget.

Figure 5.17 is representative of the typical behavior observed for a pull out fracture. A pull out fracture was identified by the nugget of the weld remaining intact during the fracture mechanism in addition to the fracture propagation through the base material. In other words, the pull out mechanism was defined as fracture around the nugget resulting in fracture and deformation through the base material. Figure 5.18 displays a representative image of the interfacial fracture associated with an average current of 9.5 kA. The amount of porosity observed is more widespread than that observed in the low weld current interfacial fracture. The number of cracks observed in in the weld nugget is also increased when compared to that of the low current interfacial fracture.

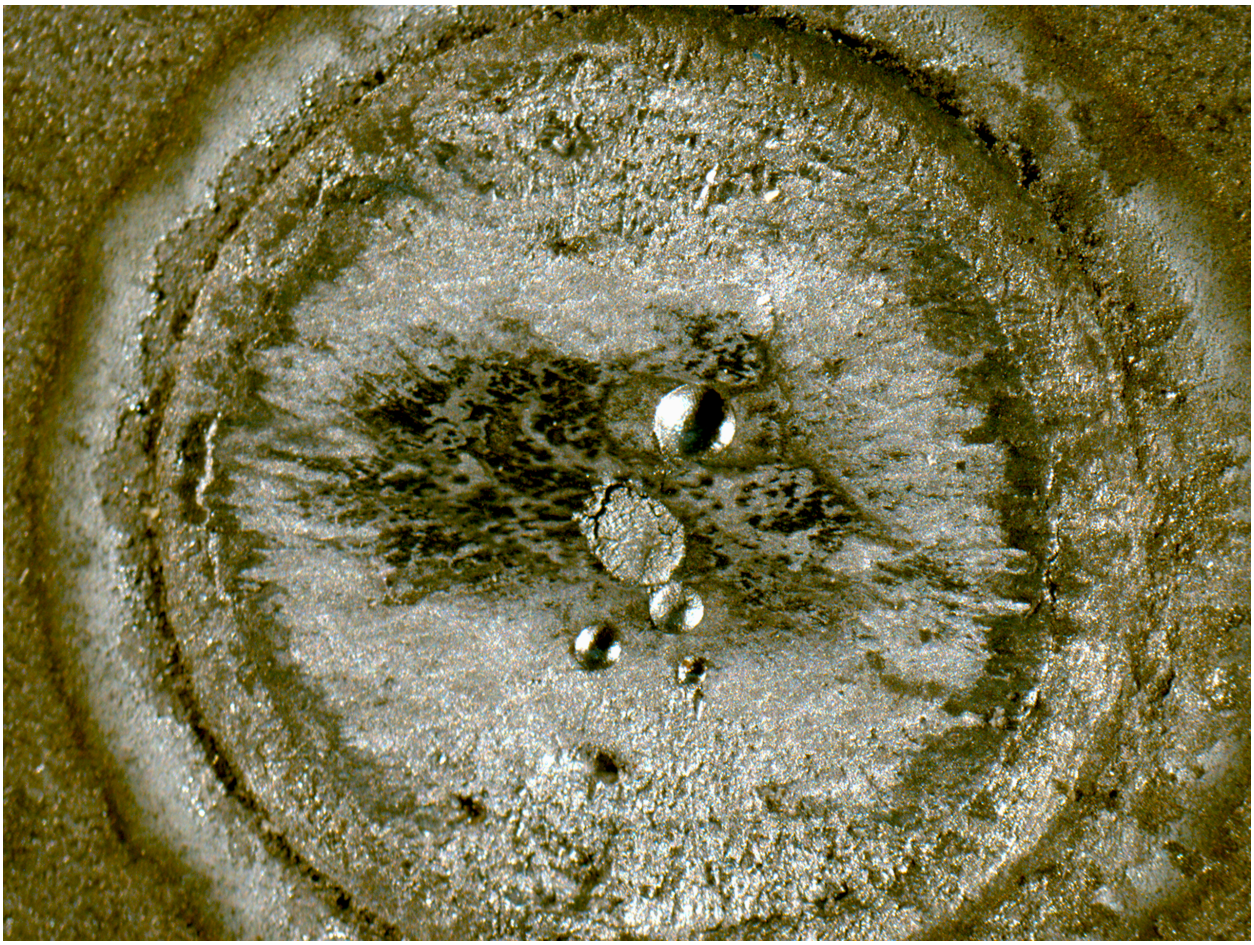

Figure 5.16 Image of full interfacial failure observed in TRIP steel welded with an average current of 6.5 kA

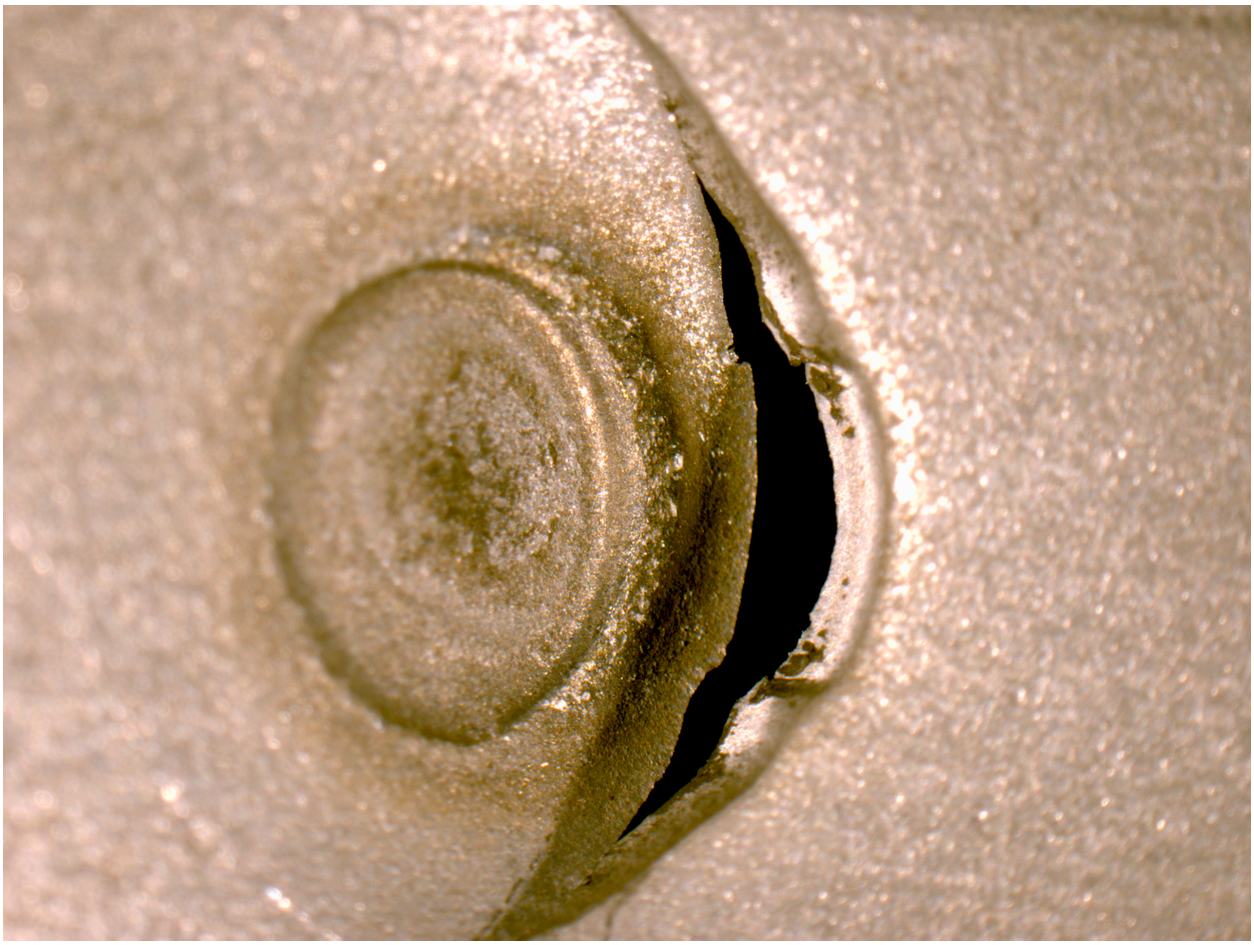

Figure 5.17 Image of nugget pull out failure observed in TRIP steel welded with an average current of 8 kA

Figure 5.18 Image of full interfacial failure observed in TRIP steel welded with an average current of 9.5 kA

5.6 Summary

During the development of the weld schedule for the TRIP 780 steel used in this study, the occurrence of interfacial failure became a point of interest and was explored by varying the effect of squeeze force and current on the occurrence of interfacial failure during shear lap tensile tests. Altering the weld current resulted in not only a change in the strength of the spot weld joint but also the occurrence of interfacial failure. Varying the squeeze force did not have an effect on the occurrence of interfacial fracture.

In this study the dependence of the microstructure on the high cycle fatigue life of the TRIP steel was investigated. In order to produce a spot weld in the shear lap configuration that achieves good strength, good fatigue life, and minimizes the occurrence of interfacial fracture, several weld schedules were examined. The weld force used to produce a spot weld in TRIP 780 does not have a significant effect on the fracture mode of the specimen given the average current is constant. The average current used to produce a spot weld in TRIP 780 has a significant effect on the fracture mode of the spot weld for several squeeze forces. No interfacial failures were observed for the fatigue tested specimens. This data is consistent with the observed behavior in the literature in the low fatigue load regime.

The effect of multiple pulse welding on the high cycle fatigue life of the steels is negligible. It is apparent that the microstructural changes that are capable of being made *in-situ* will not significantly effect the high cycle fatigue life of the TRIP 780 steel, nor the fracture mode, when

a proper current and force are used to mitigate interfacial fracture. Both methods of welding fatigue specimens behaved similarly suggesting that the high cycle fatigue life of the spot weld joint may be dictated by the joint geometry rather than the HAZ microstructure.

The Marya et al. model proves to be a good estimate of the recorded failure strength for the samples that failed via pullout, with the equation estimating a value of 22,514 N. The observed failure forces ranged from approximately 21,700 N - 24,500 N. The tensile strength of spot welds that did not experience interfacial failure were not as large as the tensile strengths achieved by some of the welds that did experience both button pullout and interfacial failure. Interfacial failure of spot welded TRIP 780 can be mitigated using a certain range of currents when welding. This appears to come as a tradeoff for sacrificing strength of the joint. Higher values of weld strength were obtainable; however, welds that failed with higher strengths also experienced interfacial failure. It is apparent that a weld schedule can be created to eliminate interfacial failure in both the fatigue regime of 10^4 and above cycles to failure as well as the overload condition for shear lap spot welded TRIP 780.

Chapter 6

Fracture Mechanics Model to Spot Weld Durability

This chapter will discuss the steps undertaken to characterize the spot weld durability in the high cycle fatigue regime using existing approaches as well as introducing a new model to predict the life of a spot welded steel joint.

6.1 Use of Existing Spot Weld Durability Models

As stated previously in this study a model currently exists to calculate an equivalent stress intensity factor for the tensile shear spot weld joint. The equations presented by Zhang were used to calculate an equivalent stress intensity factor for all of the fatigue samples used in this study (Zhang 1997, Zhang 1998, Zhang 2001). The equation used to calculate the equivalent stress intensity is shown below:

$$K_{eq} = 0.694\left[\frac{F}{d\sqrt{t}}\right], \tag{6.1}$$

where

F = Force (N),

d = Nugget diameter (mm),

t = Sheet thickness (mm),

This equation was used to calculate a maximum and minimum stress intensity value, K_{max} and K_{min}, corresponding to the maximum and minimum load applied to the fatigue specimen. The difference of these values was taken to calculate and equivalent stress intensity range:

$$\Delta K_{eq} = K_{\max} - K_{\min}, \tag{6.2}$$

where

K_{max} = Stress Intensity associated with Maximum Load (MPa√mm),

K_{min} = Stress Intensity associated with Minimum Load (MPa√mm),

ΔK_{eq} = Equivalent Stress Intensity Range (MPa√mm)

The stress intensity range was calculated for each fatigue sample used in this study, using the loading conditions stated previously. The results of this calculation were plotted on a log-log axis against the number of cycles to failure and presented as Figure 6.1. The number of cycles to failure used in this plot is the same as defined previously for shear lap specimens.

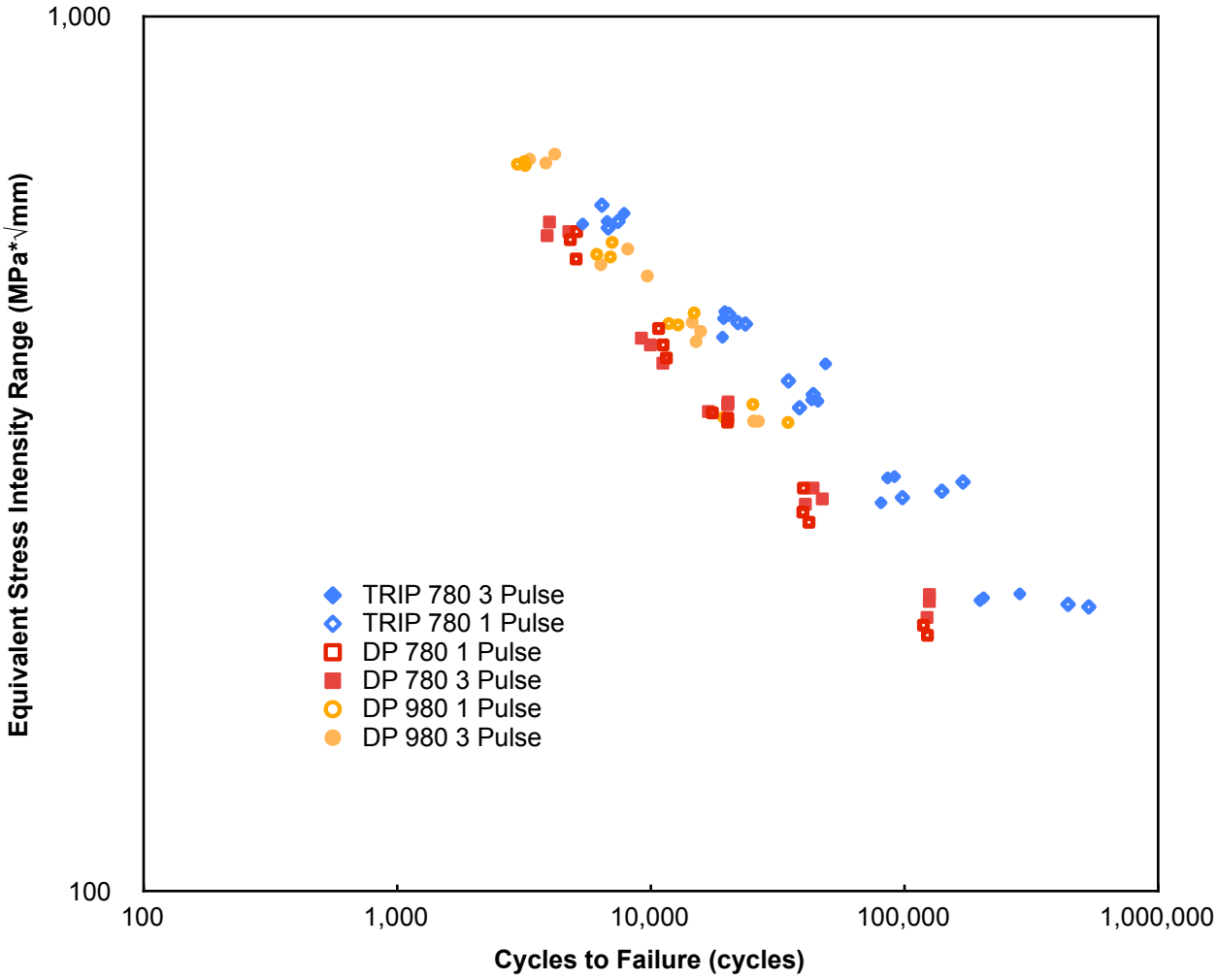

Figure 6.1 Equivalent stress intensity range calculated from using Zhang equations versus cycles to failure for AHSS steel in present study

It is plainly seen that after applying this calculation to the data a common trend is observed. The data is grouped in a trend that can be modeled by a Paris law equation. This trend has been noted by several recent studies (Dong 2011, Rathbun 2003, Zhang 1997, 2001). Figure 6.1 shows that both the DP steels and the TRIP steels used in this study behave in a similar manner not unlike previous studies.

6.2 Relation to Established Models of Fatigue Crack Growth in Steels

The purpose of this calculation is to show the correspondence between the tested specimens and these estimates which are based on established material constants. The crack growth rates observed for a plate with a center crack, using material properties that describe the HAZ microstructure of spot welds, behave much closer to the observed behavior, then the base material properties.

It has been suggested that all spot welded steel joints behave similarly, regardless of the base material. As mentioned in Chapter 2, several studies have shown that geometric differences and varying material properties can effect the fatigue life of the spot welded joint, many of these differences are negligible in the high cycle fatigue regime. It is worth noting that the largest amount of disparity in Figure 6.1 is concurrent with the portion of the curve with the highest cycles at failure. This is likely due to the fact that a greater percentage of the fatigue life of the cracks developed in the spot weld joint are spent growing through the parent material. The applied force is lower for samples with a longer number of cycles to failure, thus, increasing the

size of the flaw required to cause fast fracture, in other words meet or exceed K_{Ic}. In the case of many steels, the fracture toughness of the base material is higher than that of the fracture toughness associated with the local microstructure following welding. The differences in the fatigue are also governed to a greater extent by material properties during propagation through the base material.

To develop a predictive model for the high cycle regime of a steel spot weld joint it is important to take into consideration a comparison to known material properties. The Paris law for sub-critical crack growth was used to compare the results obtained to accepted values of crack growth behavior for two different classes of steel.

The material constants used for this analysis are found in (Dowling, 2007, Rolfe and Barsom, 1977), C and m, for ferrite - pearlite steel and martensitic steel were used in this analysis. These values were chosen because of the path of crack growth typically observed in the spot weld joint. As noted previously, fatigue crack growth in spot welded joints typically originates near the tongue structure and propagates through the thickness of the sheet through the HAZ and adjacent to the weld nugget. The fatigue crack growth observed in this study followed this trend. Microstructures of the HAZ and weld nugget are comprised of primarily of ferrite and martensite. This is a common trait shared by a majority of steel spot welded joints.

In order to use the Paris Law with the aforementioned material properties a specimen geometry and loading case must also be described. For the purpose of this comparative analysis the

geometry of a center cracked plate with an applied tensile stress was chosen. To calculate a value of stress intensity range for use in the Paris law equation, the following equation is used to calculate stress intensity (Tada and Paris, 1985):

$$\Delta K = f(g)\Delta\sigma\sqrt{\pi a}, \tag{6.4}$$

where

$f(g)$ = geometry factor,

$\Delta\sigma$ = applied stress range (MPa),

a = flaw size (mm).

The geometry factor used in the calculation was found in (Tada and Paris, 1985) for the geometry of a center cracked plate. For simplification the geometry factor is assumed to remain constant for each loading cycle. The value used for the stress range was calculated based on the loading conditions from the fatigue tests performed in this study, a value of the applied stress range was calculated corresponding to forces the used in the fatigue test.

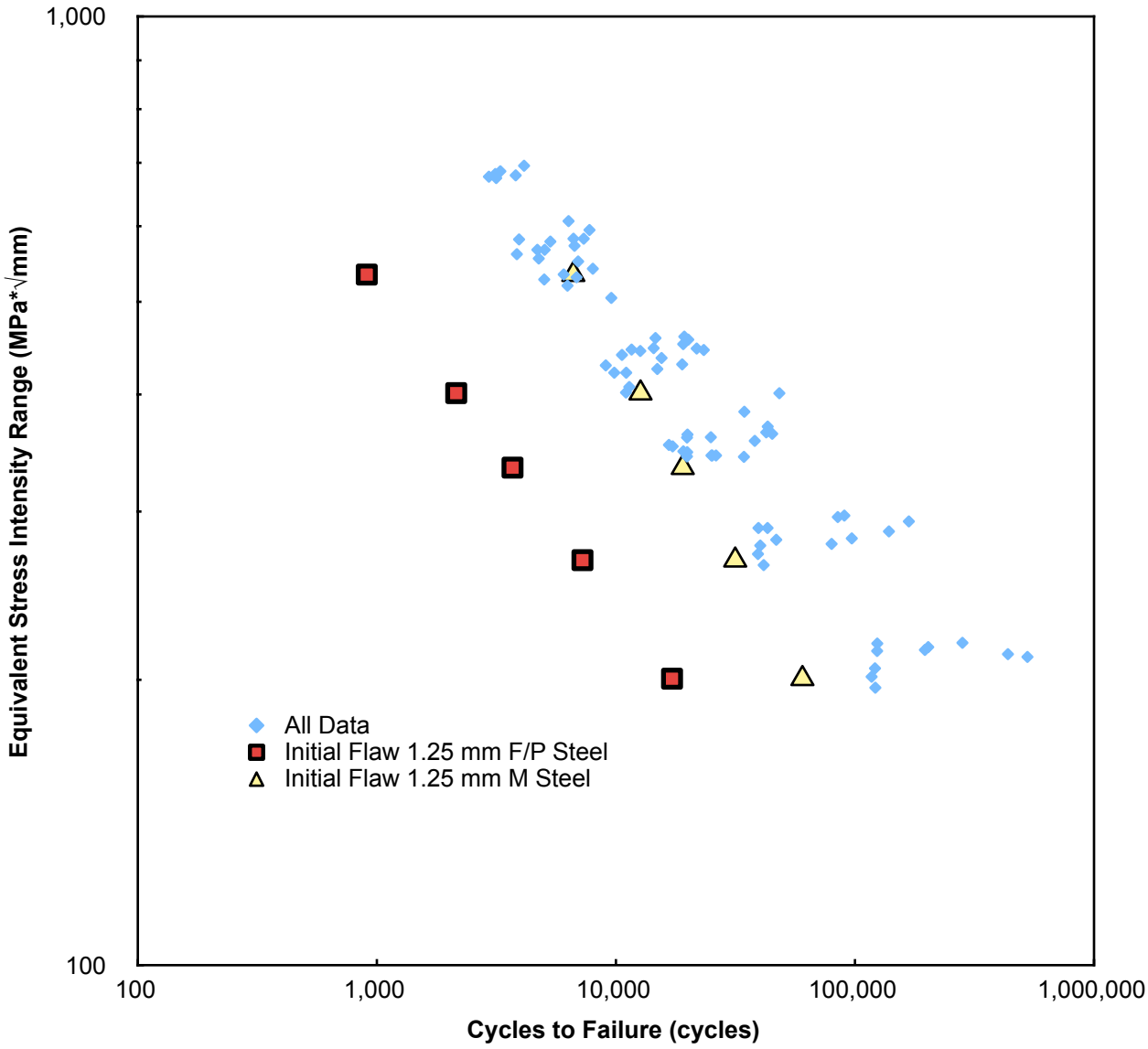

Figure 6.2 Equivalent stress intensity range versus cycles to failure for AHSS steel in present study with established material constant models

To begin the calculation an initial flaw size must be assumed. The values assumed for the initial flaw size for the calculations displayed were based on values proportional to the nugget diameter. The initial flaw size was chosen as approximately 10% of the circumference of the nugget diameter used in this study. After the assumed initial flaw size is chosen the stress intensity range calculation can be performed. The value calculated for the stress intensity range,can then be used in the Paris Law to calculate the crack growth rate.

This value found for the crack growth rate was used to find the crack extension for that particular loading cycle. The crack extension was then added to the initial flaw size value and the calculation is repeated. This method of calculation was continued until the flaw size achieved a value, approximately 5 mm. This final flaw size was chosen based on observations of the tested shear lap fatigue samples. The number of cycles required to achieve this final flaw size was then counted and used as the value for the number of cycles to failure.

The value of the stress intensity range found from the initial flaw size and the number of cycles to failure for each loading level was then plotted and compared to the values recorded for the shear lap specimens. These results are shown in Figure 6.3 for both the martensitic and ferrite-pearlite material properties.

6.3 Comparison to Previous Studies

To further illustrate the trends observed between steels of different chemistry and strength, data from a previous study was also examined. The data from (Kang, 1999) was obtained for a comparison to the AHSS results. In the study by Kang, the fatigue durability of a type of mild steel spot weld joint was investigated. The specific chemistry of the steel is not specified; however, mild steel typically consists of a microstructure predominately composed of ferrite, due to the relatively low amount of carbon. Spot welds produced using a mild steel base material will result in a nugget and HAZ microstructure that contains much less martensite and bainite than that of the microstructures discussed in this study for the AHSS steels.

The spot weld joints produced in the Kang study were produced in a geometry similar to that of the shear lap geometry used in this study. The mild steel shear lap joints were tested at a variety of mean load levels, load amplitudes, and R ratios ranging from 0 to 0.67. Using the same method stated previously, the maximum and minimum load were used to calculate the equivalent stress intensity range for the mild steel spot weld joints used in the Kang study.

The equivalent stress intensity range values and number of cycles to failure were plotted along with the data from the present study. The data is presented as Figure 6.3. It is again obvious that the spot weld joints comprised of steels of varying chemistry, and base material strength, behave relatively similar.

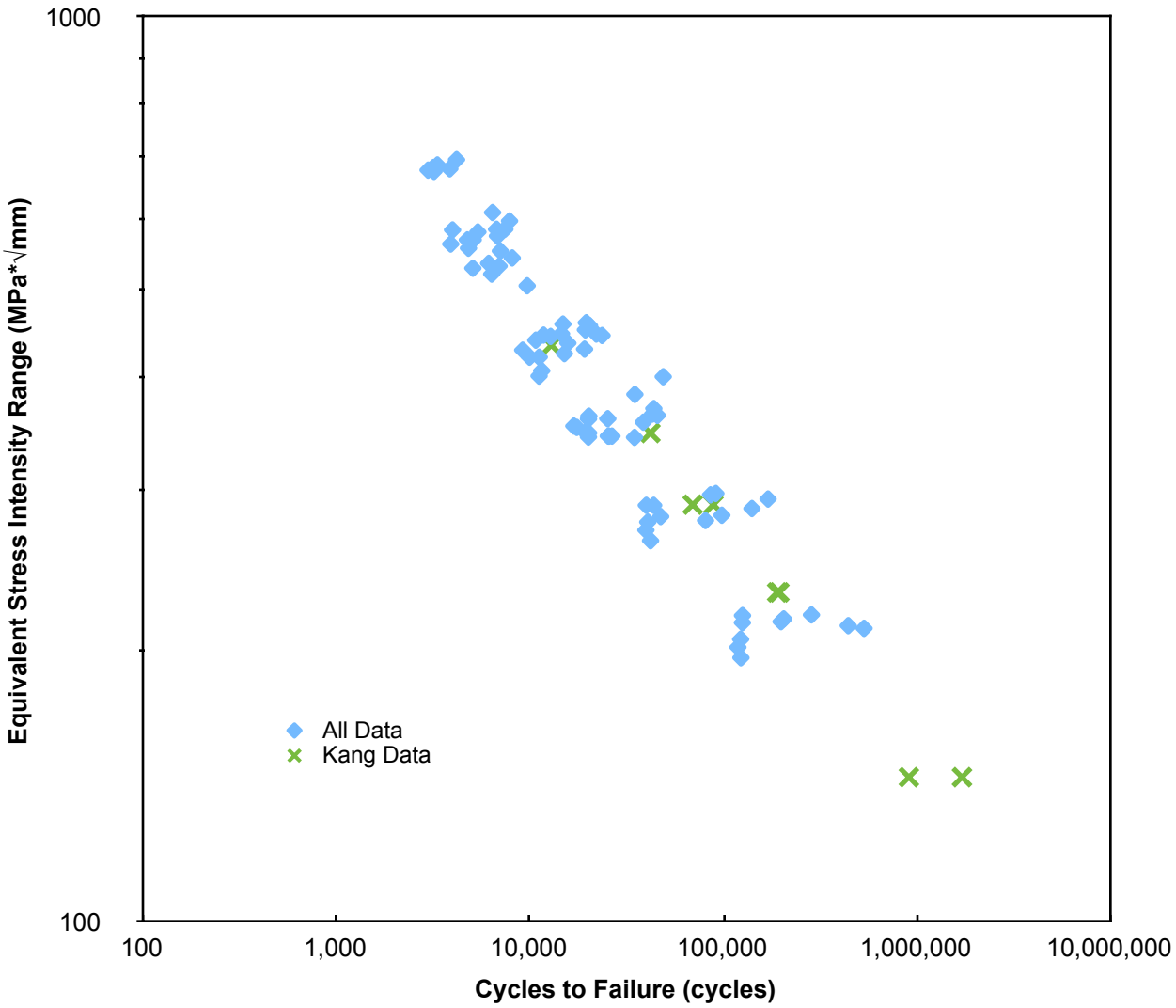

Figure 6.3 Equivalent Stress Intensity Range versus cycles to failure for AHSS steel in present study and data from Kang study.

6.4 Development of a Steel Spot Weld Durability Model

By analyzing the data presented previously a new model for spot weld durability can be established. It is apparent and has been shown by previous studies as well as the current study that spot weld joint spends a large majority of the fatigue life in the crack growth stage as opposed to the crack initiation phase. The crack growth path for steel spot welds, in the high cycle fatigue regime has consistently been described as through the HAZ adjacent to the weld nugget. This region of a steel spot weld consistently is composed of primarily ferrite and martensite. The phases certainly may occur in various concentrations and morphologies, dependent on the specific base material chemistry, weld schedule, cooling rates, etc; however, the crack growth behavior through these microstructures in steel spot weld joints is at the least similar in the high cycle fatigue regime, regardless of specific base material and processing parameters.

The first comparison utilized is that of a "hybrid material model". The hybrid material model estimates the life of the spot weld by manipulating the material constants used for the Paris power law, m and C. A similar model was used as stated previously for the case of a plate with a center through crack. Several iterations using varying values of C and m were considered; however, one case in particular modeled the data relatively well. When a value of m corresponding to martensitic steel, as described by (Dowling, 2007, Rolfe and Barsom, 1977) is used in combination with a differing C value the fit is reasonable. The model was evaluated using a 0.75 mm through crack is used in concert with a C of $6.89*10^{-13}$ and m of 0.3. The

results of this analysis are presented as Figure 6.4. The data is plotted with error bars of 30% in the positive and negative x direction. The equation that this model represents is shown below:

$$\frac{da}{dN} = 6.89^{-13}\Delta K^{0.3}, \qquad (6.5)$$

This model appears to give a good conservative estimate regarding the high cycle fatigue life of steel spot weld for shear lap spot weld samples with a nugget size of approximately 8 mm. The value of m that fits the model is reasonable considering the local microstructure which most fatigue cracks tend to propagate through. The value of C in this case appears to be dictated by the specimen geometry. For all of the samples tested there is a consistency in the geometry. The samples evaluated were all shear lap type specimens, and all had a nugget diameter of approximately 8 mm. The samples, analyzed are all steels that have a base material microstructure consisting primarily of ferrite; however, the weld nugget and HAZ contain microstructures that contain significantly more martensite and bainite then the base material. This local HAZ microstructure, directly adjacent to the weld nugget is relatively consistent amongst all of the materials examined in this study regardless of specific base material chemistry and/or strength as related to processing.

It is worth noting that the TRIP and DP steels considered in the present study also contain relatively low amounts of carbon, similar to the mild steel considered in the study by Kang.

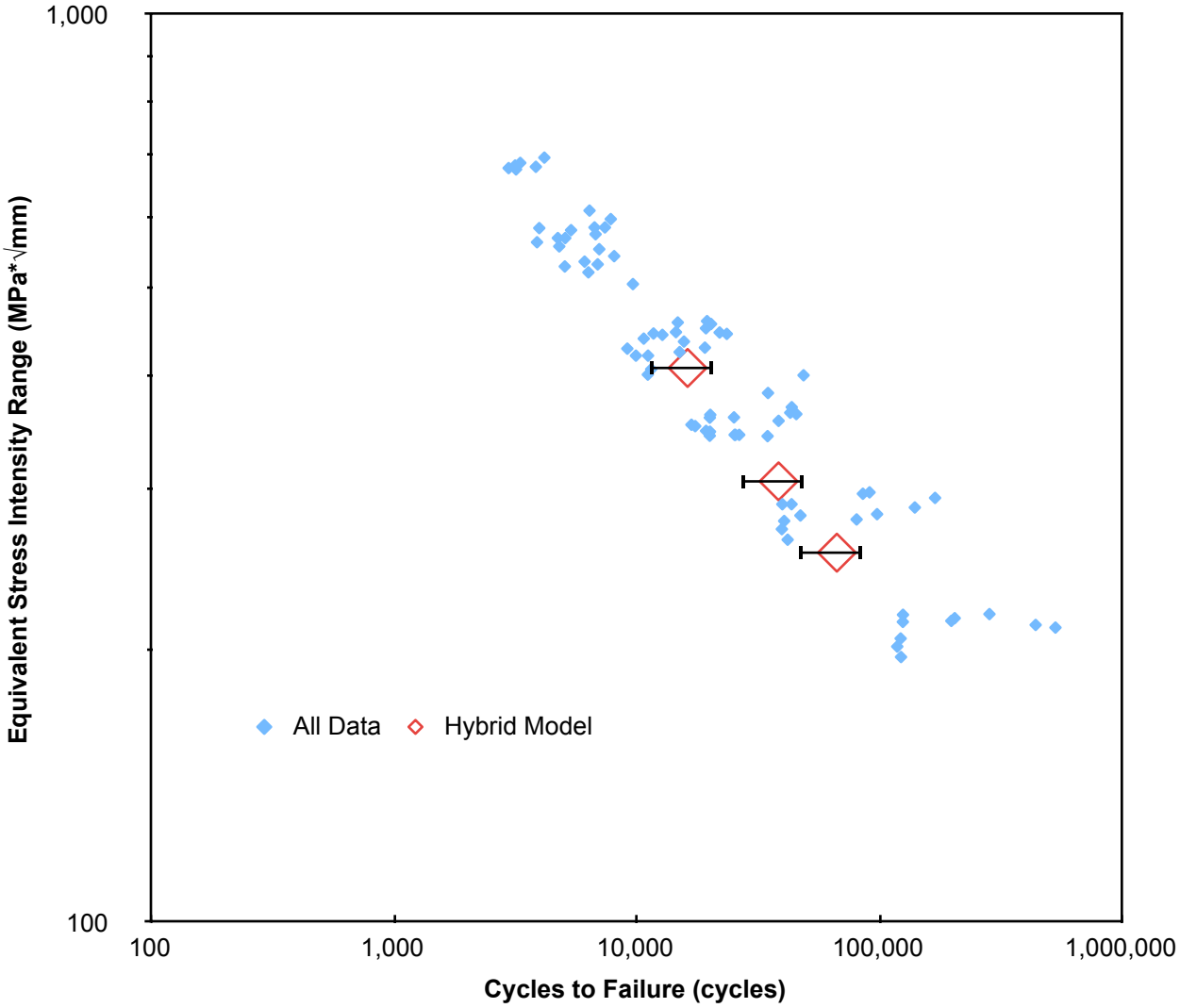

Figure 6.4 Hybrid material model plotted along with subject data

Chapter 7

Conclusions and Topics for Future Work

In the present study, the fatigue and tensile tests of AHSS shear lap coupons were conducted with varying welding parameters. The results of the test were used to develop an adjusted material model that provides a conservative estimate of the fatigue life of not only the AHSS used for this study, but also for a low carbon steel welded with a similar nugget diameter in a different study.

During the development of the weld schedule for the TRIP 780 steel used in this study, the question of interfacial failure became a point of interest and was explored by varying the effect of squeeze force and current on the occurrence of interfacial failure during shear lap tensile tests. Altering the weld current resulted in not only a change in the strength of the spot weld joint but also the occurrence of interfacial failure. Varying the squeeze force did not have an effect on the occurrence of interfacial fracture.

In this study the dependence of the microstructure on the high cycle fatigue life of the AHSS steels, specifically the TRIP steel was investigated. In order to produce a spot weld in the shear lap configuration that achieves good strength, good fatigue life, and minimizes the occurrence of interfacial fracture, it is apparent that the microstructure will not significantly effect the high cycle fatigue life of the AHSS. The results obtained from the fatigue testing performed were

used in combination with a stress intensity solution in an attempt to normalize the results for the varying material geometries and forces used for the different materials. When this calculation is performed it is apparent that the fatigue life observed for all of the AHSS steels were similar. The results of a second study conducted by Kang were also used for comparison. The Kang study was conducted on a low carbon steel with a similar nugget diameter. A similar fatigue life is observed in both sets of data.

A fracture mechanics approach to estimating the fatigue life through a modified Paris law approach was also used. This model uses material constants found for martensitic steel, the same phase that is found in the weld nugget of spot welded steels and a constant that fits the function to the data, this constant is a structural constant and will vary for different sheet thicknesses and nugget sizes.

7.1 Conclusions

From these studies the following conclusions can be made:

1. Varying the squeeze force alone during spot welding TRIP 780 will not reduce the occurrence of interfacial failure.

2. Varying the weld current will effect the occurrence of interfacial failure in spot welded TRIP 780.

3. In general, increasing the weld current used to produce TRIP 780 shear lap specimens will result in a higher achievable tensile strength; however, in the case of high current it appears that higher strengths are achievable when the interfacial fracture mechanism is the fracture mechanism.

4. The high cycle fatigue life of AHSS is not effected by altering the microstructure of the spot weld through in-situ weld tempering through multiple pulse welding.

5. The change in the weld nugget size and the transition from a primarily martensitic structure and a ferrite structure is not significantly effected by the multiple pulse welding process. The change in the hardness profile observed was found to be a drop of approximately four HRC in the three pulse welds when compared to the one pulse.

6. When the results of the fatigue tests performed are normalized using a stress intensity calculation, the fatigue life of the steels in the high cycle regime are remarkably similar. The fatigue life in the high cycle regime of the AHSS steels are essentially the same, indicating that the fatigue life of the spot welded joint is likely dictated by the structure of the joint and the varying base material microstructures and base material properties manifest as negligible differences in the fatigue life of the joints.

7. The fatigue data was compared to the results of a separate study conducted on a low carbon steel using a different fixture and test frame. The high cycle fatigue life of the spot weld samples were found to be similar. The results further suggest that the effect of the specific base material strength and/or microstructure on the high cycle fatigue life of spot weld joints is negligible.

8. The fracture mechanics model developed provides a good conservative estimate for the high cycle fatigue life of not only AHSS steels but other similar low carbon steels. This model is only valid for spot weld structures of similar nugget size, 7.5 - 8.5 mm.

7.2 Topics for Future Research

1. This study only examined steels with a low carbon content with varying other alloying elements. It is recommended that the same approach be used to study steels of varying carbon content. The behavior observed in this study indicates that the carbon content of the alloy may influence the high cycle fatigue life of steel spot weld joints due to the importance of the weld nugget and the influence of carbon concentration on the formation of martensite.

2. A fracture mechanics analysis should be undertaken to better understand the influence on the stress intensity threshold associated with interfacial failure and the influence of individual stress intensity modes. This may also require a thorough fractographic study of

the interfacial fracture surfaces in order to document the proper area that represents the joint, which may be influenced by weld cracking, porosity, etc.

3. The effectiveness of the proposed weld schedule on suppressing interfacial failure has only been tested using quasi-static loading conditions. Dynamic loading conditions should also be used to evaluate the occurrence of interfacial failure at various currents, squeeze forces, etc.

References

Abe, H., Kataoka, S. and Satoh, T. (1986). “Empirical Formula for Fatigue Strength of Single-Spot-Welded Joint Specimens under Tensile-Shear Repeated Load,” *SAE technical report No. 860606*, Detroit, Michigan.

ASM Handbook Volume 1. ASM International.

ASM Handbook Volume 9. ASM International.

ASTM, "E8 Standard Test Methods of Tension Testing of Metallic Materials,"Annual Book or ASTM Standards, American Society for Testing and Materials, Vol. 3.01

ASTM, “E3 Standard Guide for Preparation of Metallographic Specimens” Annual Book or ASTM Standards, American Society for Testing and Materials, Vol. 3.01

ASTM, "E140 Standard Hardness Conversion Tables for Metals (Relationship Between Brinell Hardness, Vickers Hardness, Rockwell Hardness, Rockwell Superficial Hardness, and Knoop Hardness)," Annual Book or ASTM Standards, American Society for Testing and Materials, Vol. 3.01

ASTM, “E384 Standard Test Method for Knoop and Vickers Hardness of Materials” Annual Book or ASTM Standards, American Society for Testing and Materials, Vol. 3.01

ASTM, "E466 Standard Practice for Conducting Constant Amplitude Axial Fatigue Tests of Metallic Specimens," Annual Book or ASTM Standards, American Society for Testing and Materials, Vol. 3.01

ASTM, "E468 Standard Practice for Presentation of Constant Amplitude Fatigue Test Results for Metallic Specimens," Annual Book or ASTM Standards, American Society for Testing and Materials, Vol. 3.01

ASTM, "E739 Standard Practice for Statistical Analysis of Linear or Linearized Stress-Life (S-N) and Strain-Life (ε-N) Fatigue Data," Annual Book of ASTM Standards, American Society for Testing and Materials, Vol. 3.01

AWS D8.9 Recommended practices for test methods for evaluating the resistance spot welding behavior of automotive sheet steel materials. Miami, FL: American Welding Society; 1998.

Barkey, M. E. and Kang, H. (1999). "Testing of Spot Welded Coupons in Tension and Shear," *Experimental Techniques*, Vol. 23, No. 5, pp. 20-22.

Barkey, M.E. and Stevenson, M.E. (2007). "Failure Modes of Electrical Resistance Spot Welds," Materials Science & Technology 2007 Conference and Exposition, Detroit, MI submitted March 2007.

Barsom, J.M. and Rolfe, S.T. Fracture and Fatigue Control in Structures: Applications of Fracture Mechanics, Third Edition. ASTM. 1999.

Bhadeshia, H.K.D.H. (2002). "TRIP-Assisted Steels?" ISIJ International 42:1059-1060.

Chatterjee, S. and Bhadeshia, H.K.D.H. (2002). "TRIP-assisted steels: cracking of high-carbon martensite" *Materials Science and Technology* 22:645-648.

Chatterjee, S. and Bhadeshia, H.K.D.H. (2007). "Transformation induced plasticity assisted steels: stress or strain affected martensitic transformation?" *Materials Science and Technology* 23:1101-1104.

Chuko, W.L. and Gould, J.E. (2002). "Development of Appropriate Resistance Spot Welding Practice for Transformation-Hardened Steels," *AWS Welding Journal* January 2002.

Davidson, J. A. (1983). "Design-Related Methodology to Determine the Fatigue Life and Related failure Mode of Spot-Welded Sheet Steels," *International Conference on Technology and Applications of High Strength Low Alloy (HSLA) Steels*, Philadelphia, Pa.

Davidson, J. A. and Imhof, E. I. (1984). "The Effect of Tensile Strength on the Fatigue Life of Spot Welded Sheet Steels," *SAE technical report No. 840110*, Detroit, Michigan.

Dowling, N. E. "Mechanical Behavior of Materials: Engineering Methods for Deformation, Fracture, and Fatigue. Third Edition. Pearson Prentice Hall. 2007.

El-Sayed, M.E.M. (1996). "Fatigue Analysis of Spot-Welded Joints Under Variable Amplitude Load History," *Engineering Fracture Mechanics* 55:363-369.

Environmental Protection Agency (EPA) and National Highway Transportation Safety Administration (NHTSA). 2017 and Later Model Year Light-Duty Vehicle Greenhouse Gas Emissions and Corporate Average Fuel Economy Standards (EPA-HQ-OAR-2010-0799). Washington, DC: Government Printing Office.

Fredriksson, K. Melander, A., Hedman, M. (1988). "Influence of prestraining and ageing on fatigue properties of high-strength sheet steels," *Intl. Journal of Fatigue* 10:139-151.

Gould, J.E. and Workman, D. (1998). "Fracture Morphologies of resistance spot welds exhibiting hold time sensitivity behavior." *Eight Sheet Metal Working Conference. Miami, FL.*: American welding Society.

Gould, J.E., Khurana, S. P. and Li, T. (2002). "Predictions of Microstructures when Welding Automotive Advanced High-Strength Steels." *AWS Welding Journal* January 2002: 111-116.

Hilditch, T.B., Speer, J.G., and Matlock, D.K. (2007). "Effect of susceptibility to interfacial fracture on fatigue properties of spot-welded high strength sheet steel" *Materials and Design* 28:2566-2576.

Hou, Wenkao. "Re: UA spot welding" Message to Eric R. Weishaupt. February 6, 2008. E-mail.

Jung, W. W., Jang, P. K., and Kang, S. S. (1996). "Fatigue Failure and Reinforcing Method of Spot Welded Area at the Stage of Vehicle Development," *SAE technical report No. 960553*, Detroit, Michigan.

Kang, H., Barkey, M. E., and Lee, Y. (2000). "Evaluation of Multiaxial Spot Weld Fatigue Parameters for Proportional Loading," *International journal of Fatigue*, Vol. 22, pp 691-702.

Kang, H. and Barkey, M. E. (1999). "Fatigue life Estimation of Spot-Welded Joints Using An Interpolation/Extrapolation Technique," *International journal of Fatigue*, Vol. 21, No. 8, pp 769-777.

Krauss, G. Principles of Heat Treatment of Steels. American Society for Metal. 1980.

Krauss, G. Steels Processing, Structure, and Performance. ASM International. 2005.

Kitagawa, H., Satoh, T., and Fujimoto, M. (1985). "Fatigue Strength of Single Spot-Welded Joints of Rephosphorized High-Strength and Low-Carbon Steel Sheets," *SAE technical report No. 850371*, Detroit, Michigan.

Long, X., Khana, S.K. (2007). "Fatigue Properties and failure characterization of spot welded high strength sheet steel," *Intl. Journal of Fatigue* 29:879-886.

Ma, C., Chen, D.L., Bhole, S.D., Boudreau, G., Lee, A., Biro, E. (2007). "Microstructure and fracture characteristics of spot-welded DP600 steel." *Materials Science and Engineering A.*, 1-13.

Marya, M., Wang, K., Hector Jr., L.G., Gayden, L.G. (2006). "Tensile-Shear Forces and Fracture Modes in Single and Multiple Weld Specimens in Dual-Phase Steels." *Journal of Manufacturing Science and Engineering*. 128:287-298.

Matsumura, O., Sakuma, Y. and Takechi, H. (1987). "Enhancement of elongation by retained austenite in intercritical annealed 0.4C – 1.5Si – 0.8Mn steel", *Trans. Iron Steel Inst. Jpn*, 27, 570–579.

Matsumura, O., Sakuma, Y. and Takechi, H. (1987). "TRIP and its kinetic aspects in austempered 0.4C – 1.5Si – 0.8Mn steel", *Scr. Metall.*, 27, 1301–1306.

Pan, N. and Sheppard S.D. (2002). “Stress intensity factors in spot welds,” Engineering Fracture Mechanics, Volume 70, Issue 5, Pages 671-684.

Paris, P., Erdogan, F. (1963). “A critical analysis of crack propagation laws.” *Journal Of Basic Engineering*, 85(4), 528-534.

Pollard, B., (1982). “Fatigue Strength of Spot Welds in Titanium-Bearing HSLA Steels,” *SAE technical report No. 820284*, Detroit, Michigan.

Pook, L.P., (1975). “Approximate Stress Intensity Factor for Spot Welds and Similar Welds,” *Report No. 588*, National Engineering Laboratory, UK.

Pook, L.P., (1975). “Fracture Mechanics analysis of the Fatigue Behavior of Spot Welds,” *International Journal of Fracture*, 11, pp. 173-176.

Radaj, D. and Zhang, S., (1991). “Simplified Formulae for Stress Intensity factors of Spot Welds,” *Engineering Fracture Mechanics*, Vol. 40, No. 1, pp. 233-236.

Radaj, D. and Zhang, S., (1991). “Stress Intensity Factors for Spot Welds Between Plates of Unequal Thickness,” *Engineering Fracture Mechanics*, Vol. 39, No. 2, pp. 391-413.

Radaj, D. and Zhang, S., (1992). “Stress Intensity Factors for Spot Welds Between Plates of Dissimilar Materials,” *Engineering Fracture Mechanics*, Vol. 42, No. 3, pp. 407-426.

Radaj, D., Zheng, Z., and Mohrmann, W., (1991). “Local Stress Parameters at the Weld Spot of Various Specimens,” *Engineering Fracture Mechanics,* Vol. 37, No. 5, pp. 933-951.

Rathbun, R.W., Matlock, D.K., and Speer, J.G. (2003). “Fatigue Behavior of Spot Welded High-Strength Sheet Steels,” *AWS Welding Journal* August 2003.

Sakuma, Y., Matsumura, O. and Akisue, O. (1991). “Influence of C content and annealing temperature on microstructure and mechanical - properties of 400C transformed steel containing retained austenite”, *ISIJ Int*., 31, 1348–1353.

Sakuma, Y., Matsumura, O. and Takechi, H. (1991). "Mechanical–proper- ties and retained austenite in intercritically heat-treated bainite- transformed steel and their variation with Si and Mn additions", *Metall. Mater. Trans. A,* 22A, 489–498.

Shang, D., Barkey, M.E., Wang, Y., and Lim, L.C. (2004). ''Fatigue Damage and Dynamic Natural Frequency Changes of Spot Welded Joints,'' SAE Technical Paper 2003-01-0695, selected for publication in 2003 *SAE Transactions: Journal of Materials & Manufacturing*, September 2004

Tada, H., Paris, P. C. (1985). The stress analysis of cracks handbook: by Hiroshi Tada, with the cooperation of Paul C. Paris and George R. Irwin. 2d. ed. Saint Louis: Paris Productions & (Del Research Corp.).

Timokhina, I.B., Hodgson, P.D., and Pereloma, E.V. (2004). "Effect of Microstructure on the Stability of Retained Austenite in Transformation-Induced-Plasticity Steels," *Metallurgical and Materials Transactions A* 35A:2331-2341.

Wang, G. and Barkey, M.E. (2005). ''Fatigue Crack Identification in Tensile-Shear Spot Welded Structure by Dynamic Response Characteristics,'' *ASME Journal of Engineering Materials and Technology*, Vol 127, pp. 310-317.

Wang, G. and Barkey, M.E. (2006). ''Investigation of Spot Weld Fatigue Crack Growth Process Using X-ray Imaging," *AWS Welding Journal Research Supplement*, Volume 85 No. 4, pp. 84S-90S.

Wilson, R. B. and Fine, T. E. (1981). "Fatigue Behavior of Spot Welded High Strength Steel Joints," *SAE technical report No. 810354*, Detroit, Michigan.

Yan, B. and Urban, D. (2003). "Characterization of Fatigue and Crash Performance of New Generation High Strength Steels for Automotive Applications," Report prepared to the U.S. Department of Energy, January 2003.

Zhang, S. (1997). "Stress Intensities at Spot Welds*," International Journal of Fracture*, Vol. 88, pp. 167-185.

Zhang, S. (1998). “Stress Intensities Derived from Stresses Around a Spot Weld,” *International Journal of Fracture*, Vol. 99, pp. 239-257.

Zhang, S. (2001). “Fracture Mechanics Solutions to Spot Welds,” *International Journal of Fracture*, Vol. 112, pp. 247-274.

Zhang, X., Barkey, M.E., Lee, Y., Lu, M., Pakalnins, E., Orsette, C., Trojanowski, W. (2008). “DOE Analysis of Factors Affecting Ultimate Strength of Multiple Resistance Spot Welded Joints,” *SAE 2007 Transactions Journal of Passenger Cars – Mechanical Systems*, June 2008

Appendix A

Base Material Fatigue Testing Results

DP 980 (UTS Load 28 kN)	
Cycles	Load (Percent UTS)
2365	0.9
1004	0.9
30333	0.8
38197	0.8
146519	0.7
205322	0.7
81312	0.7
676855	0.7
1313746	0.67
2269046	0.65
4000000	0.65
4000000	0.6

DP 780 (UTS Load 20 kN)	
Cycles	Load (Percent UTS)
42	0.9
13	0.9
30802	0.8
9989	0.8
108654	0.7
92960	0.7
150445	0.65
257484	0.65
1140120	0.64
2000000	0.64
2000000	0.62
2000000	0.6
2946363	0.6

TRIP 780 (UTS Load 22.7 kN)	
Cycles	Load (Percent UTS)
651	0.9
389	0.9
31754	0.8
27420	0.8
130148	0.7
123141	0.7
145405	0.7
177761	0.66
150106	0.66
2000000	0.65
2000000	0.65
223969	0.65
2000000	0.6

Appendix B

Spot Weld Fatigue Testing Results

DP 980 1 Pulse (UTS Load 28 kN)	
Cycles	Load (Percent UTS)
3194	0.36
2977	0.36
3166	0.36
6119	0.27
7032	0.27
6928	0.27
12797	0.225
14811	0.225
11764	0.225
19370	0.18
34721	0.18
25245	0.18

DP 980 3 Pulse (UTS Load 28 kN)	
Cycles	Load (Percent UTS)
3854	0.36
3324	0.36
4177	0.36
6346	0.27
9678	0.27
8100	0.27
15704	0.225
15074	0.225
14555	0.225
25402	0.18
26537	0.18
25598	0.18

DP 780 1 Pulse (UTS Load 20 kN)	
Cycles	Load (Percent UTS)
5072	0.36
5093	0.36
4812	0.36
11171	0.27
11510	0.27
10725	0.27
17473	0.225
20105	0.225
20062	0.225
42001	0.18
39751	0.18
39936	0.18
123124	0.135
118780	0.135

DP 780 3 Pulse (UTS Load 20 kN)	
Cycles	Load (Percent UTS)
3981	0.36
4748	0.36
3897	0.36
9177	0.27
9958	0.27
11148	0.27
20071	0.225
20160	0.225
16862	0.225
47410	0.18
43584	0.18
40636	0.18
125269	0.135
125433	0.135
122688	0.135

TRIP 780 1 Pulse (UTS Load 22.7 kN)	
Cycles	Load (Percent UTS)
6412	0.36
6791	0.36
7420	0.36
22029	0.27
23585	0.27
20311	0.27
34860	0.225
38542	0.225
43660	0.225
170031	0.18
140347	0.18
98119	0.18
532786	0.135
441564	0.135
1300067	0.135

TRIP 780 3 Pulse (UTS Load 22.7 kN)	
Cycles	Load (Percent UTS)
7844	0.36
6722	0.36
5382	0.36
19159	0.27
19345	0.27
19551	0.27
45593	0.225
48841	0.225
43049	0.225
80787	0.18
91333	0.18
85756	0.18
204890	0.135
198404	0.135
284858	0.135